EARTHQUAKE RISK AND LIQUEFACTION HAZARD ASSESSMENT FRAMEWORK: MARMARA REGION A CASE STUDY

A thesis submitted for the degree of Doctor of Philosophy
in the Faculty of Engineering of the University of Sheffield

By

Ilya Sianko

(BSc, MSc)

Department of Civil & Structural Engineering
The University of Sheffield

June 2021

To my family
for their love, support,
patience and
faith in me.

ACKNOWLEDGMENTS

Firstly, I would like to express gratitude and appreciation to my supervisor Dr. Zuhal Ozdemir for her continuous support, encouragement and guidance during my PhD research. She provided me with all the necessary tools to complete this thesis and her support allowed me to grow personally and professionally.

Secondly, this research would not have been possible without the help and support of my co-supervisors Prof. Kypros Pilakoutas and Dr. Iman Hajirasouliha. Their vast knowledge and priceless advice helped me to successfully overcome any difficulties during this project. I would like to thank Dr. Reyes Garcia, who has provided me with a lot of support and motivation in the early stages of my research.

I appreciate the financial assistance provided by the RCUK-TUBITAK Research Partnerships Newton Fund Awards and the British Council Newton Fund.

Most of all I am thankful to my parents, without their endless support and belief in me I would not have the opportunity to undertake doctoral research. A final big thank you is to my wife Olga who encouraged me at every step and who was always patient and supportive.

ABSTRACT

The devastation of the past earthquake events such as Kocaeli (1999), Kashmir (2005) and Haiti (2010) highlights the need for an earthquake risk assessment (ERA) framework, which can be applied to developing countries to reduce future earthquake losses. Although there are several ERA frameworks used in current practice, these frameworks are not flexible or applicable to the areas with limited input data and lacking assessment of earthquake induced secondary hazards. One of them is liquefaction, which is capable of causing settlement, tilting or even collapse of the structures. As an example, numerous liquefaction manifestations in Adapazari during 1999 Kocaeli and 1999 Chi-Chi earthquakes caused damage to a significant number of buildings due to ground failures. This past experience highlighted the importance of the integration of liquefaction hazard assessment into the existing or future earthquake risk assessment frameworks.

This research presents the development of the multi-hazard ERA framework, which can be applied to the areas with limited input data available. The proposed framework is based on Monte-Carlo simulations and consists of three main modules: Probabilistic Seismic Hazard Analysis (PSHA), Probabilistic Liquefaction Hazard Analyses (PLHA) and Seismic Risk Assessment.

The developed PSHA module generates earthquake catalogues using Monte-Carlo simulations to represent future seismicity of the region of interest. In this module, both Poisson and time dependent (renewal) models are adopted to quantify the effect of temporal dependencies between seismic events, while near-field rupture directivity effects are also taken into account. The Marmara region in Turkey is selected as a case study region. The PSHA results compare well with the recent studies performed for the study region.

The PLHA module of the framework uses Monte-Carlo simulations and simplified liquefaction assessment procedures to predict earthquake induced liquefaction hazard in a probabilistic way. The module provides a relatively flexible approach to treat uncertainties of the earthquake and soil related input parameters by including such parameters with distribution functions. Liquefaction Potential Index (LPI) and Liquefaction Severity (L_S) procedures are adopted for the prediction of liquefaction hazard. The PLHA module is applied to the city of Adapazari in Turkey, which is located in a liquefaction prone area. A set of probabilistic liquefaction hazard maps are derived for Adapazari as there were no PLHA studies performed

for the city. The PLHA module is verified with a scenario earthquake and observed liquefaction from the 1999 Kocaeli earthquake.

Seismic risk assessment module uses readily available data such as building stock and population data from census, global shear-wave velocity maps and satellite images. Seismic risk assessment module is applied to Adapazari. An exposure model for buildings in the case study area is developed by mapping buildings footprints from aerial and satellite images and using remote street survey. The risk results are presented in terms of loss curves and probabilistic mean damage ratio (MDR) maps considering various return periods and vulnerability models. Casualty models are incorporated into the framework for estimation of fatalities associated with earthquakes in the city of Adapazari. Social and economic losses are verified with a scenario earthquake similar to 1999 Kocaeli earthquake.

The developed ERA framework can serve as an efficient tool for the assessment of liquefaction hazard and seismic risk in the areas with limited data available. Although, due to lack of reliable procedures for accounting damage due to liquefaction in large scale seismic risk studies, the risk module of the framework should be used with caution in the areas prone to liquefaction. The proposed framework and its outcomes can be used by policy and stakeholders for earthquake preparedness and developing emergency response and recovery strategies.

TABLE OF CONTENTS

Contents

LIST OF FIGURES

LIST OF TABLES

ABBREVIATIONS

AFAD	The Disaster and Emergency Management Presidency
BPT	Brownian Passage Time
BSZ	Background Source Zone
CE	Common Era
CNAF	Central Branch of North Anatolian Fault
DF	Degree of Freedom
EFL	Epicentral Fault Line
ERA	Earthquake Risk Assessment
FSZ	Fault Source Zone
GEM	Global Earthquake Model
GMPE	Ground Motion Prediction Equation
GSHAP	Global Seismic Hazard Assessment Program
GWL	Ground Water Level
IM	Intensity Measure
MC	Monte-Carlo
MDR	Mean Damage Ratio
MSRF	Multi-Scale Random Field
NAF	North Anatolian Fault
NNAF	North Branch of North Anatolian Fault
PDF	Probability Density Function
PGA	Peak Ground Acceleration
PGV	Peak Ground Velocity
PLHA	Probabilistic Liquefaction Hazard Analysis
POE	Probability of Exceedance
PEER	Pacific Earthquake Engineering Research Centre
PSHA	Probabilistic Seismic Hazard Analysis
RC	Reinforced Concrete
RLD	Subsurface Rupture Length
RW	Rupture Width
Sa	Spectral Acceleration
Sd	Spectral Displacement

SHARE	Seismic Hazard Harmonization in Europe
SNAF	South Branch of North Anatolian Fault
SPT	Standard Penetration Test
SRL	Surface Rupture Length
TL	Turkish Lira

NOTATIONS

a	Constant in Gutenberg–Richter relationship
a_{max}	Peak horizontal ground acceleration
b	Constant in Gutenberg–Richter relationship
CRR	Cyclic resistance ratio
CSR	Cyclic stress ratio
$d4$	Number of buildings collapsed
$d5$	Number of buildings extensively damaged
$D5$	Number of buildings collapsed
E	Number of expected events
F_S	Safety factor against liquefaction
K_{FC}	Fines content
K	Number of death
$L4$	Lethality rate for extensive damage
$L5$	Lethality rate for collapse
LPI	Liquefaction potential index
L_S	Liquefaction severity index
M_L	Local magnitude
M_{char}	Characteristic magnitude
M_{max}	Maximum magnitude
M_{min}	Minimum magnitude
M_s	Surface wave magnitude
M_w	Moment magnitude
M	Earthquake magnitude
$M1$	Population per building
$M2$	Occupancy rate at the time of an earthquake
$M3$	Occupants trapped by collapse
$M4$	Lethality rates for collapse
$M5$	Lethality rates for post-collapse
MSF	Magnitude scaling factor
m_b	Body-wave magnitude

N_{max}	Annual number of earthquakes exceeding M_{max}
N_{min}	Annual number of earthquakes exceeding M_{min}
N_{rndB}	Number of events from Poisson distribution for BSZ
n	Total number of cells used in the chi-squared test
O	Number of observed events in synthetic catalogue
P_L	Probability of liquefaction
P_a	Reference stress
P_{char}	Annual probability of occurrence of characteristic magnitude
$P_{cond}(T, \Delta T)$	Conditional probability of the future characteristic event
P_{max}	Probabilities of annual occurrence for an event exceeding M_{max}
P_{min}	Probabilities of annual occurrence for an event exceeding M_{min}
P_{rndB}	Random number sampled from standard normal distribution
P_{rndF}	Random number sampled from standard normal distribution
$P(\alpha)$	Probability of observing a pulse at α
R	Source-site distance
R_{hyp}	Distance to hypocentre
R_{JB}	Shortest distance to surface projection of the fault rupture
R_{eff}	Effective Poisson annual probability
R_{epi}	Distance to epicentre
R_{rup}	Shortest distance to the fault rupture
r	Site-to-source geometric parameter
r_d	Shear stress reduction factor
s	Site-to-source geometric parameter
T	Period
T_p	Period of the pulse
ΔT	Exposure period
V_{S1}^*	Limiting upper value of shear-wave velocity for liquefaction
V_{s1}	Overburden-stress-corrected
V_{S10}	Average shear-wave velocity across the top 10m of soil
V_{S20}	Average shear-wave velocity across the top 20m of soil
V_{S30}	Average shear-wave velocity across the top 30m of soil
$V_{s,12m}$	Average shear-wave velocity across the top 12m of soil

$V_{s1,\mathrm{cs}}$	Stress-corrected shear wave velocity
X^2	Chi-squared
α_p	Aperiodicity
μ	Mean return period
$\mu_{\ln T_p}$	Mean period of the pulse
$\sigma_{\ln T_p}$	Standard deviation of mean period of the pulse
$\sigma_{\varepsilon_{r_d}}$	Standard deviation of r_d
σ'_v	Effective overburden stress
σ_v	Total overburden stress
α	Orientation of interest
τ	Between-event residual
φ	Within-event residual
$f(t)$	Probability density function
z	Depth
ε	Standard normal variable
σ	Standard deviation

Chapter 1: Introduction

1.1 Background

Earthquakes may have a huge negative impact on economic welfare and resilience of communities, particularly in developing countries. Previous major earthquakes such as 2005 Kashmir (Pakistan), 2008 Chengdu (China), 2010 Haiti and 2011 Tohoku (Japan) earthquakes demonstrated the destructive social and economic consequences of such events. The urbanisation of earthquake prone areas has increased significantly over the last few decades and seismic risk assessment has become more and more important. Seismic risk assessment has three main components: seismic hazard, vulnerability and exposure.

Probabilistic seismic hazard analysis (PSHA) is a complex process as it often deals with different uncertainties and unknown parameters. Nevertheless, there are existing probabilistic seismic hazard analysis (PSHA) models available to the public that provide hazard results at the regional or country level. However, these models only provide data for specific return periods or soil conditions (e.g. SHARE project and Unified Hazard Tool by USGS). The hazard results from these models are available for a limited number of regions or countries for which they were developed. In addition to the seismic hazard models, there are commercial risk assessment tools that are normally used by insurance and reinsurance industries. Often these tools are presented as “black boxes” and the user is limited to the pre-defined procedures and input parameters (Bommer et al., 2006). As a result, region specific modifications to the hazard and vulnerability models cannot be easily implemented. The assumptions and uncertainties adopted in these commercial tools are locked or are not shown to the user (Bommer et al., 2006). Moreover, the processes within the commercial software that convert input to output are not deconstructed (Musson and Winter, 2012).

To address some of the above issues, Global Earthquake Model (GEM, https://www.globalquakemodel.org/) was initiated in 2006 to develop an open-source earthquake risk assessment tool, which is called OpenQuake (Pagani et al., 2014). This tool has greatly improved the earthquake hazard and risk assessment standards (Erdik, 2017). Although OpenQuake (version 3.11.2) is a very comprehensive and transparent risk assessment tool, it still lacks some flexibility in certain areas, such as time-dependent PSHA and consideration of the near-fault directivity. Time-dependent hazard models can provide better hazard estimates compared to Poisson hazard models for the areas where information on periodicity of the faults ruptures with characteristic magnitude earthquakes is available (Schwartz and Coppersmith, 1984). In some cases it is important to consider near-fault directivity effects as they are known to cause pulselike ground motions at near-fault sites (Shahi and Baker, 2011). These pulses can place huge earthquake demands on buildings and previously caused extensive damage in past earthquake events (Akkar et al., 2005, Luco and Cornell, 2007). To make the PSHA module more comprehensive both time-dependent and near-fault directivity procedures need to be incorporated into a seismic hazard assessment tool. Another limitation of OpenQuake is that it is designed to predict only the strong ground motion hazard and it is not capable of predicting secondary hazards like liquefaction, landslides etc. The assessment of secondary hazards might be crucial for areas where there is evidence that they may occur. Past experience has demonstrated that such hazards may cause substantial damage to structures in addition to strong ground motions.

Often in areas with presence of soft soil and ground water level close to the surface, earthquakes may trigger liquefaction, which can cause damage to lifelines and structures. Ground and foundation failures due to liquefaction were widely observed during the 1999 Kocaeli and Duzce (Turkey) and 1999 Chi-Chi (Taiwan) earthquakes. During the 1999 Kocaeli earthquake hundreds of buildings were subjected to settlement, tilting and overturning due to

liquefaction in the city of Adapazari (Mollamahmutoglu et al., 2003, Bray et al., 2004, Bakır et al., 2005). To mitigate future risks from liquefaction there are different procedures developed for assessing liquefaction hazard. Simplified methods are commonly employed by geotechnical engineers to evaluate the liquefaction potential of soils due to the difficulty and the cost of obtaining high-quality undisturbed samples (Juang et al., 2001). The stress method developed by Seed and Idriss (1971) is the most commonly used method in assessing liquefaction susceptibility of soils. The method uses the peak ground acceleration (PGA) along with a representative earthquake magnitude to calculate the seismic stress that causes soil to liquefy. The PGA used in the analysis usually corresponds to the value observed in the past events (e.g. Holzer et al., 2006; Sonmez and Ulusay, 2008; Rahman et al., 2015). The main drawback of using scenario earthquake is that it does not consider all possible future earthquake events that are capable of triggering liquefaction. The approaches such as proposed by Juang et al. (2008) and Kramer and Mayfield (2007) are based on seismic hazard curves and disaggregation of results from PSHA and are limited to the areas where this data is available. Therefore, there is a need for a PLHA module that is more flexible and complete in providing liquefaction hazard prediction at a given location in comparison to a conventional liquefaction estimation procedure.

The development of an exposure model for seismic risk assessment is a challenging process as the model needs to include data about the location, fragility and value of the structures. Satellite imagery and remote street view survey may be used as an alternative to field building surveys. A simple procedure is proposed in this work for cost effective and rapid building stock assessments using satellite imagery and remote street view survey.

1.2 Research Aim and Objectives

The main aim of this research is to develop a seismic risk assessment framework that is capable of predicting seismic risk and liquefaction hazard in seismically active regions and apply it to a selected case study area. The main objectives of the presented work can be given as follows:

1. To develop a comprehensive event-based PSHA procedure based on generated synthetic catalogues, that will utilise readily available data for analysis.
2. To develop a procedure for probabilistic liquefaction hazard analysis (PLHA) and verify it with a case study.
3. To develop a simple methodology for building exposure model for structures and identify suitable fragility/vulnerability models.
4. To apply the seismic risk framework to a case study area to produce seismic hazard maps, loss curves and risk maps.
5. Estimate the casualties for a case study area using a probabilistic approach that considers various return periods. Verify results with comparing to casualties from a past event and modelled scenario earthquake.

1.3 Structure of the Thesis

This thesis consists of five chapters and three appendices. The first and last chapters are written in normal thesis format while chapters 2 to 4 are written in journal paper format.

Chapter 2, which is entitled “A Practical Probabilistic Earthquake Hazard Analysis Tool: Case Study Marmara Region” is a journal paper published in Bulletin of Earthquake Engineering. It addresses objective 1. This chapter describes the development of the probabilistic seismic hazard analysis (PSHA) module of the proposed seismic risk assessment framework. To demonstrate the applicability of the proposed methodology, the Marmara region

in Turkey is used as a case study area. Both Poisson and time-dependent (renewal) seismic hazard models are developed for the case study area. In addition, the procedure for accounting near-field rupture directivity effects in an event-based PSHA is proposed. The results of the proposed PSHA are compared with results from recent PSHA studies.

Chapter 3, which is entitled "A Practical Probabilistic Liquefaction Hazard Analysis Tool Based on Monte-Carlo Procedure", was submitted for publication in peer-reviewed journal, and addresses objective 2. In this work, a PLHA procedure based on Monte-Carlo simulations is proposed for assessing liquefaction hazard for seismic prone regions. Different liquefaction prediction methods are integrated into the procedure to quantify liquefaction hazard. Small and large scale case studies are performed for the city of Adapazari and the Marmara region of Turkey. The liquefaction hazard maps prepared for the city of Adapazari are compared with observed liquefaction following the 1999 Kocaeli earthquake.

Chapter 4, which is entitled "Probabilistic Seismic Risk Assessment Framework: case study Adapazari, Turkey", is ready for submission to publish in a peer-reviewed journal, and addresses objectives 3-5. In this work, a probabilistic seismic risk framework is proposed. The developed framework is applied to the city of Adapazari in Turkey by using readily available data. An exposure model for buildings and population is developed based on the information from building footprints mapped and census data. Fragility/vulnerability functions for Turkey are selected and integrated into the framework to predict seismic damage. Seismic loss curves and mean damage ratios maps are obtained for the study area for different return periods. In addition, casualty models are employed in to the framework to estimate number of fatalities in the city of Adapazari. The scenario earthquake based on the 1999 Kocaeli earthquake is used to compare predictions of structural damage and number of casualties with that past event.

Chapter 5 provides concluding remarks and includes recommendations for future work.

References

Akkar, S., Yazgan, U. & Gülkan, P. 2005. Drift estimates in frame buildings subjected to near-fault ground motions. *Journal of Structural Engineering*, 131, 1014-1024.

Bakır, B. S., Yılmaz, M. T., Yakut, A. & Gülkan, P. 2005. Re-examination of damage distribution in Adapazarı: Geotechnical considerations. *Engineering Structures*, 27, 1002-1013.

Bommer, J., Spence, R. & Pinho, R. Earthquake loss estimation models: time to open the black boxes. *First European Conference on Earthquake Engineering and Seismology*. Geneva, 2006.

Bray, J. D., Sancio, R. B., Durgunoglu, T., Onalp, A., Youd, T. L., Stewart, J. P., Seed, R. B., Cetin, O. K., Bol, E. & Baturay, M. B. 2004. Subsurface characterization at ground failure sites in Adapazari, Turkey. *Journal of Geotechnical and Geoenvironmental Engineering*, 130, 673-685.

Erdik, M. 2017. Earthquake risk assessment. *Bulletin of Earthquake Engineering*, 15, 5055-5092.

Holzer, T. L., Bennett, M. J., Noce, T. E., Padovani, A. C. & Tinsley Iii, J. C. 2006. Liquefaction hazard mapping with LPI in the greater Oakland, California, area. *Earthquake Spectra*, 22, 693-708.

Juang, C. H., Chen, C. J. & Jiang, T. 2001. Probabilistic framework for liquefaction potential by shear wave velocity. *Journal of geotechnical and geoenvironmental engineering*, 127, 670-678.

Juang, C. H., Li, D. K., Fang, S. Y., Liu, Z. & Khor, E. H. 2008. Simplified procedure for developing joint distribution of a max and M w for probabilistic liquefaction hazard analysis. *Journal of Geotechnical and Geoenvironmental Engineering*, 134, 1050-1058.

Kramer, S. L. & Mayfield, R. T. 2007. Return period of soil liquefaction. *Journal of Geotechnical and Geoenvironmental Engineering*, 133, 802-813.

Luco, N. & Cornell, C. A. 2007. Structure-specific scalar intensity measures for near-source and ordinary earthquake ground motions. *Earthquake Spectra*, 23, 357-392.

Mollamahmutoglu, M., Kayabali, K., Beyaz, T. & Kolay, E. 2003. Liquefaction-related building damage in Adapazari during the Turkey earthquake of August 17, 1999. *Engineering Geology*, 67, 297-307.

Musson, R. M. W. & Winter, P. 2012. Objective assessment of source models for seismic hazard studies: with a worked example from UK data. *Bull Earthquake Eng*, 10, 367-378.

Pagani, M., Monelli, D., Weatherill, G., Danciu, L., Crowley, H., Silva, V., Henshaw, P., Butler, L., Nastasi, M., Panzeri, L. and Simionato, M. 2014. OpenQuake engine: An open hazard (and risk) software for the global earthquake model. *Seismological*

Research Letters, 85, 692-702.

Rahman, M. Z., Siddiqua, S. & Kamal, A. M. 2015. Liquefaction hazard mapping by liquefaction potential index for Dhaka City, Bangladesh. *Engineering geology*, 188, 137-147.

Schwartz, D. P. & Coppersmith, K. J. 1984. Fault behavior and characteristic earthquakes: Examples from the Wasatch and San Andreas fault zones. *Journal of Geophysical Research: Solid Earth*, 89, 5681-5698.

Seed, H. B. & Idriss, I. M. 1971. Simplified procedure for evaluating soil liquefaction potential. *Journal of Soil Mechanics & Foundations Div.*, 97(9), 1249-1273.

Shahi, S. K. & Baker, J. W. 2011. An empirically calibrated framework for including the effects of near-fault directivity in probabilistic seismic hazard analysis. *Bulletin of the Seismological Society of America*, 101, 742-755.

Sonmez, B. & Ulusay, R. 2008. Liquefaction potential at Izmit Bay: comparison of predicted and observed soil liquefaction during the Kocaeli earthquake. *Bulletin of Engineering Geology and the Environment*, 67, 1-9.

Chapter 2: A Practical Probabilistic Earthquake Hazard Analysis Tool: Case Study Marmara Region

***Sianko, I.**, Ozdemir, Z., Khoshkholghi, S., Garcia, R., Hajirasouliha, I., Yazgan, U. and Pilakoutas, K., 2020. A practical probabilistic earthquake hazard analysis tool: case study Marmara region. Bulletin of earthquake engineering, 18(6), pp.2523-2555.*

ABSTRACT

Earthquakes have a damaging impact on the economic welfare and resilience of communities, particularly in developing countries. Seismic Hazard Assessment is the first step towards performing prevention, preparedness, and response or recovery actions to reduce seismic risk. This paper presents a computation tool for predicting the seismic hazard at the macro level as a part of a comprehensive multi-hazard framework on Earthquake Risk Assessment (ERA). The Probabilistic Seismic Hazard Analysis (PSHA) procedure is based on the Monte-Carlo (MC) approach, and particular attention is paid to the definition of source zones assigned in the study area. Both Poisson and time dependent (renewal) models are adopted to quantify the effect of temporal dependencies between seismic events, while near-field rupture directivity effects are also taken into account. Marmara region in Turkey is selected as a case study area to perform a new seismic hazard analysis and verify the accuracy of the proposed tool. The results show good agreement with results from the recent SHARE project and the latest Turkish Earthquake Design code hazard maps. This confirms that the proposed PSHA method can be an attractive alternative to the direct integration based methods due to its practicality and powerful handling of uncertainties.

2.1 Introduction

Seismic risk is determined by combining the likelihood of seismic events over a pre-defined timeframe at a specific site or area/region and the consequences of this event on assets in the area. Hence, seismic hazard, vulnerability and value of exposed infrastructure are the main components of earthquake risk assessment (Silva et al., 2015). Whilst the occurrence of earthquakes cannot be predicted accurately, current understanding of global tectonics and seismology allows to make reasonable estimates of seismic hazard in most regions of the world. However, detailed seismic risk estimation for a site/area is still a complex task as it requires huge amounts of data such as seismo-tectonic structure, seismicity, soil conditions, building stock and population of the considered area.

The seismic hazard at a site can be quantified by undertaking deterministic or probabilistic seismic hazard analysis (PSHA) (Erdik, 2017). In the deterministic approach, a particular earthquake scenario, called controlling earthquake, is used to estimate hazard at a site. On the other hand, PSHA can be used to quantify the probability of exceedance of various ground motion levels at a site/region for different return periods of earthquakes. Contrary to the deterministic approach, the probabilistic approach can take into account all potential earthquake sources with the inclusion of uncertainties arising from earthquake size, location and occurrence time.

Conventional PSHA calculations (e.g. Cornell, 1968) are carried out using the total probability theorem, for which the contribution of all possible seismic events along with their associated probability of occurrences are combined. Alternatively, stochastic modelling approaches using Monte-Carlo (MC) simulation method can be used to generate synthetic earthquake catalogues by randomizing key parameters (in a controlled way) obtained from past seismicity, tectonic settings and geological data to represent the future seismic behaviour of a

region. Unlike the conventional probabilistic seismic hazard analysis initially proposed by Cornell (1968), the MC method is more flexible in treating uncertainty as most parameters can be presented as distribution functions.

Due to its advantages, the MC-based PSHA has been utilised in several seismic hazard assessment studies. For example, Musson (1999) proposed a relatively straightforward PSHA procedure based on MC simulations and used hazard analysis results for the Island of Spetses in Greece, to identify the design earthquake representing the most likely combination of distance and magnitude that would produce the calculated hazard ground motion at the site/area of interest. This approach is simpler than the approach proposed by McGuire (1995) for conventional PSHA, where a disaggregation procedure is used to determine the contribution made to the overall hazard by each magnitude-distance bin. In a follow-up study, Musson (2000) performed a sensitivity analysis to check the effect of the number of simulations used in the MC procedure on the hazard curve using the UK as a study area. This study demonstrated that if the number of simulations is sufficiently large, the results of the MC approach come close to the results of the conventional method. More recently, Musson and Winter (2012) proposed a statistical procedure by using MC simulations to reduce errors associated with the subjective decisions used for the definition of areal source zones.

Previous research has confirmed that time-dependent (renewal) models are also easier to apply in the MC approach to predict the probability of exceedance of various ground motion levels for particular return periods in comparison to the direct integration based method (Musson, 2000). Nevertheless, to improve the computational efficiency and practicality of the developed tool in the present paper, an alternative method of converting conditional time-dependent probabilities into effective Poisson probabilities is utilised. Future earthquakes of a certain magnitude occurring periodically on the fault segments can be predicted more accurately using the time-dependent model, given that it is enough data about faults to assume

them characteristic (Cramer et al., 2000; Akinci et al., 2009; Console et al., 2013). On the other hand, the Poisson model which treats all events independent from each other, is a better choice when seismicity and tectonic data are relatively limited.

Pulse-like ground motions can have devastating impact on tall structures with long fundamental periods of vibration (Malhotra, 1999). For areas close to faults, near-fault directivity becomes an important feature to include in a PSHA study. In the work presented by Akkar and Cheng (2015) this effect was included in MC-based PSHA together with the multi-scale random fields (MSRFs) approach. The results of their study indicated that the application of MSRFs to this method can considerably increase the complexity and computational cost of the MC simulations, and therefore, an alternative and simpler approach for considering near-fault directivity effects in MC method is needed. Furthermore, there are limited PSHA studies and hazard assessment frameworks that account for pulse-like ground motions at the regional scale.

There are seismic risk and hazard assessment frameworks available to the public for performing seismic hazard analysis at the regional level. However, the seismic hazard models used in these tools are mainly based on predefined data sets and designed to be applicable only in specific areas. Therefore, these tools cannot be easily adopted to regions/areas where the large amount of required data regarding seismicity, tectonics, and geotechnics of the region are not readily available. On the other hand, GEM (Global Earthquake Model) developed the open-source earthquake risk assessment software OpenQuake (www.globalquakemodel.org), which has greatly improved the earthquake hazard and risk assessment standards (Erdik, 2017). Although the OpenQuake is a very comprehensive software, it still lacks some flexibility in certain areas, such as time-dependent PSHA and consideration of the near-fault directivity. Time-dependent PSHA module in OpenQuake requires manual input from a user regarding sets of fault ruptures and their corresponding probabilities of occurrence over a specified time

span. Whereas, the time-dependent PSHA procedure employed in this paper calculates the annual rates for the desired exposure period automatically using the input information related to the characteristics of fault segments based on Brownian passage-time (BPT) and log-normal models. While only those two models are coded and can be used automatically, the developed PSHA tool is also capable of accepting manual input from the user. The near-fault directivity procedure employed in the OpenQuake software can only utilise the GMPE developed by Chiou and Youngs (2014). Therefore, this will not give flexibility to use other GMPEs for the PSHA calculations for different regions. Whereas, the near-fault directivity procedure developed by Shahi and Baker (2011) is incorporated in the developed tool as it can be applicable to any other conventional GMPE. Even though the only pulse occurrence model developed by Shahi and Baker (2011) is available in the developed computational tool, this model allows for the use of a wide range of GMPEs, and therefore, could be more practical, especially when multiple GMPEs are utilised for analysis (e.g. logic tree).

There are also commercial hazard assessment tools available that are usually expensive and rely on detailed information that is costly to obtain (Bommer et al., 2006), particularly for developing countries. These tools are normally available as "black boxes", and therefore, modifications to incorporate different or uncommon seismic parameters cannot be easily implemented. The assumptions and uncertainties used in these commercial tools cannot always be changed or are not revealed to the user. Therefore, the influence of underlying assumptions on the analysis results is not completely clear to the user (Krinitzsky, 2003; Bommer et al., 2006; Musson and Winter, 2012). These issues highlight a need to develop a flexible and comprehensive earthquake hazard assessment tool.

This study aims to develop a practical yet comprehensive PSHA tool based on MC simulations to perform regional seismic hazard assessment. The developed procedure utilises both Poisson and time-dependent models, as well as near-field directivity. The developed tool

will be incorporated in the Earthquake Risk Assessment (ERA) framework specifically developed for areas, for which generally limited information related to seismic risk parameters exist.

The Marmara region (Turkey), which is capable of producing an earthquake with $M > 7$ in the near future, is chosen as a case study area to validate the developed hazard assessment tool of the framework. For the case study area, catalogue homogenisation, completeness and declustering analyses are performed, while derived background zones are verified via a statistical test developed by Musson and Winter (2012). A set of hazard maps are derived for Marmara using Poisson or time-dependent models, and incorporating the near-field forward rupture directivity effect for higher periods of spectral acceleration (Sa). In addition, the design earthquake for the city centre of Istanbul is identified. Although this work is applied to an area with readily available data, the presented tool can be practical and easily modified to an area with less earthquake-related data available. The main steps of the proposed tool are described in the following sections of the article.

2.2 Catalogue Refinement

Earthquake catalogues are needed in the PSHA method to quantify the seismicity of the area, determine seismic source zones and calculate associated seismic parameters. The first step towards performing PSHA is taken by merging existing historic and instrumental catalogues through i) homogenisation, ii) declustering and iii) completeness analyses.

i) Homogenisation. Different magnitude scales are used to record earthquakes in catalogues. Hence, magnitude conversion equations are required to homogenise earthquakes for PSHA. Equations specifically developed for a region of interest can reduce errors associated with magnitude conversion.

ii) Declustering. There are a number of techniques to decluster earthquake catalogues (e.g. Gardner and Knopoff, 1974; Reasenberg, 1985; Knopoff, 2000; Aldama Bustos, 2009), which in general employ fixed time and space windows to find clustered earthquake events. The method proposed by Knopoff (2000) provides window parameters for events in the magnitude range of M=4.2 to M=6.0. Aldama Bustos (2009) modified the Knopoff (2000) procedure by extrapolating spatial and temporal windows for events with M>6.0 by following the tendency of the time and space windows from Gardner and Knopoff (1974).

iii) Completeness. The earthquake recurrence (Gutenberg-Richter) relationship requires a complete catalogue to define the seismicity of the earthquake source zone. For each magnitude level, the catalogue completeness period may start from a different point in time. For small magnitudes, catalogue completeness starts from recent dates, while for large magnitudes, completeness starts from earlier dates in time. Catalogue completeness periods for different magnitude levels are normally computed following the procedure proposed by Stepp (1972).

2.3 PSHA using MC Simulations

In both conventional and MC-based PSHA studies, two different types of seismic source models can be used to represent seismicity of an area: area source zone model, and area source zone model combined with fault source zone model. In the former, seismicity is homogenised over source zones, where a future earthquake can occur randomly in space. In the latter model, the hazard resulting from active faults with a characteristic magnitude is concentrated in fault source zones (FSZs), while seismic events without identified faults are assumed to occur randomly in areal background source zones (BSZs). In this paper, the latter model is adopted as it more suitable to the study region having well-defined faults.

2.3.1 Background Source Zones (BSZs)

Based on geological, seismological and spatial distribution of earthquakes, the study area is divided into a number of areal BSZs. Earthquakes associated with each BSZ are used to determine the Gutenberg-Richter recurrence parameters (*a* and *b* values). Once source zone geometry and recurrence parameters are defined for each BSZ, then synthetic catalogues (occurrence, magnitude and location of event in a particular year) are produced by following the procedure proposed by Crowley and Bommer (2006):

1) Minimum and maximum magnitudes are assigned to each BSZ. There are different approaches to determine maximum magnitude M_{max}. One subjective approach is to add 0.5 units to the maximum observed magnitude. Other methods include using relations proposed by Wells and Coppersmith (1994), or using the statistical procedure by Kijko (2004). The minimum magnitude M_{min} is usually taken between 4.0 and 5.5, so as to define minimum threshold magnitude level capable of causing damage to structures. It should be noted that, for practical purposes, some damage is experienced if the PGA exceeds 0.05g.

2) The Gutenberg-Richter relationship is rearranged to calculate N_{min} and N_{max}, which represent annual number of earthquakes exceeding M_{min} and M_{max}, respectively:

$$N_{min} = 10^{a-bM_{min}} \tag{2.1}$$

$$N_{max} = 10^{a-bM_{max}} \tag{2.2}$$

3) A random real number, P_{rndB} is sampled from a uniform distribution between 0 and 1 for each year in the catalogue.

4) Probabilities of annual occurrence P_{min} and P_{max} for an earthquake event exceeding M_{min} and M_{max} are obtained as follows:

$$P_{min} = 1 - exp^{-N_{min}} \tag{2.3}$$

$$P_{max} = 1 - exp^{-N_{max}} \tag{2.4}$$

5) The assigned random number P_{rndB} is compared with P_{min} and P_{max} to decide if a seismic event is occurring in that year of synthetic catalogue. If P_{rndB} is less than P_{min} and greater than P_{max} ($P_{min} > P_{rndB} > P_{max}$), then an earthquake event is generated in that year. If this condition is not satisfied, no seismic event occurs in that year.

6) The magnitude of the occurring event is calculated using P_{rndB} by rearranging the terms in the Poisson distribution and recurrence equations:

$$N_{rndB} = -\ln(1 - P_{rndB}) \tag{2.5}$$

$$M = \frac{a - \log(N_{rndB})}{b} \tag{2.6}$$

7) A synthetic event can take place at any location within the boundary of a BSZ. A random location is assigned for an earthquake event within the boundary of an associated BSZ. Fig. 2.1 shows how intensity spreads from an event occurring within BSZs.

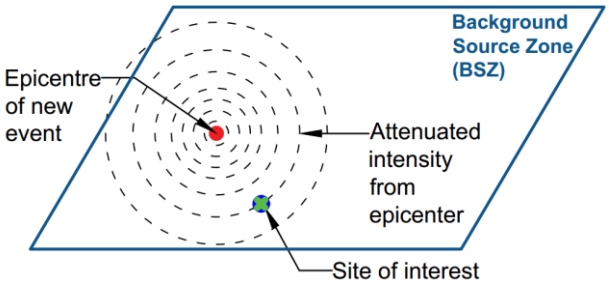

Figure 2.1 Generated random event occurring within BSZs and spreading from epicentre in circles.

8) Steps 1 to 7 are repeated for each year of synthetic catalogue until all years of synthetic catalogue are simulated.

The procedure described above assumes that maximum one earthquake event can be generated per catalogue year in a synthetic catalogue. However, Eqs. (2.3) - (2.4) take into account events occurring more than once in a year. This means that the occurrence of any multiple events is distributed along the whole length of a synthetic catalogue. An analysis was performed to assess the effect of this assumption on the total number of generated events and their magnitude distribution in a synthetic catalogue. The Poisson distribution probabilities of events occurring once, twice, three times and so on in a year were calculated separately to find the number of events and their associated magnitudes. The comparison of the synthetic catalogues generated using both methods showed no significant difference.

2.3.2 Fault Source Zones (FSZs)

The procedure to generate a synthetic catalogue for fault segments is slightly different from that for BSZs. Instead of using the recurrence relationship, the characteristic magnitude and associated annual occurrence rate are used to generate the events, as summarised below:

1) A random number, P_{rndF} is sampled from a uniform distribution between 0 and 1 for each year of the catalogue.

2) The assigned random number is compared with the annual probability of occurrence of characteristic magnitude, P_{char}, on that fault segment to decide if a seismic event is occurring in that year of synthetic catalogue. If P_{rndF} is less than P_{char} ($P_{rndF} < P_{char}$), an earthquake with characteristic magnitude M_{char} is generated in that year, otherwise no seismic event occurs. Empirical relationships proposed by Wells and Coppersmith (1994) and Youngs and Coppersmith (1985) can be used to calculate M_{char} and the associated recurrence intervals, respectively, by using fault geometry and slip rates.

3) For an earthquake event occurring on an active fault, the epicentre of each new event is assumed as random within a segment boundary. In this case, the epicentral fault line (EFL) representing the rupture length is defined parallel to the general direction of the active fault in that segment, as illustrated in Fig. 2.2.

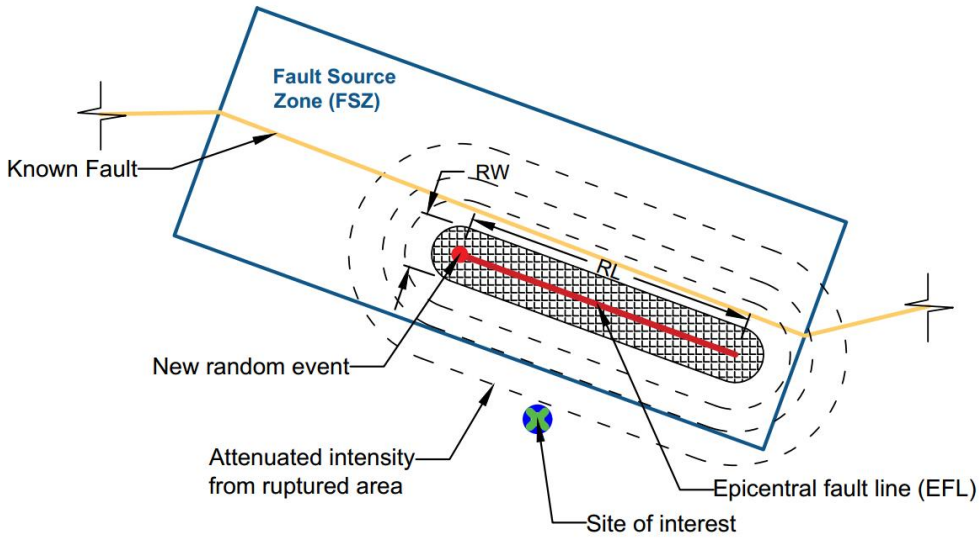

Figure 2.2 Generated random event occurring at fault segment and spreading from obtained fault line.

4) The geometry of the EFL can be estimated using magnitude relationships proposed by Wells and Coppersmith (1994):

$$\log(SRL) = -3.22 + 0.69\,M_w \tag{2.7}$$

$$\log(RLD) = -2.44 + 0.59\,M_w \tag{2.8}$$

$$\log(RW) = -1.01 + 0.32\,M_w \tag{2.9}$$

where *SRL* and *RLD* are the surface and subsurface fault rupture length in kilometres (km), respectively; *RW* is the downdip fault rupture width in kilometres (km); and M_w is the moment magnitude. The rupture length, RL, is assumed to be the maximum value of *SLR* and *RLD*. The fault segmentation model considers that a segmentation boundary exists, but it does not necessarily stop all the ruptures. The length of the rupture is calculated from Wells and

Coppersmith (1994) equation and randomized with a given standard deviation. If the calculated length of the rupture is greater than the length of a segment, it will extend to another segment; hence, multi-segment rapture is considered in a way.

For a BSZ or FSZ, the total number of years of simulated earthquakes is equal to the catalogue length times the number of simulations. However, it should be noted that it is only the total number of simulated years that matters for analysis rather than the catalogue length or number of simulations individually (Musson, 2012). Therefore, a catalogue with sufficient number of simulated years is necessary to capture rare events. In MC-based PSHA calculations, the period length of a synthetic catalogue is usually taken as 50 or 100 years.

2.3.3 Verification of Background Source Zones

Delimitation of BSZs is not always a straightforward process, as expert opinion and subjective judgement influence this process. For example, the areal source model of the Anatolian region proposed by Erdik et al. (1999) is based on tectonic information, whereas the areal source model of Northern Europe used in the GSHAP project (Grunthal and Group, 1999) follow the past seismicity pattern of the region. Moreover, seismic source models for the same study region employed by different researchers can also show variations. For instance, the seismic source zones for the Persian Gulf (also known as Arabian Gulf) defined by Peiris et al. (2006), Musson et al. (2006), Abdalla and Al-Homoud (2004), and Aldama-Bustos et al. (2009) all differ in size and shape.

To avoid subjectivity, an objective method for assessing BSZ is necessary. The methodology described by Musson and Winter (2012) can be used to verify source zone models by assessing them in a statistical manner via the chi-square (X^2) test. In this test, the study area under consideration is divided into equally sized grids and the number of past events from the existing earthquake catalogue is counted for each cell of the grid. If the number of events in

the cell is less than a minimum threshold (determined based on cell size and number of events in the catalogue), then the cell is disregarded in the test. The next step is to assess the validity of the source model by comparing the number of real events that occurred in the past with the events predicted in the synthetic catalogue using the X^2 value:

$$X^2 = \sum_{i=1}^{n} \frac{(O_i - E_i)^2}{E_i} \tag{2.10}$$

where *n* is total number of cells used in the test: O_i is the number of observed (events in the synthetic catalogue) events from MC simulation; and E_i is the number of expected (original catalogue) events obtained from earthquake catalogue in the cell i. The degrees of freedom (DF) are defined as:

$$\mathrm{DF} = \mathrm{n} - 1 \tag{2.11}$$

The X^2 and DF values obtained from Eqs. (2.10) and (2.11) are checked in the X^2 distribution table to find the significance level (or probability of a larger value of X^2) of null hypothesis to be rejected. The source model can be considered to offer a viable depiction of seismicity pattern if the significance level is large enough to not reject the null hypothesis. Conventionally, a significance level of 0.05 is used as a boundary between significant and non-significant results. It should be noted that if the test is applied in a sensible way (e.g. source zones are not under-generalised) it can help to indicate a problem if the zones are too big or are in the wrong place. While Musson and Winter (2012) adopted method does not completely eliminate subjectivity, it can reduce the effects of subjectivity in the delineation of the BSZs.

2.3.4 Ground-Motion Prediction Equations

Ground-motion prediction equations (GMPEs) estimate ground motion intensity (e.g. PGA, PGV or SA values at certain periods) at a site of interest and generally take the following form:

$$\ln(IM) = \overline{\ln(IM)}\,(M, R, \theta) + \sigma(M, R, \theta) \cdot \varepsilon \tag{2.12}$$

where $\ln(IM)$ represents the natural logarithm of a ground motion intensity measure, which is considered to be a normally distributed random variable (Erdik, 2017); $\overline{\ln(IM)}$, σ and ε are the mean, standard deviation (consists of within-event (φ) and between-event (τ) standard deviations (SDs)) and standard normal variable, respectively; M is earthquake magnitude; R is source-site distance; and θ represents the effect of style-of-faulting, soil conditions and similar parameters. The variability in $\ln(IM)$ is achieved by adding the product of σ and ε to the mean value, where ε is a standard normal variable. To include ground motion variability in MC-based PSHA within-event (φ) and between-event (τ) SDs should be considered. For each earthquake generated in the synthetic catalogue, a random number sampled from the standard normal probability distribution is multiplied by within-event (φ) SD. Another draw from the standard normal probability distribution for each site of interest is multiplied by between-event (τ) SD. Obtained values are added to the $\ln(IM)$ to find estimated ground motion value at each site of interest.

Different alternatives exist to calculate the value of *R*. Fig. 2.3 shows the different distance metrics used in ground motion prediction equations (GMPEs) available in the literature. These include distance to hypocentre, R_{hyp}; the shortest distance from a site to the fault rupture, R_{rup}; distance to epicentre, R_{epi}; and the shortest horizontal distance to the point on the surface projection of the fault rupture ('Joyner-Boore distance') R_{JB} (Joyner and Boore, 1981).

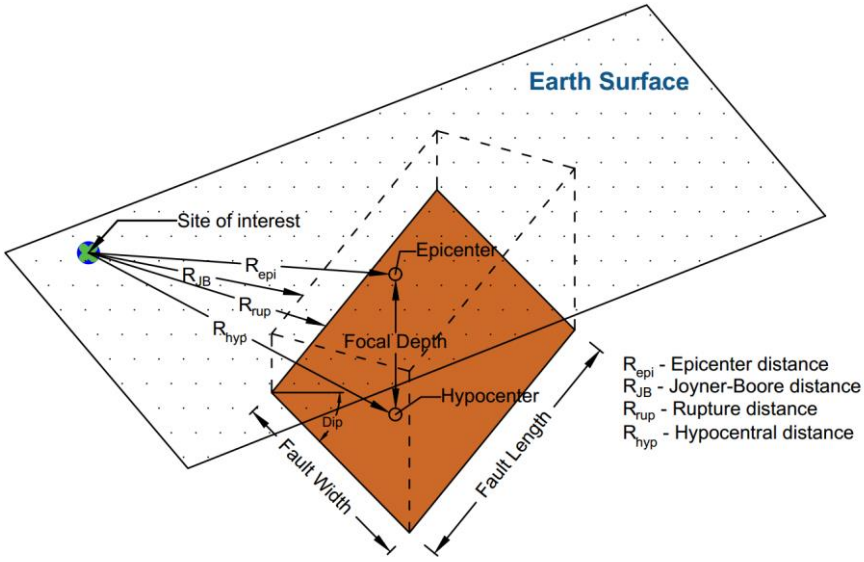

Figure 2.3 Fault geometry and projection on to the surface with distance metrics used in GMPEs.

If the selected GMPEs were a function of R_{hyp} and R_{rup}, integration over depth would be required in the conventional PSHA method (Bommer and Scherbaum, 2008). However, in the MC-based PSHA method, there is an easy and practical way to include depth related uncertainty into hazard calculations, as depth can be entered as a distribution function during the generation of synthetic catalogues (Musson, 2000).

2.3.5 Hazard Calculation for the Desired Probability of Exceedance Level

Once synthetic catalogues for both BSZs and FSZs are generated, the probability of exceedance of ground shaking intensities (PGA, PGV or Sa) can be calculated at a site of interest. For each year of a synthetic catalogue, all earthquakes occurring in that year across all source zones are used to identify the largest ground shaking intensity at the site. In other words, the worst-case scenario from all seismic sources affecting the site of interest is stored as an annual maximum outcome. This step is repeated for all simulations. The results of each simulation are combined into a single list. The probability of exceedance of ground shaking intensities can be found by sorting annual outcomes in descending order and by selecting the

N^{th} value in the sorted list. For the desired probability of exceedance (PoE), N can be calculated using the following equation:

$$N = (\frac{1}{PoE} \times \text{Catalogue length} \times \text{Number of simulations}) + 1 \quad (2.13)$$

The flowchart for predicting seismic hazard at a site of interest using MC PSHA method is shown in Fig. 2.4.

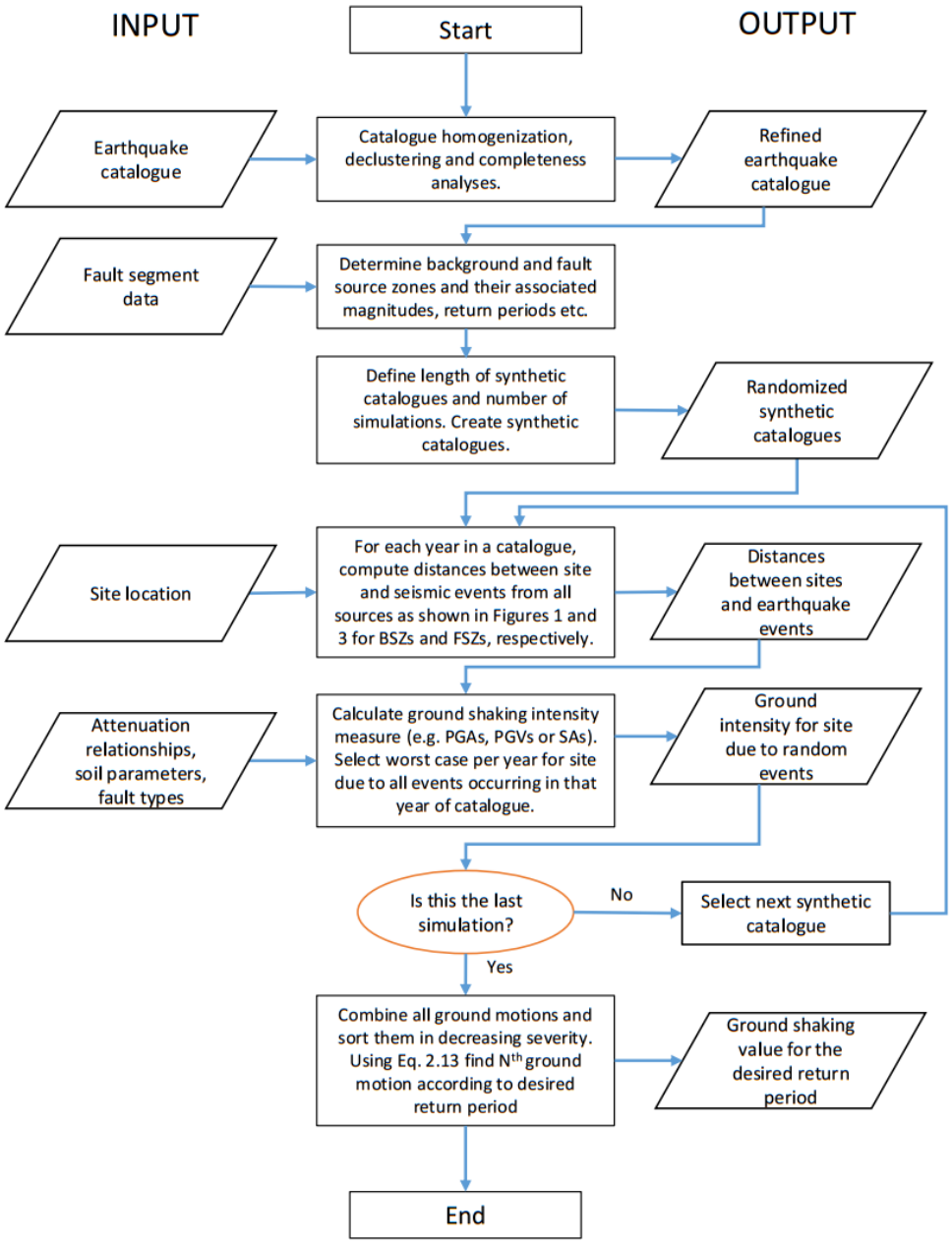

Figure 2.4 Procedure for predicting seismic hazard at a site of interest using MC-based PSHA.

2.3.6 Near-Fault Directivity

Pulselike ground motions caused by near-fault forward directivity effects can have devastating consequences on structures located nearby the ruptured fault. If the rupture propagation direction and the slip direction on the fault are all aligned with the site of interest, and if the speed of the rupture propagation is similar to that of the shear wave velocity, forward rupture directivity effects can lead to the development of a single pulse of large amplitude (Archuleta and Hartzell, 1981; Somerville et al. 1997; Somerville, 2003; Akkar et al., 2018). It should be noted that traditional GMPEs are based on data coming from both pulselike and non-pulselike ground shaking records. Hence, they are expected to underestimate spectral acceleration for pulselike motions (Shahi and Baker, 2011).

Several approaches were developed to take into account forward directivity effects on spectral acceleration values (e.g. Somerville, 2003; Shahi and Baker, 2011; Spudich et al., 2013). In this work, the probabilistic approach developed by Shahi and Baker (2011) is chosen for implementation, due to its effectiveness as verified through comparison with other method by Akkar et al., (2018) and its relative ease of application within MC-based PSHA method. In this approach, the probability of observing a pulse at α, $P(\alpha)$, is calculated in accordance with Eqs. (2.14) - (2.16) using the product of a probability derived from site-to-source geometry, and the probability of observing the pulse in the orientation of interest:

$$P(\alpha) = P(\alpha|\text{pulse}) \times P(\text{pulse}|r, s) \tag{2.14}$$

$$P(\alpha|\text{pulse}) = \min[0.67; 0.67 - 0.0041(77.5 - \alpha)] \tag{2.15}$$

$$P(\text{pulse}|r, s) = \frac{1}{1 + e^{(0.642 + 0.167r - 0.075s)}} \tag{2.16}$$

where α is orientation of interest measured in degrees, and *r* and *s* are site-to-source geometric parameters measured in km, as schematically shown in Fig. 2.5. It is important to note that Eq. (2.16) is valid for strike-slip faults only.

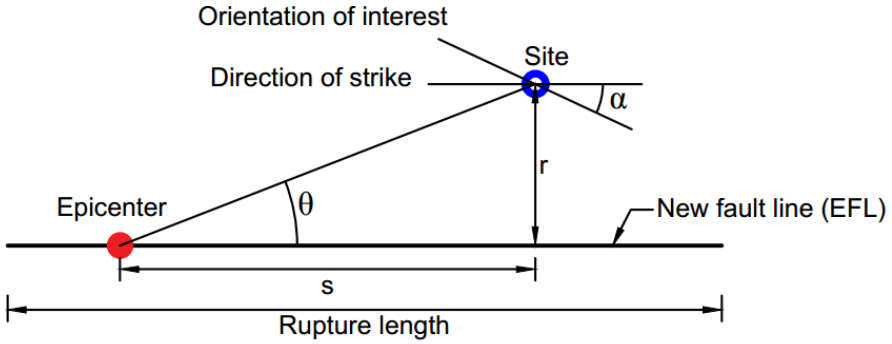

Figure 2.5 Plan view explaining the parameters needed to fit in Eq. 16 for strike-slip faults.

The directivity effect is experienced mostly in the fault-normal component of the ground motion, and therefore, the highest probability of observing pulse is when the orientation of interest is perpendicular to the strike (α=90°) and the lowest when the orientation is parallel to the strike (α=0).

Once $P(\alpha)$ is calculated, occurrence of pulselike ground motion at the site of interest needs to be determined. For each year of a synthetic catalogue with an earthquake occurrence, a random number between 0 and 1 from a uniform distribution is generated. If the random number is less than $P(\alpha)$ obtained from Eq. (2.16), a pulselike event occurs in that year, else it does not. For events that are producing pulselike ground motions, the mean period of the pulse $\mu_{\ln T_p}$ and its standard deviation $\sigma_{\ln T_p}$ are calculated as:

$$\mu_{\ln T_p} = -5.73 + 0.99M \tag{2.17}$$

$$\sigma_{\ln T_p} = 0.56 \tag{2.18}$$

where T_p is the period of the pulse; and M is the earthquake magnitude.

Amplification and de-amplification factors to modify GMPEs to account for pulselike and non-pulselike behaviour are given in Shahi and Baker (2011), as well as equations of observing pulse in case of strike-normal type of faulting.

2.3.7 Time-Dependent (Renewal) Analysis

The Poisson model is generally applicable to low seismicity regions or regions without major faults, as it considers earthquakes as independent events in time. Paleoseismic studies and historical seismicity observations have shown that earthquakes with similar characteristic magnitudes (same size) and similar time intervals between events tend to occur on known fault segments (Schwartz and Coppersmith, 1984). It is also suggested, that for the faults with an adequate information on return period of M_{char}, a time-dependent model may be better at estimation of the short-term hazard assessment than a Poisson model (Akinci et al., 2009). In the renewal model, if the time interval that passed from the previous event is known for a fault segment, the conditional probability of a future characteristic event rupturing in that segment in the next ΔT years , $P_{cond}(T, \Delta T)$, can be calculated as follows:

$$P_{cond}(T, \Delta T) = \frac{\int_{T}^{T+\Delta T} f(t)dt}{\int_{T}^{\infty} f(t)dt} \tag{2.19}$$

where $f(t)$ is the probability density function (PDF) for earthquake recurrence time interval; T is the time passed since the last characteristic event occurred on the fault segment; and ΔT is the exposure period, taken as 50 years for typical buildings. $P_{cond}(T, \Delta T)$ is conditional, as it changes with time elapsed since the last earthquake. $f(t)$ can be represented with Gaussian, log-normal, Weibull, Gamma and Brownian Passage Time (BPT) models. Among these, the BPT model (which is similar to the log-normal distribution) is deemed to represent adequately the earthquake distribution (Ellsworth WL et al., 1999). The PDF for the BPT distribution can be calculated as:

$$PDF(t,\mu,\alpha_p) = \left(\frac{\mu}{2\pi\alpha_p{}^2 t^3}\right)^{\frac{1}{2}} \exp\left(-\frac{(t-\mu)^2}{2\alpha_p{}^2\mu t}\right)^{\frac{1}{2}} \quad (2.20)$$

where μ is mean return period; and α_p is the aperiodicity (an equivalent to the coefficient of variation). Small values of α_p mean that the characteristic earthquakes are highly periodical. As α_p increases the conditional probability of the future characteristic event, $P_{cond}(T,\Delta T)$, it becomes similar to Poisson probabilities (Erdik et al., 2004). Many studies suggested a standard value of 0.5 for α_p (Cramer et al., 2000 and Erdik et al., 2004). Fig. 2.6a-b show the PDF and $P_{cond}(T,\Delta T)$ for BPT model for a mean return period of μ=300 years and exposure period of ΔT=50 years. Fig. 2.6 show that the conditional probability of having a new event in the next 50 years, $P_{cond}(T,50)$, does not significantly increase after an approximate elapsed time of 400 years since the last event.

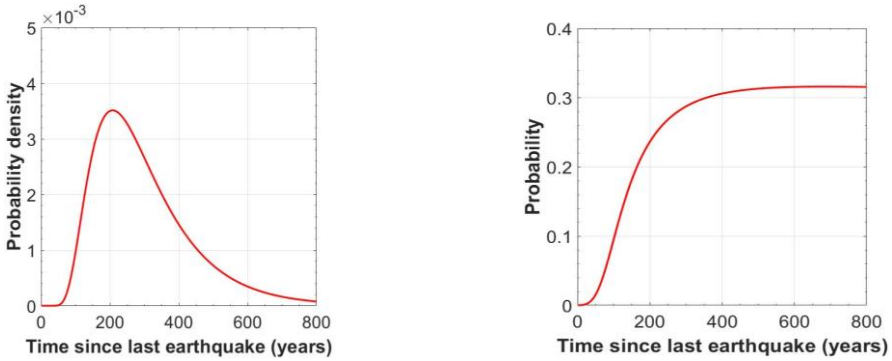

a) b)

Figure 2.6 (a) PDF and (b) conditional probability for BPT distribution with a mean return period of 300 years and α=0.5.

Once conditional probabilities for a specific exposure period are calculated from Eq. (2.19), they can be converted to the effective Poisson annual probabilities, R_{eff} using the following equation (WGCEP94, 1995):

$$R_{eff} = -\ln(1 - P_{cond}(T,\Delta T))/\Delta T \quad (2.21)$$

2.3.8 Uncertainty in PSHA

There are two types of uncertainties that exist in earthquake hazard analysis: aleatory and epistemic uncertainties. Aleatory uncertainty represents the natural randomness in a process, while epistemic uncertainty is the lack of knowledge introduced in a model that tries to represent an actual behaviour. The aleatory variability arises from the randomness of the earthquake generation process, and is usually taken into account with a probability distribution. Epistemic uncertainty on the other hand arises from the lack of knowledge about the true single value of a variable. Parameters that define a probability density function (e.g. mean and standard deviation of a normal distribution) have in fact one true value, which we don't know.

In PSHA analysis, the standard deviation of GMPEs can be used to deal with aleatory uncertainty. Epistemic uncertainty can be addressed with a logic tree, in which weights are applied to the branches to reflect confidence in given options (Bommer et al., 2005; Scherbaum et al., 2005). Fig. 2.7 shows an example of a logic tree that utilises several GMPEs.

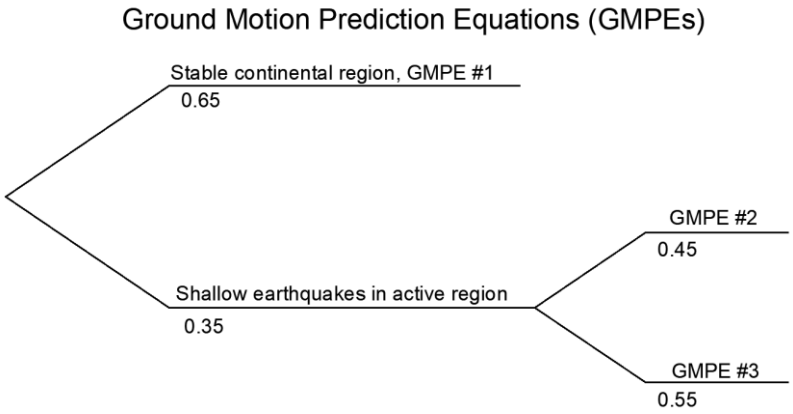

Figure 2.7 An example of the logic tree for ground motion prediction equations.

It should be noted that logic trees can be used to include different hypotheses in PSHA. For example, they are often used for altering recurrence rates of faults, geometry of seismic source zones, and characteristic magnitudes. The use of a MC-based approach in PSHA can reduce

the number of parameters employed in the logic trees because many of the mentioned parameters are already randomized during the synthetic catalogue generation process.

The previous sections provided an overview of the components of the utilised MC-based PSHA. To demonstrate the method, the following section uses a case study region to verify the effectiveness of the developed computational tool.

2.4 The Case Study: Marmara Region, Turkey

To demonstrate the developed PSHA tool, Marmara region (Turkey) is selected as a case study area. This region is located in one of the most seismically active zones in the world. It houses one-third of Turkey's population and is a major industrial hub for the country. Both 1999 Kocaeli and Duzce earthquakes occurred in this region and caused enormous economic losses, extensive structural damage to structures and a high fatality rate. An event of similar magnitude to these earthquakes is expected to hit Istanbul in the near future. For example, Murru et al. (2016) predict the probability of having an earthquake with M≥7.0 in Istanbul to be at around 50% in the next 30 years. This earthquake is expected to be more severe and damaging compared to those of Kocaeli and Duzce as Istanbul is very densely populated and a large proportion of structures are substandard (Bal et al. 2008).

2.4.1 Tectonic Setting of Marmara Region

The North Anatolian Fault (NAF) lies across northern Turkey (see NAFZ in Fig. 2.8) for more than 1,500 km starting from Karliova in the east and extending to the Gulf of Saros in the west. The NAF is a right-lateral strike-slip transform fault system, along which the Anatolian plate is pushed westwards by the collision between the Arabian and Eurasian plates. The western portion of the NAF zone dominates the tectonic regime of the Marmara Sea area: the NAF zone continues as a single fault line east of 31.5°E, whereas to the west it splays into a complex fault system that has created multiple strong seismic events over the last century (see

Fig. 2.9). Three main branches can be identified including the northern NAF (NNAF), central NAF (CNAF) and southern NAF (SNAF) branches. The NNAF is the most active branch with slip rates of 14-24 mm/year, while CNAF and SNAF branches move only 2-8 mm/year (Murru et al. 2016). The NNAF branch enters the eastern part of the Marmara Sea at the Gulf of Izmit, then bends to the north shelf of the sea, and eventually joins NE-SW striking the Ganos fault onshore. Here, the branch extends until entering the Aegean Sea through the Gulf of Saros (Kurt et al., 2000; McNeill et al., 2004). Unlike NNAF, the CNAF and SNAF branches span to the south of the Marmara Sea. CNAF goes underwater through the Marmara Sea by entering at Gemlik Bay and emerging on land briefly. At 27.8°E, the CNAF branch turns toward south-west to join the faults in the North Aegean region.

The high-resolution bathymetric survey in the Marmara Sea provided indication of a continuous strike-slip faulting system going through the northern part of the Marmara Sea. It also provided a better understanding of the behaviour of the faults with seismic gap and linked the 1999 Kocaeli earthquake fault with the 1912 Sarkoy-Murefte earthquake fault (Erdik et al., 2004).

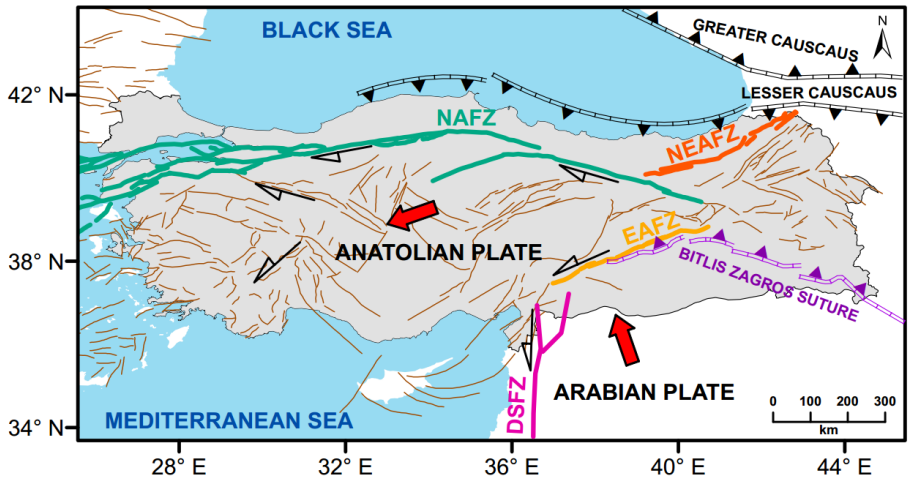

Figure 2.8 Tectonic setting of Turkey. EAFZ – East Anatolian Fault Zone, NAFZ – North Anatolian Fault Zone, NEAFZ – North East Anatolian Fault Zone, DSFZ – Dead Sea Fault Zone (Faults data is taken from http://www.efehr.org).

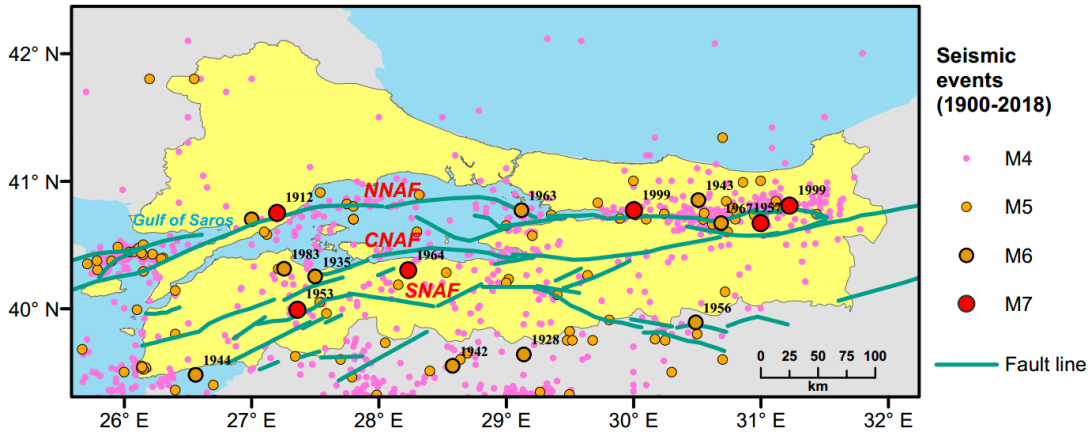

Figure 2.9 Faults system in Marmara region with epicentral location of major earthquakes occurred in 20th century (Faults data is taken from http://www.efehr.org)

2.4.2 Seismicity of the Marmara Region

As the capital of both Byzantine and Ottoman empires, Istanbul has been populated for millennia and therefore there is evidence of historical seismicity. Furthermore, the effect of past earthquakes can be tracked by observing damage and repairs on historical structures, which can serve as an indicator of previous seismic events. During the 20th century, Marmara has experienced relatively high seismicity with several M >7.0 earthquakes occurring on the NAF. Table 2.1 summarises the magnitudes and dates of major historical events of $M_s \geq 7$ since 1500 CE. The table shows a recent series of strong earthquakes, which ruptured along the NAF, starting further east with the M_w =7.8 Erzincan earthquake (1939) and propagating towards the west into the Marmara region. The Kocaeli (1999) and Duzce (1999) earthquakes were the last events associated with the westward propagation at the NAF (Alpar and Yaltirak, 2002).

It is well-established that there is a potential seismic gap in the region of the Marmara Sea to the south of Istanbul (Bohnhoff et al., 2013). The fault in this area has not ruptured for at least 200 years, although there is evidence of large historical events taking place around this seismic gap (e.g. the 1766 Istanbul earthquake). The length of the gap is around 150 km and it has a potential of generating an earthquake with M >7.0 similar to previous earthquakes at this

location (Hubert-Ferrari et al., 2000). An earthquake of that magnitude and proximity to Istanbul would have devastating consequences and, therefore, it is crucial to understand the potential hazard associated with this seismic gap to develop appropriate seismic mitigation and prevention strategies.

Table 2.1 List of $M_s \geq 7$ earthquakes in Marmara Region from 1500 CE to present (adapted from Ambraseys and Jackson (2000) and Erdik et al. (2004)).

M_s	Date	Name
7.2	10.09.1509	Istanbul earthquake
7.2	10.05.1556	Near Bandirma
7.4	25.05.1719	Izmit earthquake
7.0	06.03.1737	Near Biga
7.1	22.05.1766	Istanbul earthquake
7.4	05.08.1766	Ganos earthquake
7.1	28.02.1855	Bursa earthquake
7.3	10.07.1894	Istanbul earthquake
7.3	09.08.1912	Murefte earthquake
7.3	01.02.1944	Bolu–Gerede earthquake
7.1	18.03.1953	Yenice-Gonen earthquake
7.2	26.05.1957	Abant earthquake
7.4	17.08.1999	Kocaeli earthquake
7.2	12.11.1999	Duzce earthquake

2.4.3 Homogenisation, Clustering and Completeness of the Earthquake Catalogue

In this study, the instrumental earthquake catalogue developed by Turkey's Disaster and Emergency Management Presidency (AFAD) (https://deprem.afad.gov.tr/) is utilised for the case study area. This catalogue consists of seismic events with $M \geq 4$ that occurred between

1900 and 2018 in the Marmara region. Most of the earthquake data are reported in terms of surface-wave magnitude scale, M_s, for the first half of 20th century, while more magnitude scales are used for more recent events. Historical events that occurred in the region are included in the catalogue using data from Ambraseys and Jackson (2000). A catalogue homogenisation was necessary to convert M_s, M_L and m_b magnitude scales into moment magnitude, M_w, and this was done using conversion equations specifically developed for Turkey by Kadirioğlu and Kartal (2016).

After homogenisation, the data need to be declustered for the removal of dependent events (fore- and after-shocks). Table 2.2 lists the number of mainshocks and dependent events according to each method in the refined earthquake catalogue. It can be seen from this table that Gardner and Knopoff (1974) approach removes 50.88% of events in catalogue due to the fact that the time and space windows are larger compared to those obtained with the modified Knopoff (2000) method. Consequently, the former method leads to smaller earthquake occurrence rates. Therefore, this work uses the modified Knopoff (2000) method for subsequent analysis to stay on the conservative side.

Table 2.2 Summary of dependent events removed for final catalogue using different algorithms.

Algorithm	**Mainshocks**	**Removed events**	**Percentage of events removed**	**Total energy of events removed**	**Clusters**	**Total events in catalogue**
Gardner and Knopoff (1974)	417	432	50.88%	1.64%	110	849
Modified Knopoff (2000)	524	325	38.28%	1.41%	91	849

After homogenization and declustering, the number of event below M_w<4.1 was found to be considerably low. Therefore, for the catalogue obtained for the study area the minimum completeness magnitude was set to M_w=4.1. Fig. 2.10a-d shows the results of completeness analysis performed for the case study area following procedure described by Aldama Bustos (2009). In this figure, black dashed vertical lines show the start of the completeness period, and red horizontal lines show the estimated mean occurrence rate for the completeness period.

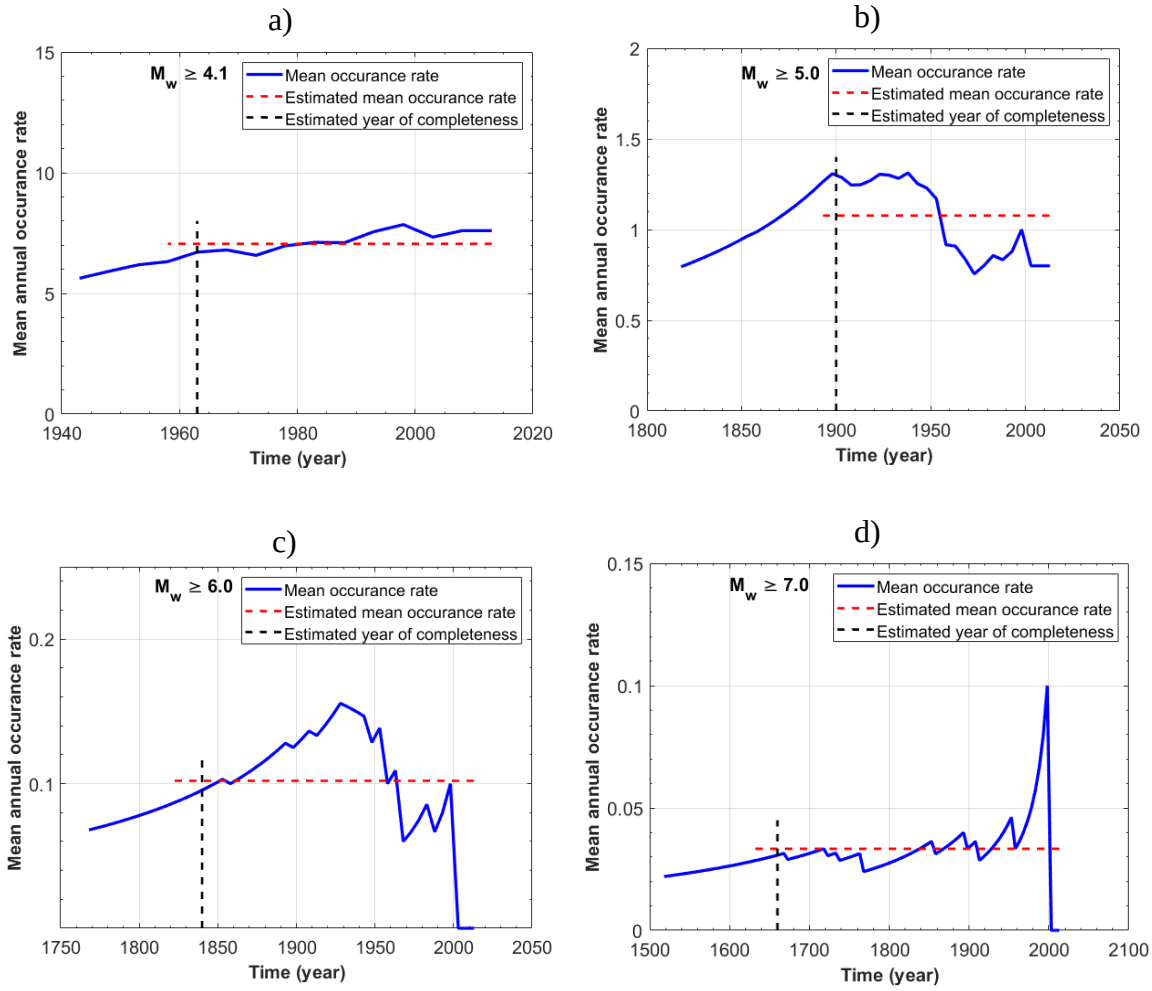

Figure 2.10 Instrumental earthquake catalogue completeness analysis showing mean annual occurrence rate of events for (a) Mw ≥ 4.2, (b) Mw ≥ 5.0, (c) Mw ≥ 6.0, and (d) Mw ≥ 7.0

The results in Fig. 2.10a-d indicate that the declustered catalogue may be regarded as being complete above M_w=4.1 from 1963 onwards, M_w=5.0 from 1900 onwards, M_w=6.0 from 1840

and M_w=7.0 from 1660. Levels of completeness are adopted for other magnitudes and periods following the chosen algorithm.

It should be noted that catalogue homogenization, completeness analysis and declustering presented are incorporated into the code and automated. Nevertheless, user intervention and judgement are always required for a rigorous treatment of the catalogue issues such as determination of completeness date.

2.4.4 Source Zones

The seismicity of the Marmara region is represented with the fault segmentation and background seismicity model. Table 2.3 provides information on the seismicity parameters for each of the BSZs used in this study (such as *a* and *b* parameters of the Gutenberg–Richter relationship, and the minimum and maximum earthquake magnitudes, M_{min} and M_{max}, associated with each source zone). M_{max} is based on the maximum observed magnitude in the source zone from historical data. BSZs are delineated by the user, but by utilising X^2 test validation zones are altered until satisfactory result is obtained. Fig. 2.11 shows the derived BSZs for the Marmara region. A source zone number is assigned to each BSZ, as shown in the figure. The maximum likelihood estimation procedure developed by Weichert (1980) is integrated into the code to estimate the *b* parameter of the Gutenberg-Richter relationship by accounting for different years of completeness period for each magnitude range. The location of synthetic earthquakes within BSZs and FSZs are randomized with a uniform distribution to treat aleatory uncertainty. Also, the code developed allows the user to treat earthquakes in BSZs as points or ruptures. For the case study example, earthquakes occurring within BSZs are assumed as point sources for a computational efficiency. In general, this does not make a big difference, except for a few zones where the M_{max} is high.

The validity of the source model is verified via the X^2 test, as explained in Section 2.3. Fig. 2.12a shows the locations of the instrumental historical earthquake events in the Marmara region, whereas Fig. 2.12b illustrates the earthquake locations from one of the synthetic catalogues. By counting and comparing the cell counts in each BSZ from instrumental and synthetic catalogues, X^2 values are calculated using Eq. 2.10. Cells with less than 15 events are excluded from the analysis (e.g. brown coloured cell in Fig. 2.12a). The process is repeated for each of the 1,000 simulated catalogues and the X^2 statistic is calculated to be 5.24, thus proving the hypothesis that there was no significant difference between the synthetic catalogue and the recorded events.

Table 2.3 Seismicity parameters for BSZs used in this study.

BSZ #	M_{min}	M_{max}	a	b	σ(b)
1	4.0	5.5	2.20	0.69	0.13
2	4.0	5.6	1.96	0.62	0.11
3	4.0	6.0	3.33	0.83	0.08
4	4.0	6.8	3.57	0.86	0.08
5	4.0	6.7	2.88	0.80	0.10
6	4.0	6.9	2.27	0.62	0.08
7	4.0	5.6	2.95	0.90	0.16
8	4.0	5.6	2.98	0.89	0.15
9	4.0	6.6	2.13	0.66	0.11
10	4.0	6.9	3.22	0.87	0.10
11	4.0	6.6	2.58	0.82	0.15
12	4.0	5.9	3.68	1.00	0.13
13	4.0	6.6	2.69	0.88	0.19
14	4.0	6.7	2.60	0.90	0.24
15	4.0	5.5	3.79	0.98	0.11
16	4.0	6.2	2.26	0.72	0.13
17	4.0	6.1	3.01	0.81	0.10

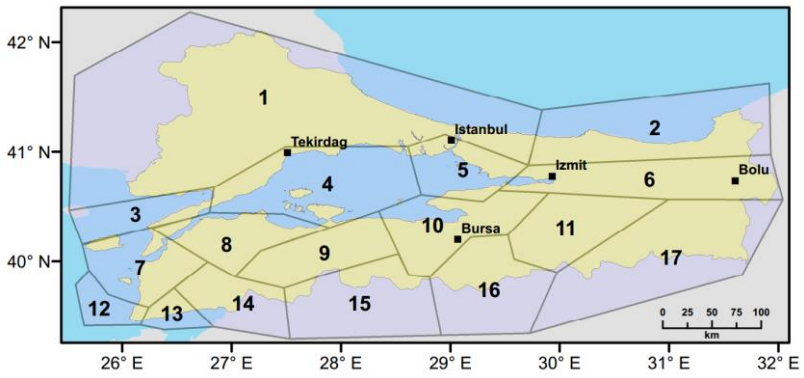

Figure 2.11 Background source model used in the PSHA presented in this study. Zone numbers and corresponding parameters are listed in Table 2.3.

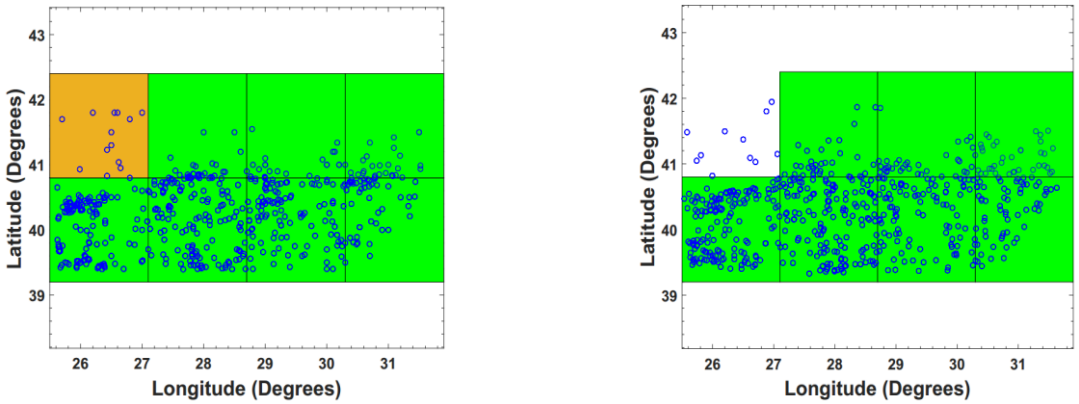

(a) (b)

Figure 2.12 Distribution of (a) historical events and (b) events in one of the simulated catalogues occurred in the Marmara region.

Aggregate testing (Musson and Winter, 2012) can be utilised to compare activity rates obtained from original and synthetic catalogues for each BSZ. Mean magnitude and total number of events are then calculated for each synthetic catalogue generated in the MC process. The data obtained from all synthetic catalogues are then grouped into magnitude-total number of seismic event bins. The number of catalogues coinciding to each mean magnitude and number of event ranges result in a surface plot, where the peak value shows the most repeating value for the number of event vs mean magnitude. The pair of mean magnitude and number of events calculated from the original catalogue provides a point for a comparison with this distribution. If the point is relatively close to the peak of distribution, the model can be

considered to adequately represent the activity rate of the background zone. As an example, Fig. 2.13 shows the result of analysis for one of the BSZ (# 3) showing 100 years' seismicity. One can see from this figure that the synthetic catalogues result in a modal value of 63 events and mean magnitude of 4.63, whereas historical outcome produces 63 events with a mean magnitude of 4.53. Relatively close values imply that the activity rates assigned to the considered BSZ are consistent with the past earthquake data.

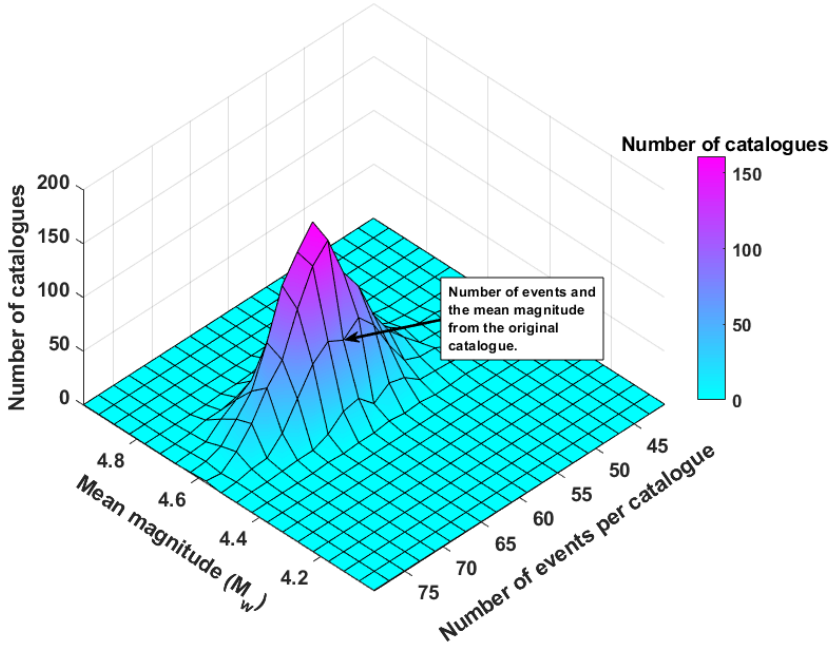

Figure 2.13 Frequency plot showing 100 years' seismicity generated for one of a BSZs produces by the model. The arrow indicates the point of values obtained from original catalogue in that BSZ.

The segmentation model proposed by Erdik et al. (2004) (see Fig. 2.14), which assumes that the total accumulated energy along well-defined fault segments of the region is released through characteristic earthquakes is adopted for this region. The developed code is capable of calculating return period from slip rates and M_{char} for each fault segment if available, which are computed through empirical relations (Wells and Coppersmith, 1994), but for the case study area M_{char} values and Poissonian rates were adopted from Erdik et al. (2004) with a manual input. The main parameters associated with the faults segments are shown in Table 2.4. The table also lists calculated annual rates of time-dependent method described in the Section 3.7.

Table 2.4 Poisson and time-dependent annual rates for the fault segmentation model adopted from Erdik et al. (2004).

Segment number	Char. Magnitude (M_w)	Mean recurrence time (years)	Time since last earthquake (years)	Poisson annual rate	Time-dependent annual rate
1	7.2	140	19	0.0071	0.0021
2	7.2	140	19	0.0071	0.0021
3	7.2	140	19	0.0071	0.0021
4	7.2	140	19	0.0071	0.0021
5	7.2	175	127	0.0057	0.0103
6	7.2	210	267	0.0048	0.0104
7	7.2	250	255	0.0040	0.0082
8	7.2	250	255	0.0040	0.0082
9	7.2	200	465	0.0050	0.0114
10	7.2	200	1,000	0.0050	0.0110
11	7.5	150	109	0.0067	0.0122
12	7.2	250	54	0.0040	0.0010
13	7.2	600	1,000	0.0017	0.0037
14	7.2	600	1,000	0.0017	0.0037
15	7.2	1000	1,000	0.0010	0.0020
19	7.5	250	77	0.0040	0.0023
21	7.2	250	19	0.0040	0.0001
22	7.2	250	64	0.0040	0.0015
25	7.5	1,000	1,000	0.0010	0.0020
40	7.2	1,000	166	0.0010	0.0000
41	7.2	1,000	1,000	0.0010	0.0020
42	7.2	1,000	1,000	0.0010	0.0020
43	7.2	1,000	284	0.0010	0.0002
44	7.2	1,000	1,000	0.0010	0.0020
45	7.2	1,000	68	0.0010	0.0000

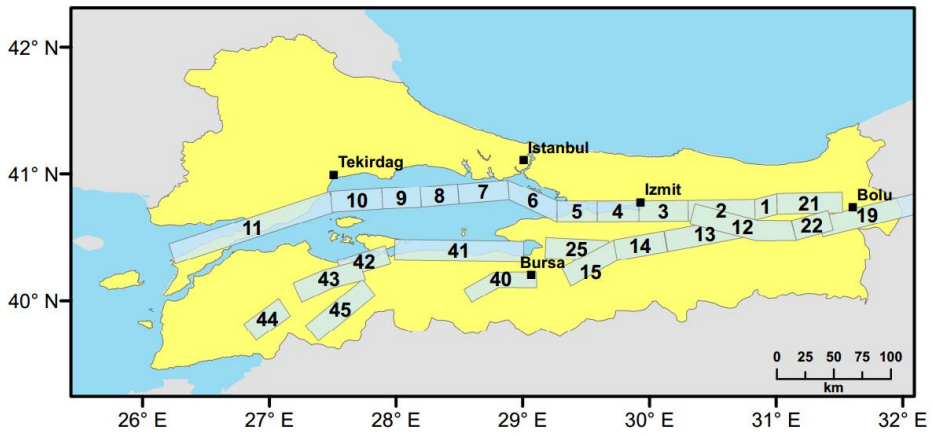

Figure 2.14 The fault segmentation model proposed by Erdik et al. (2004) for the Marmara.

To take into account aleatory uncertainty, the mean of the M_{char} value is randomized with a uniform distribution by sampling value between -0.25 and 0.25 and adding it to the mean of the M_{char}.

2.4.5 Ground Motion Prediction Equations (GMPEs) used for the study area

In this study, the GMPEs proposed by Akkar et al. (2014) and Boore et al. (2014) are employed to calculate the earthquake hazard in terms of PGA and SAs. To treat epistemic uncertainty, a logic tree is used, allocating weights of 0.7 and 0.3 to each branch for the GMPEs of Akkar et al. (2014) and Boore et al. (2014), respectively. Higher weight is given to Akkar et al. (2014) equation because such model contains a large proportion of recordings from Turkey. Moreover, in this GMPE, the majority of recordings for strike-slip mechanism events with M>7 are taken from earthquakes which occurred in the Marmara region. The GMPE proposed by Boore et al. (2014) is one of the few GMPEs that satisfy the requirements for use in PSHA specified by Bommer et al. (2010). In this GMPE, inter-event and intra-event variabilities are calculated for different magnitude ranges based on period, distance or soil conditions. It also employs a correction factor for various seismic active regions around the world including Turkey.

2.5 Results and Conclusions

The procedures presented in this paper are implemented for the region using a Matlab code. Hazard maps considering these models for PGA and SA at T=0.2 sec and T=1.0 sec for a Probability of Exceedance (POE) of 10% (i.e. a return period of 475 years) and 2% in 50 years (return periods of 2475 years) are generated for the region. Design earthquakes are also derived for a specific location in the Marmara region.

2.5.1 Hazard Maps

Figs. 2.15 and 2.16 show PGA hazard maps derived using Poisson and time-dependent models, respectively. Both maps are for a return period of 475 years. It is shown that there is a noticeable difference between the PGA values obtained using the Poisson and time-dependent models, even though nearly two decades have passed since the 1999 Kocaeli earthquake. The annual rates calculated for the time-dependent model for the fault segments (1 to 4 from Table 2.4) relatively close to Izmit area are about a third of those used in the Poisson model. As a result of this, lower hazard levels are obtained in the time-dependent model for the eastern part of the Marmara region. On the other hand, hazard levels are slightly higher in the western part of the Marmara region, due to the fact that no fault ruptures occurred since the 18^{th} century. Both models predict PGA levels between 0.30g and 0.45g for a 475 year return period for Istanbul's metropolitan area, which creates a high risk for this densely populated city. The hazard level for Istanbul area is considerably higher in the time-dependent model than that obtained using the Poisson model. This is because some unruptured NAF segments (seismic gap) in the Marmara Sea have a higher probability of generating characteristic events with M>7. In both figures, the highest PGAs are predicted in the southern part of Istanbul, where the Bosporus meets with the Marmara Sea. The expected seismic hazard gradually reduces towards the north of the city. Predicted hazard levels for PGA corresponding to a return period

of 2475 years are given in Figs. 2.17 and 2.18 using the Poisson and time-dependent models, respectively. It can be seen that the maximum PGA levels for rock conditions using the Poisson and time-dependent models are as high as 0.80g for 475 years return period and 1.36g for 2475 years return period across the case study area.

Hazard maps for SA at T=0.2 sec with return periods of 475 and 2475years for the Poisson model are compared in Figs. 2.19 and 2.20, respectively. The maximum values of SA at T=0.2 sec is found to be as high as 1.67g and 2.61g for 475 and 2475 years of return periods, respectively. Figs. 2.21 and 2.22 show the hazard maps for SA at T=1.0 sec with return periods of 475 and 2475 years, respectively, calculated using the Poisson model. In this case, the maximum values of SA at T=1.0 sec are found to be as high as 0.50g and 0.92g for 475 and 2475 years of return periods, respectively.

Seismic hazard maps with and without consideration of near-field effect are also compared in Figs. 2.23 and 2.24, respectively, for T=2.0 sec and POE 2% in 50 years. It is found that near-field directivity increases SA values around active faults (e.g. Izmit area) by approximately SA of 10-20%.

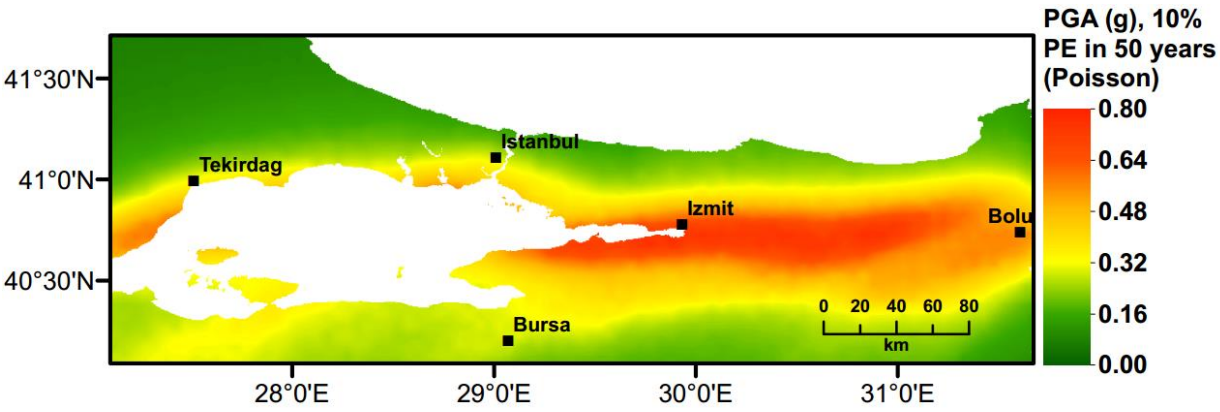

Figure 2.15 Seismic hazard map of Marmara region for PGA (g) considering 10% probability of exceedance in 50 years (the Poisson model).

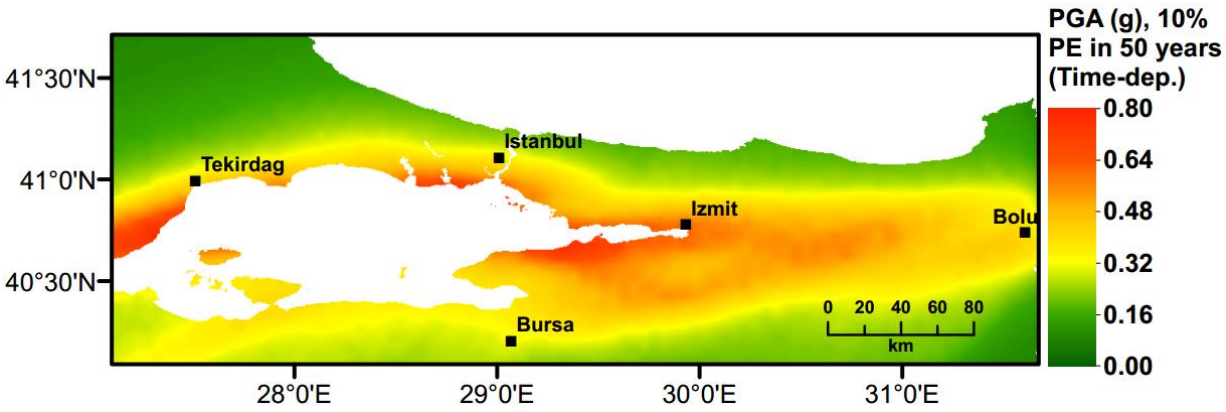

Figure 2.16 Seismic hazard map of Marmara region for PGA (g) considering 10% probability of exceedance in 50 years (Time-dependent model).

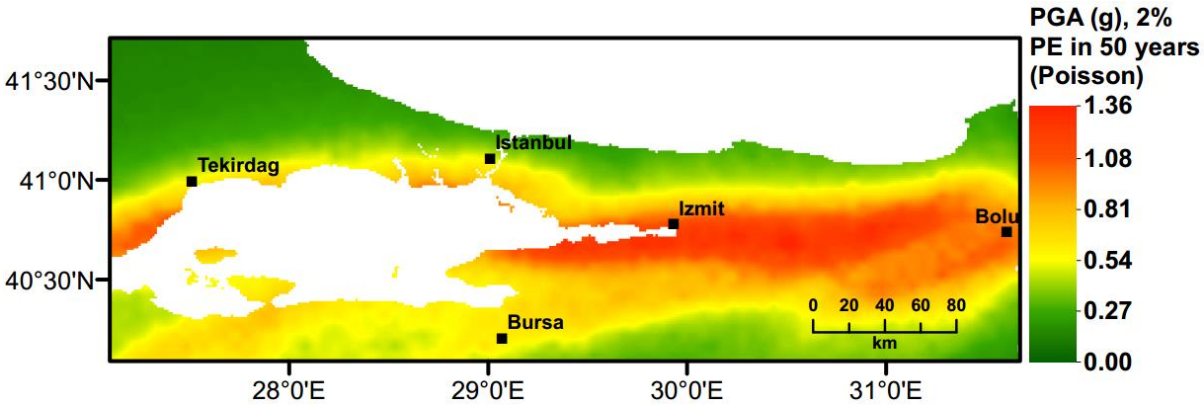

Figure 2.17 Seismic hazard map of Marmara region for PGA (g) considering 2% probability of exceedance in 50 years (the Poisson model).

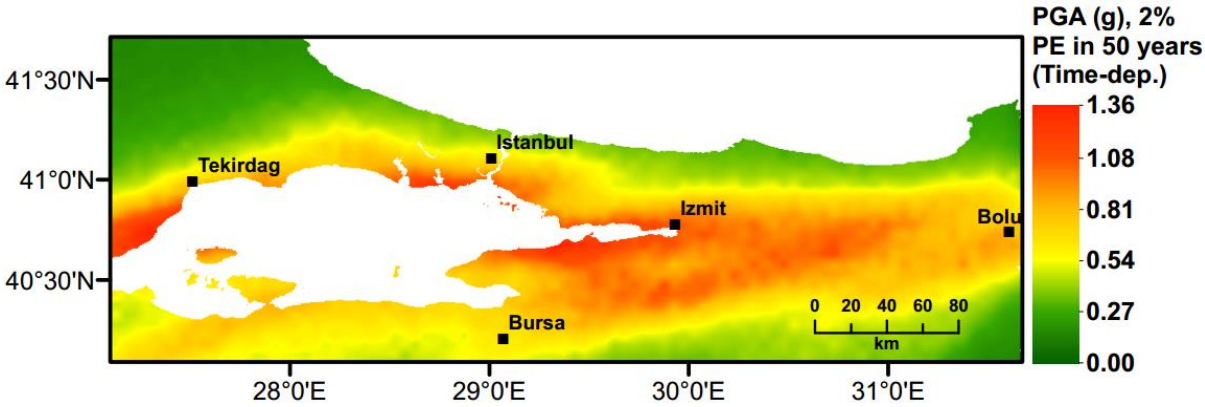

Figure 2.18 Seismic hazard map of Marmara region for PGA (g) considering 2% probability of exceedance in 50 years (Time-dependent model).

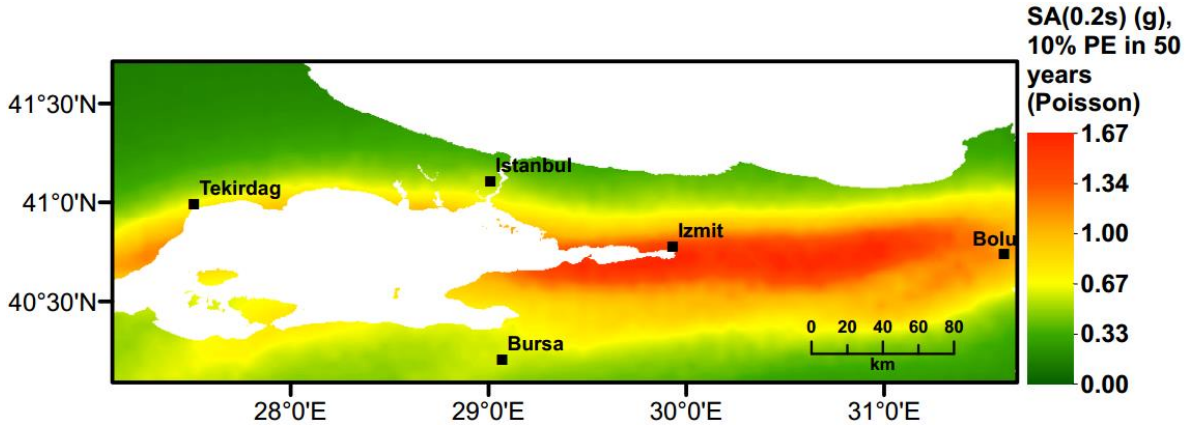

Figure 2.19 Seismic hazard map of Marmara region for SA (g) T=0.2 sec considering 10% probability of exceedance in 50 years (the Poisson model).

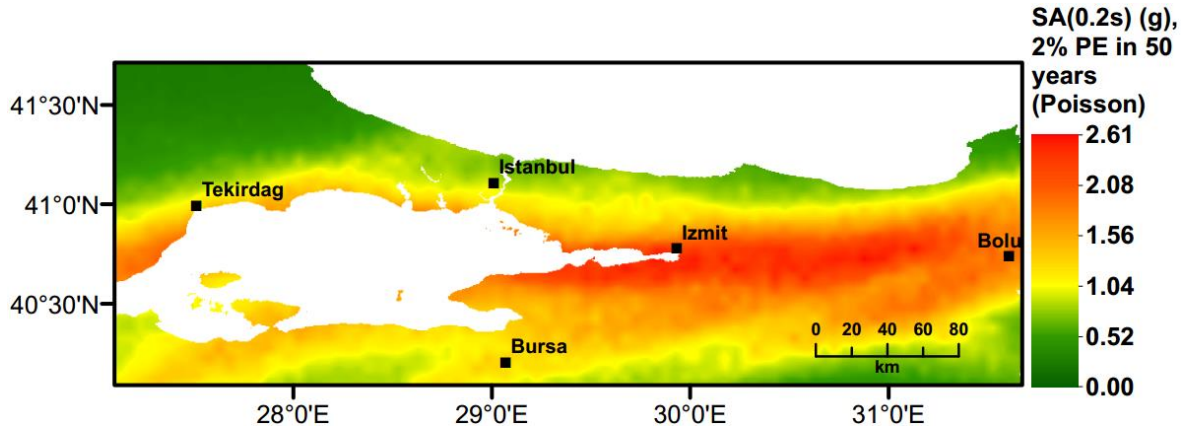

Figure 2.20 Seismic hazard map of Marmara region for SA (g) T=0.2 sec considering 2% probability of exceedance in 50 years (the Poisson model).

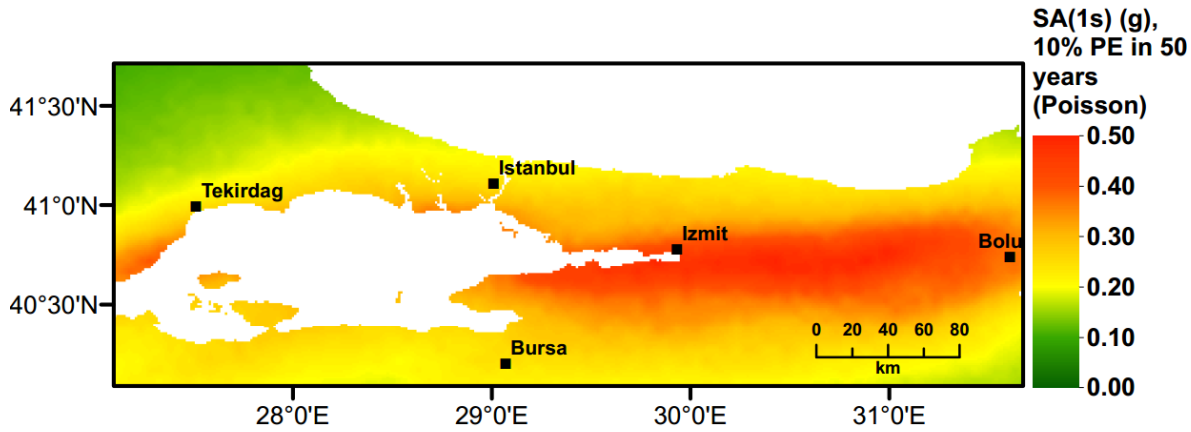

Figure 2.21 Seismic hazard map of Marmara region for SA (g) T=1.0 sec considering 10% probability of exceedance in 50 years (the Poisson model).

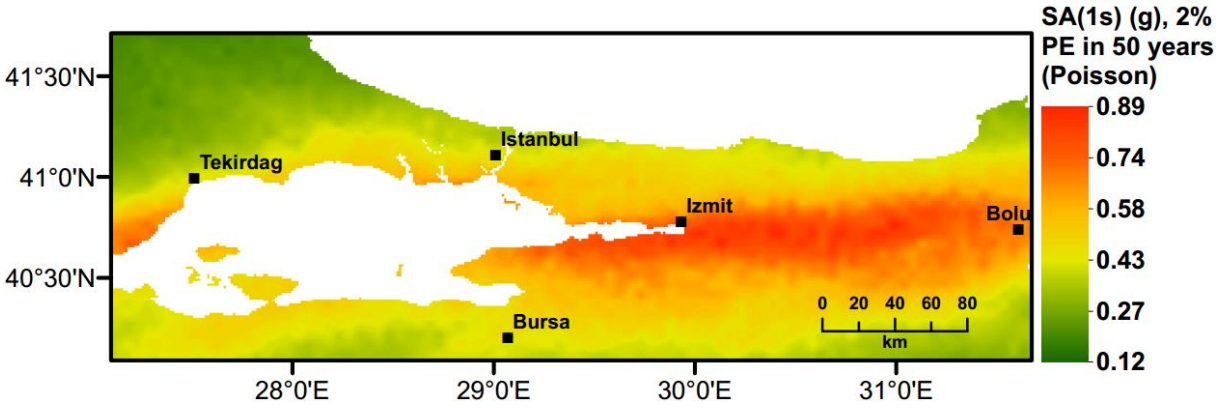

Figure 2.22 Seismic hazard map of Marmara region for SA (g) T=1.0 sec considering 2% probability of exceedance in 50 years (the Poisson model).

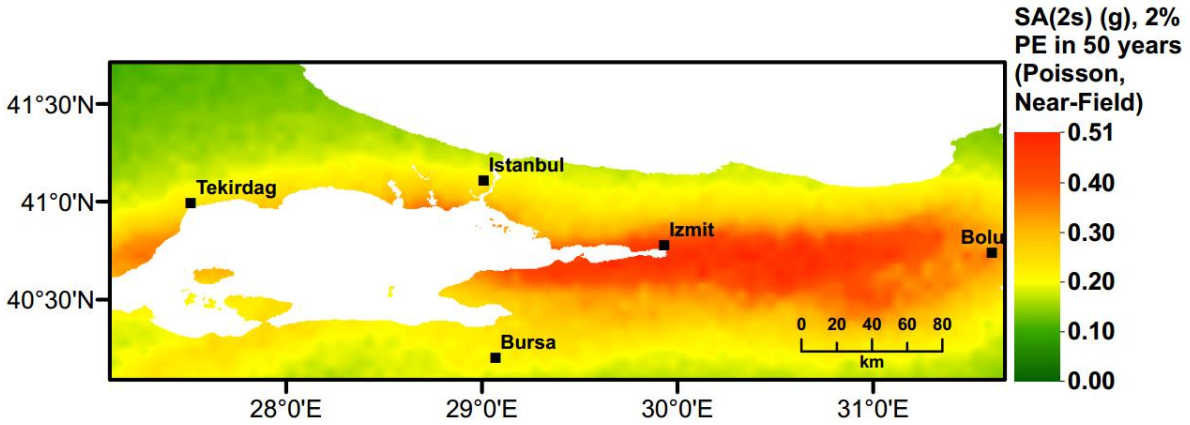

Figure 2.23 Seismic hazard map of Marmara region for SA (g) T=2.0 sec considering 2% probability of exceedance in 50 years employing the Poisson model including near-field directivity effects.

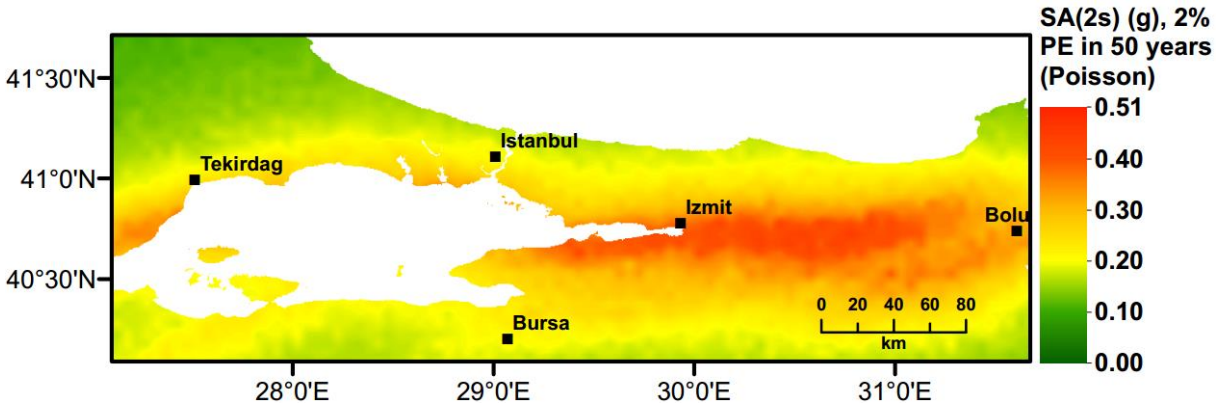

Figure 2.24 Seismic hazard map of Marmara region for SA (g) T=2.0 sec considering 2% probability of exceedance in 50 years (the Poisson model).

The results in Table 2.5 indicate that the directivity effect can have influence the predicted PSHA results by up to 20%, as can be observed for Izmit. For the areas at some distance from the fault, the directivity effect has no effect (e.g. Bursa). Particularly, this may have impact on the structures with long periods.

Table 2.5 Comparison of SA(2s) results for 475 years return period with and without directivity effect for major cities of Marmara region.

	SA(2s), Poisson	SA(2s), Poisson, Near-field
Istanbul	0.21g	0.23g
Izmit	0.39g	0.47g
Bursa	0.21g	0.21g
Tekirdag	0.23g	0.23g

The results of the study were validated via comparison with the other PSHA studies for the study area, mainly to confirm they are not an outlier. This also provides some indication how realistic the results are in the presented study, given that a different approach has been used for PSHA. The hazard maps are compared with those developed by the recent SHARE project Woessner et al. (2015), by Kalkan et al. (2008), and by Turkey's AFAD (AFAD, 2018). It should be noted that AFAD's map is included in the latest version of the Turkish Earthquake Design code Sesetyan et al. (2018). Table 2.6 compares the estimated PGA levels for a return period of 475 years obtained for major cities in the Marmara region. The differences between PGA (g) values obtained from this study and SHARE project (EFEHR, 2018) is also shown as a colour map in Fig. 2.25. It can be concluded that, despite some differences, there is a good overall agreement between the results of this study with those reported in SHARE project for a return period of 475 years.

Table 2.6 Comparison of PGA results with those from other studies for 475 years return period, major cities of Marmara region.

	This study				
	Poisson (PGA)	Time-Dependent (PGA)	AFAD (PGA)	Kalkan *et al*. (2008) (PGA)	SHARE (PGA)
Istanbul	0.29g	0.37g	0.32g	0.31g	0.31g
Izmit	0.70g	0.59g	0.72g	0.43g	0.47g
Bursa	0.29g	0.39g	0.35g	0.37g	0.38g
Tekirdag	0.35g	0.37g	0.40g	0.41g	0.37g
Bolu	0.51g	0.40g	0.63g	0.53g	0.49g

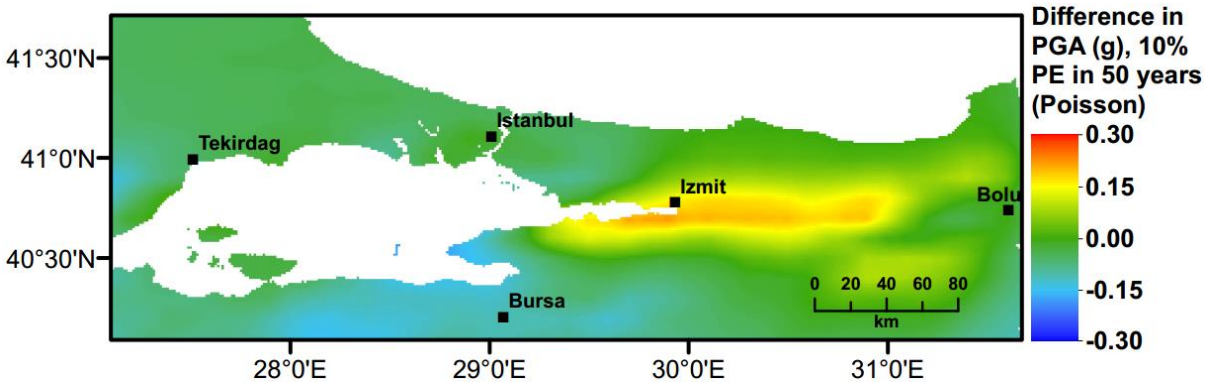

Figure 2.25 Comparison of results of this study with SHARE project, shown as difference in PGA values for 475 years return period.

2.5.2 Identification of Design Earthquakes

One of the main uses of the proposed MC-based PSHA tool is that it can be used to identify design earthquakes at sites of interest. To achieve this, all earthquake events that produce the target hazard value according to a probability of exceedance (with a plus/minus tolerance level) are extracted from the synthetic catalogues. Then, a 3D surface graph is created for a range of magnitude and distance combinations, and with a third dimension showing the number of occurrences of events. The peaks in the graph identify potential design earthquakes in terms of

magnitude and distance. As an example, for a location in central Istanbul, the PGA value of 0.35g with a return period of 475 years is assumed. Fig. 2.26 shows that this PGA value at the site is most likely to be produced by a modal earthquake of M_w=7.25 at a distance of 10 km. This information can be used as input data for the assessment of secondary hazards (e.g. landslides or liquefaction), or to help select appropriate time-history earthquake records for earthquake structural analysis.

The framework as a whole can be applicable to regions where fault data exist. On the other hand, in the areas of low seismicity, where there are no active faults, BSZs procedure alone described in the paper can be still used to perform PSHA.

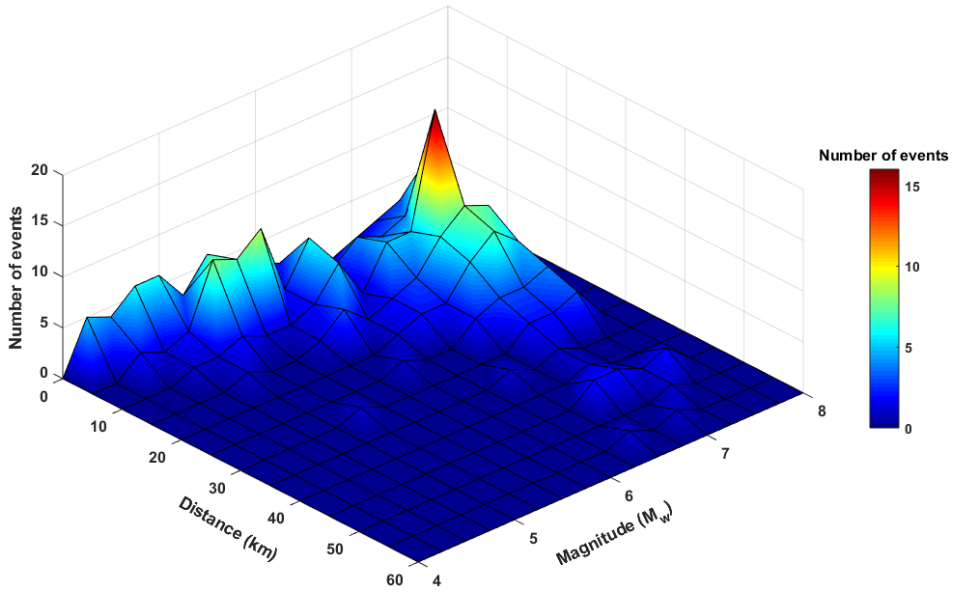

Figure 2.26 Design earthquakes in terms of distance and magnitude for a design PGA=0.35g (±0.01g) for a location in Istanbul, with POE of 10% in 50 years and calculated using a Poisson model.

2.5.3 Conclusions

This article proposes a practical MC-based PSHA tool for which synthetic earthquake catalogues are created by using readily available information on the seismo-tectonic structure,

seismicity and geology of a region. Fault segmentation and background seismicity models are used to represent seismicity. The proposed background zones are verified via the X^2 test with associated seismicity parameters to check if the seismic zones can replicate the (instrumental) past seismicity. Both Poisson and time-dependent (renewal) seismic hazard models are adopted and near-field rupture directivity effects are accounted for in the model. To demonstrate the proposed computational tool, the Marmara region in Turkey is used as a case study area. The results show that the generated hazard maps compare well with results from recent PSHA studies (AFAD and SHARE). The hazard results are used to identify the design earthquake for central Istanbul. The developed tool will be incorporated into a multi-hazard seismic risk assessment framework, which will provide decision-makers, government, insurance industry and practitioners with practical risk evaluation methodologies to reduce earthquake-related losses and promote sustainable development of earthquake prone areas in the world. By using the proposed tool, designers can assess the expected seismic hazard by taking into account the time-dependent renewal characteristics of the seismic sources. Moreover, the likely impact of near-field directivity effects on the probable seismic actions can be considered directly. The decision makers can utilize the proposed tool for developing strategies by assessing the risk with a greater level of resolution. They can effectively differentiate in between the risks associated with different subregions within their area of interest, by modelling the directivity effects associated with the probable rupture scenarios.

References

Abdalla, J. A. & Al-Homoud, A. S. 2004. Seismic hazard assessment of United Arab Emirates and its surroundings. *Journal of earthquake engineering*, 8, 817-837.

AFAD 2018. Republic of Turkey Prime Ministry Disaster and Emergency Management Authority. Accessed on 27 November, 2018.

Akinci, A., Galadini, F., Pantosti, D., Petersen, M., Malagnini, L. & Perkins, D. 2009. Effect of time dependence on probabilistic seismic-hazard maps and deaggregation for the Central Apennines, Italy. *Bulletin of the Seismological Society of America*, 99, 585-610.

Akkar, S. & Cheng, Y. 2015. Application of a Monte- Carlo simulation approach for the probabilistic assessment of seismic hazard for geographically distributed portfolio. *Earthquake Engineering and Structural Dynamics*, 45, 525-541.

Akkar, S., Moghimi, S. & Arıcı, Y. 2018. A study on major seismological and fault-site parameters affecting near-fault directivity ground-motion demands for strike-slip faulting for their possible inclusion in seismic design codes. *Soil Dynamics and Earthquake Engineering*, 104, 88-105.

Akkar, S., Sandıkkaya, M. & Bommer, J. 2014. Empirical ground- motion models for point- and extended- source crustal earthquake scenarios in Europe and the Middle East. *Official Publication of the European Association for Earthquake Engineering*, 12, 359-387.

Aldama-Bustos, G., Bommer, J., Fenton, C. & Stafford, P. 2009. Probabilistic seismic hazard analysis for rock sites in the cities of Abu Dhabi, Dubai and Ra's Al Khaymah, United Arab Emirates. *Georisk*, 3, 1-29.

Aldama Bustos, G. 2009. An exploratory study of parameter sensitivity, representation of results and extensions of PSHA: case study-United Arab Emirates. Imperial College London.

Alpar, B. & Yaltirak, C. 2002. Characteristic features of the North Anatolian Fault in the eastern Marmara region and its tectonic evolution. *Marine Geology*, 190, 329-350.

Ambraseys, N. N. & Jackson, J. 2000. Seismicity of the Sea of Marmara (Turkey) since 1500. *Geophysical Journal International*, 141, F1-F6.

Archuleta, R. J. & Hartzell, S. H. 1981. Effects of fault finiteness on near-source ground motion. *Bulletin of the Seismological Society of America*, 71, 939-957.

Bal, İ. E., Crowley, H., Pinho, R. & Gülay, F. G. 2008. Detailed assessment of structural characteristics of Turkish RC building stock for loss assessment models. *Soil Dynamics and Earthquake Engineering*, 28, 914-932.

Bohnhoff, M., Bulut, F., Dresen, G., Malin, P. E., Eken, T. & Aktar, M. 2013. An earthquake gap south of Istanbul. *Nature communications*, 4, 1999.

Bommer, J., Spence, R. & Pinho, R. Earthquake loss estimation models: time to open the black boxes. *First European Conference on Earthquake Engineering and Seismology*. Geneva, 2006.

Bommer, J. J., Douglas, J., Scherbaum, F., Cotton, F., Bungum, H. & FäH, D. 2010. On the selection of ground-motion prediction equations for seismic hazard analysis. *Seismological Research Letters*, 81, 783-793.

Bommer, J. J. & Scherbaum, F. 2008. The use and misuse of logic trees in probabilistic seismic hazard analysis. *Earthquake Spectra*, 24, 997-1009.

Bommer, J. J., Scherbaum, F., Bungum, H., Cotton, F., Sabetta, F. & Abrahamson, N. A. 2005. On the use of logic trees for ground-motion prediction equations in seismic-hazard analysis. *Bulletin of the Seismological Society of America*, 95, 377-389.

Boore DM, Stewart JP, Seyhan E, Atkinson GM (2014) NGA-West2 equations for predicting PGA, PGV, and 5% damped PSA for shallow crustal earthquakes. *Earthquake Spectra*, 30, 1057-1085

Chiou, B. S.-J. & Youngs, R. R. 2014. Update of the Chiou and Youngs NGA model for the average horizontal component of peak ground motion and response spectra. *Earthquake Spectra*, 30, 1117-1153.

Console, R., Falcone, G., Karakostas, V., Murru, M., Papadimitriou, E. & Rhoades, D. 2013. Renewal models and coseismic stress transfer in the Corinth Gulf, Greece, fault system. *Journal of Geophysical Research: Solid Earth*, 118, 3655-3673.

Cornell, C. A. 1968. Engineering Seismic Risk Analysis. *Bulletin of the Seismological Society of America*, 58, 1583-1606.

Cramer, C. H., Petersen, M. D., Cao, T., Toppozada, T. R. & Reichle, M. 2000. A time-dependent probabilistic seismic-hazard model for California. *Bulletin of the Seismological Society of America*, 90, 1-21.

Crowley, H. & Bommer, J. 2006. Modelling Seismic Hazard in Earthquake Loss Models with Spatially Distributed Exposure. *Official Publication of the European Association for Earthquake Engineering*, 4, 275-275.

EFEHR (2018) European Facilities for Earthquake Hazard and Risk. On internet at http://www.efehr.org/. Accessed on 21 September, 2018.

Ellsworth Wl, Matthews Mv, Nadeau Rm, Nishenko Sp, Reasenberg Pa & Rw, S. 1999. A physically-based earthquake recurrence model for estimation of long-term earthquake. Workshop on earthquake recurrence. State of the art and directions for the future. *Istituto Nazionale de Geofisica*, Rome, Italy.

Erdik, M. 2017. Earthquake risk assessment. *Bulletin of Earthquake Engineering*, 15, 5055-5092.

Erdik, M., Biro, Y. A., Onur, T., Sesetyan, K. & Birgoren, G. 1999. Assessment of earthquake hazard in Turkey and neighboring. *Annals of Geophysics*, 42.

Erdik, M., Demircioglu, M., Sesetyan, K., Durukal, E. & Siyahi, B. 2004. Earthquake hazard in Marmara Region, Turkey. *Soil Dynamics and Earthquake Engineering*, 24, 605-631.

Gardner, J. & Knopoff, L. 1974. Is the sequence of earthquakes in Southern California, with aftershocks removed, Poissonian? *Bulletin of the Seismological Society of America*, 64, 1363-1367.

Grunthal, G. & Group, G. R. W. 1999. Seismic hazard assessment for central, north and northwest Europe: GSHAP Region 3. *Annals of Geophysics*, 42.

Hubert-Ferrari, A., Barka, A., Jacques, E., Nalbant, S. S., Meyer, B., Armijo, R., Tapponnier, P. & King, G. C. 2000. Seismic hazard in the Marmara Sea region following the 17 August 1999 Izmit earthquake. Nature, 404, 269.

Joyner, W. B. & Boore, D. M. 1981. Peak horizontal acceleration and velocity from strong-motion records including records from the 1979 Imperial Valley, California, earthquake. *Bulletin of the Seismological Society of America*, 71, 2011-2038.

Kadirioğlu, F. T. & Kartal, R. F. 2016. The new empirical magnitude conversion relations using an improved earthquake catalogue for Turkey and its near vicinity (1900-2012). *Turkish Journal of Earth Sciences*, 25, 300-310.

Kalkan, E., Gülkan, P., Öztürk, N. Y. & Çelebı, M. 2008. Seismic Hazard in the Istanbul Metropolitan Area: A Preliminary Re- Evaluation. *Journal of Earthquake Engineering*, 12, 151-164.

Kijko, A. 2004. Estimation of the maximum earthquake magnitude, m max. *Pure and Applied Geophysics*, 161, 1655-1681.

Knopoff, L. 2000. The magnitude distribution of declustered earthquakes in Southern California. *Proceedings of the National Academy of Sciences*, 97, 11880-11884.

Krinitzsky, E. L. 2003. How to combine deterministic and probabilistic methods for assessing earthquake hazards. *Engineering Geology*, 70, 157-163.

Kurt, H., Demirbağ, E. & Kuşçu, İ. 2000. Active submarine tectonism and formation of the Gulf of Saros, Northeast Aegean Sea, inferred from multi-channel seismic reflection data. *Marine Geology*, 165, 13-26.

Malhotra, P. K. 1999. Response of buildings to near-field pulse-like ground motions. *Earthquake Engineering & Structural Dynamics*, 28, 1309-1326.

Mcguire, R. K. 1995. Probabilistic seismic hazard analysis and design earthquakes: closing the loop. *Bulletin of the Seismological Society of America*, 85, 1275-1284.

Mcneill, L., Mille, A., Minshull, T., Bull, J., Kenyon, N. & Ivanov, M. 2004. Extension of the North Anatolian Fault into the North Aegean Trough: Evidence for transtension, strain partitioning, and analogues for Sea of Marmara basin models. *Tectonics*, 23.

Murru, M., Akinci, A., Falcone, G., Pucci, S., Console, R. & Parsons, T. 2016. M≥ 7 earthquake rupture forecast and time-dependent probability for the Sea of Marmara region, Turkey. *Journal of Geophysical Research: Solid Earth*, 121, 2679-2707.

Musson, R. M. W. 1999. Determination of design earthquakes in seismic hazard analysis through Monte-Carlo simulation. *Journal Of Earthquake Engineering*, 3, 463-474.

Musson, R. M. W. 2000. The use of Monte Carlo simulations for seismic hazard assessment in the UK. *Annali di Geofisica*, 43, 1–9.

Musson, R. M. W. 2012. PSHA validated by quasi observational means. *Seismological Research Letters*, 83, 130-134.

Musson, R. M. W., Northmore, K., Sargeant, S., Phillips, E., Boon, D., Long, D., Mccue, K. & Ambraseys, N. 2006. The geology and geophysics of the United Arab Emirates. Volume 4, *Geological hazards*. Ministry of Energy, United Arab Emirates.

Musson, R. M. W. & Winter, P. 2012. Objective assessment of source models for seismic hazard studies: with a worked example from UK data. *Bull Earthquake Eng*, 10, 367-378.

Peiris, N., Free, M., Lubkowski, Z. & Hussein, A. Seismic hazard and seismic design requirements for the Arabian Gulf region. *First European conference on earthquake engineering and seismology*, 2006. 4-6.

Reasenberg, P. 1985. Second-order moment of central California seismicity, 1969–1982. *Journal of Geophysical Research: Solid Earth*, 90, 5479-5495.

Scherbaum, F., Bommer, J. J., Bungum, H., Cotton, F. & Abrahamson, N. A. 2005. Composite ground-motion models and logic trees: methodology, sensitivities, and uncertainties. *Bulletin of the Seismological Society of America*, 95, 1575-1593.

Schwartz, D. P. & Coppersmith, K. J. 1984. Fault Behavior and Characteristic Earthquakes - Examples from the Wasatch and San-Andreas Fault Zones. *Journal of Geophysical Research*, 89, 5681-5698.

Sesetyan, K., Demircioglu, M. B., Duman, T. Y., Çan, T., Tekin, S., Azak, T. E. & Fercan, Ö. Z. 2018. A probabilistic seismic hazard assessment for the Turkish territory—part I: the area source model. *Bulletin of Earthquake Engineering*, 16, 3367-3397.

Shahi, S. K. & Baker, J. W. 2011. An empirically calibrated framework for including the effects of near-fault directivity in probabilistic seismic hazard analysis. *Bulletin of the Seismological Society of America*, 101, 742-755.

Silva, V., Crowley, H., Varum, H. & Pinho, R. 2015. Seismic risk assessment for mainland Portugal. Bulletin of Earthquake Engineering, 13, 429-457.

Somerville, P. G. 2003. Magnitude scaling of the near fault rupture directivity pulse. *Physics of the earth and planetary interiors*, 137, 201-212.

Somerville, P. G., Smith, N. F., Graves, R. W. & Abrahamson, N. A. 1997. Modification of empirical strong ground motion attenuation relations to include the amplitude and duration effects of rupture directivity. *Seismological Research Letters*, 68, 199-222.

Spudich, P., Bayless, J. R., Baker, J. W., Chiou, B. S., Rowshandel, B., Shahi, S. K. & Somerville, P. 2013. *Final report of the NGA-West2 directivity working group*.

Stepp, J. Analysis of completeness of the earthquake sample in the Puget Sound area and its effect on statistical estimates of earthquake hazard. *Proc. of the 1st Int. Conf. on Microzonazion, Seattle*, 1972. 897-910.

Weichert, D. H. 1980. Estimation of the earthquake recurrence parameters for unequal observation periods for different magnitudes. *Bulletin of the Seismological Society of America,* 70, 1337-1346.

Wells, D. L. & Coppersmith, K. J. 1994. New Empirical Relationships Among Magnitude, Rupture Length, Rupture Width, Rupture Area, and Surface Displacement. *Bulletin of the Seismological Society of America*, 84, 974-1002.

WGCEP94 1995. Seismic hazards in Southern California: probable earthquakes, 1994 to 2024. *Bulletin of the Seismological society of America,* 85, 379–439.

Woessner, J., Laurentiu, D., Giardini, D., Crowley, H., Cotton, F., Grünthal, G., Valensise, G., Arvidsson, R., Basili, R., Demircioglu, M. B., Hiemer, S., Meletti, C., Musson, R. W., Rovida, A. N., Sesetyan, K., Stucchi, M. & Consortium, T. S. 2015. The 2013 European Seismic Hazard Model: key components and results. *Bulletin of Earthquake Engineering*, 13, 3553-3596.

Youngs, R. R. & Coppersmith, K. J. 1985. Implications of fault slip rates and earthquake recurrence models to probabilistic seismic hazard estimates. *Bulletin of the Seismological society of America*, 75, 939-964.

Chapter 3: A Practical Probabilistic Liquefaction Hazard Analysis Tool Based on Monte-Carlo Procedure

Sianko, I.**, Ozdemir, Z., Khoshkholghi, S., Hajirasouliha, I., and Pilakoutas, K., 2021. A Practical Probabilistic Liquefaction Hazard Analysis Tool Based on Monte-Carlo Procedure. Natural hazards. **Submitted for publication.

ABSTRACT

Earthquake induced soil liquefaction has the potential to cause devastating damages to exposed buildings and infrastructure as witnessed following several major earthquake events. The few current approaches that deal with liquefaction at the regional level are deterministic and lack accuracy. This paper presents a new Probabilistic Liquefaction Hazard Analyses (PLHA) procedure based on Monte-Carlo (MC) simulations to mitigate future seismic risks associated with liquefaction. The proposed procedure provides a relatively flexible approach to treat uncertainties in earthquake and soil related input parameters by including such parameters with distribution functions. Different methods, such as Liquefaction Potential Index (LPI) and Liquefaction Severity (L_S), are adopted for the prediction of liquefaction potential. The developed procedure is applied to the high risk city of Adapazari, Turkey, for which no PLHA studies exist. For the study area, the liquefaction hazard predictions obtained from LPI and L_S methods are compared with deterministic approaches for a specific return period. Finally, the proposed procedure is used to develop indicative PLHA maps for the Marmara region. The time-dependent probabilistic seismic hazard analysis (PSHA) model is integrated into the PLHA procedure for the first time and the results are compared to those predicted using the Poisson model for the Marmara region. The findings of this work show that the developed PLHA procedure can provide designers and decision-makers with a powerful tool to predict seismic liquefaction hazard using relatively easily obtainable input data.

3.1 Introduction

Earthquake induced liquefaction poses a devastating threat to exposed structures and lifelines such as buildings, roads, pipelines and buried cables as demonstrated by several past major earthquake events (e.g. Kocaeli 1999, Chi-Chi 1999, and Tohoku 2011). To mitigate future losses associated with liquefaction, one of the important tasks at site selection and planning stages is to identify areas vulnerable to liquefaction by developing liquefaction hazard maps. Nevertheless, the current catastrophe models used by the insurance industry to account for losses due to liquefaction generally employ a basic approach, in which a factor is applied to losses associated with strong ground motions based on the liquefaction susceptibility of the area (Bird et al., 2006). Another common approach in assessing liquefaction hazard is to use deterministic methods, where earthquake magnitude is coupled with ground shaking intensity obtained from the results of a PSHA. In this approach, whilst earthquake magnitude and ground shaking intensity couples are determined probabilistically, single deterministic values are used as input for liquefaction potential evaluation (Franke, 2016). However, a range of ground shaking and magnitude intensities can occur at a site of interest, caused by multiple seismic sources, each with a different potential for causing liquefaction. Moreover, it is known that even earthquakes with relatively small magnitudes (M~5) are capable of triggering liquefaction (Musson, 1998) and as a result, the deterministic approach may underestimate the hazard potential. Furthermore, the modern approach of performance-based design requires knowledge of the probability of exceedance of liquefaction severity at the given site due to all possible ground motions for a given return period (e.g. 50 years). Hence, there is a need for a more refined approach to estimate liquefaction hazard for enhanced safety in design, loss estimation and post-event assessment studies.

There are several methods (e.g. Kramer and Mayfield, 2007; Mayfield, 2007; Finn and Wightman, 2007; Juang et al., 2008; Salloum, 2008) that combine probabilistic seismic hazard

analysis with liquefaction potential assessment procedures, such as the stress-based simplified procedure of Seed and Idriss (1971). These methods typically utilize a seismic hazard curve in terms of PGA and disaggregation of results that are obtained from probabilistic seismic hazard analysis (PSHA), to account for the joint probability distribution of PGA and moment magnitude M_w of selected earthquake scenarios. Those parameters are key inputs in the stress-based simplified liquefaction assessment procedures. In many cases such assessments are restricted by the availability of seismic hazard information, as seismic hazard estimates and deaggregation of results are available only for a few return periods and a reference soil condition. Therefore, this can restrict the use of performance-based earthquake engineering procedures for liquefaction potential evaluation (Kramer and Elgamal, 2001; Kramer and Mayfield, 2007).

To address some the above mentioned research gaps, this paper presents a new fully probabilistic liquefaction hazard analysis (PLHA) procedure that can consider all possible potential ground shaking events and associated magnitudes simulated within a Monte-Carlo (MC) process. This procedure utilises a practical MC-based PSHA tool developed in a previous study (Sianko et al, 2020), for which synthetic earthquake catalogues are created by using readily available information on the seismo-tectonic structure, seismicity and geology of a region. The PLHA procedure proposed in this work aims to estimate the return period for a particular liquefaction severity, rather than providing occurrence or non-occurrence of liquefaction for a specified earthquake scenario. In addition, different methods for the liquefaction potential prediction, such as Liquefaction Potential Index (LPI) and Liquefaction Severity (L_S), are examined in the procedure. To assess the accuracy of the developed PLHA tool, the city of Adapazari and Marmara region of Turkey are selected as small and large scale case study areas. For the Marmara region, an indicative PLHA map is prepared using freely available slope based V_{s30} data to represent soil conditions, while a more refined PLHA study

is performed for the city of Adapazari based on borehole data from multiple sources. Additionally, a parametric study is carried out to investigate the effect of stress-reduction factor r_d on liquefaction prediction parameter and the distribution of earthquake magnitudes contributing to the liquefaction hazard. Finally, the liquefaction hazard is predicted for the Marmara region using both the Poisson and time-dependent probabilistic seismic hazard analysis (PSHA) models.

3.2 Deterministic Liquefaction Potential Assessment

Deterministic liquefaction hazard is normally assessed by comparing the soil liquefaction resistance with earthquake demand. The simplified procedure developed by Seed and Idriss (1971) is commonly used for assessing the cyclic stress ratio (CSR), which represents earthquake demand for liquefaction potential. In this procedure, the safety factor against liquefaction (F_S) is calculated as the ratio of the cyclic resistance ratio (CRR) to the cyclic stress ratio (CSR) for a given layer of soil at depth z:

$$F_S = \frac{CRR}{CSR} \tag{3.1}$$

The conditions $F_S > 1$ and $F_S < 1$ indicate that the soil profiles are classified as non-liquefiable and liquefiable, respectively, while the $F_S = 1$ represents limiting equilibrium. According to procedure proposed by Seed and Idriss (1971), CSR can be expressed by:

$$CSR = 0.65\left(\frac{a_{max}}{g}\right)\left(\frac{\sigma_v}{\sigma_v'}\right)r_d \tag{3.2}$$

where a_{max} is the peak horizontal ground acceleration; g is the acceleration due to gravity; σ_v is the total overburden stress at depth z; σ'_v is the effective overburden stress at depth z; and

r_d represents the average value of shear stress reduction factor. Iwasaki (1986) suggested that r_d could be roughly approximated as linearly decreasing with depth. This procedure has been widely adopted in general practice mainly due to its simplicity. For standard structures, r_d can be calculated using relationships provided by Liao and Whitman (1986):

$$r_d(z) = \begin{cases} 1.0 - 0.00765z & for\ z \leq 9.15\ m \\ 1.174 - 0.0267z & for\ 9.15 < z \leq 23\ m \end{cases} \quad (3.3)$$

In this equation, r_d is assumed to be independent of earthquake magnitude, and therefore, it does not decrease as magnitude decreases. In the liquefaction hazard analysis, r_d can influence the minimum magnitude that is capable of triggering liquefaction, and in turn earthquake magnitude will have an effect on r_d. Cetin and Seed (2004) proposed the following relationship to estimate r_d as a non-linear function of d, M_w, a_{max} and $V_{s,12m}$ (the average shear wave velocity in top 12 m):

$for\ z < 20m$

$$r_d = \frac{\left[1 + \frac{-23.013 - 2.949a_{max} + 0.999M_w + 0.0525V_{s,12m}}{16.258 + 0.201e^{0.341(-z+0.0785V_{s,12m}+7.586)}}\right]}{\left[1 + \frac{-23.013 - 2.949a_{max} + 0.999M_w + 0.0525V_{s,12m}}{16.258 + 0.201e^{0.341(0.0785V_{s,12m}+7.586)}}\right]} \pm \sigma_{\varepsilon_{r_d}} \quad (3.4)$$

$for\ z \geq 20m$

$$r_d = \frac{\left[1 + \frac{-23.013 - 2.949a_{max} + 0.999M_w + 0.0525V_{s,12m}}{16.258 + 0.201e^{0.341(-20+0.0785V_{s,12m}+7.586)}}\right]}{\left[1 + \frac{-23.013 - 2.949a_{max} + 0.999M_w + 0.0525V_{s,12m}}{16.258 + 0.201e^{0.341(0.0785V_{s,12m}+7.586)}}\right]} - 0.0046(z - 20) \pm \sigma_{\varepsilon_{rd}} \quad (3.5)$$

where,

$$\sigma_{\varepsilon_{r_d}} = z^{0.85}0.0198 \qquad for\ z < 12m \quad (3.6)$$

$$\sigma_{\varepsilon_{r_d}} = 12^{0.85}0.0198 \qquad for\ z \geq 12m \quad (3.7)$$

In the above equations $\sigma_{\varepsilon_{r_d}}$ is the standard deviation of r_d.

In Eq. (3.1) CRR is usually calculated using soil parameters obtained from cone penetration tests (CPT) or standard penetration tests (SPT). However, Andrus and Stokoe (2000) proposed a different approach for calculating CRR using the shear-wave velocity:

$$CRR = \left[0.022\left(\frac{V_{s1,\mathrm{cs}}}{100}\right)^2 + 2.8\left(\frac{1}{V_{s1}^* - V_{s1,\mathrm{cs}}} - \frac{1}{V_{s1}^*}\right)\right] \times MSF \tag{3.8}$$

$$V_{s1,\mathrm{cs}} = V_{s1}K_{FC} = V_s\left(\frac{P_a}{\sigma_v'}\right)^{0.25} \times K_{FC} \tag{3.9}$$

where $V_{s1,\mathrm{cs}}$ is the stress-corrected shear wave velocity; V_{s1} is the overburden-stress-corrected shear-wave velocity; P_a is a reference stress of 100 kPa; V_{S1}^* is the limiting upper value for cyclic liquefaction occurrence, which varies between 200-215 m/s depending on the fines content of the soil; and K_{FC} is the adjustment factor for the fines content FC (%) and was defined by Juang et al. (2001) as follows:

$$K_{FC} = \begin{cases} 1.0 & for\ FC \leq 5\% \\ 1.0 + (\mathrm{FC} - 5)T & for\ 5\% < FC < 35\% \\ 1 + 30T & for\ FC \geq 35\% \end{cases} \tag{3.10}$$

where,

$$T = 0.009 - 0.0109\left(\frac{V_{s1}}{100}\right) + 0.0038\left(\frac{V_{s1}}{100}\right)^2 \tag{3.11}$$

In Eq. (3.8), MSF represents the magnitude scaling factor, which can be calculated as follows (Youd and Idriss, 1997):

$$MSF = \left(\frac{M_w}{7.5}\right)^{-2.56} \tag{3.12}$$

MSF reflects the number of significant cycles, and therefore, can be assumed to be related to the ground motion duration.

According to Maurer et al. (2014), severe liquefaction will generally occur if the liquefiable layer is thick, it is located close to the surface, and F_S calculated for this layer is far less than 1.0. Juang et al. (2005) found that Eq. (3.8) is conservative for calculating CRR, resulting in lower factors of safety and over-predicting liquefaction occurrence. To address this, they proposed a multiplication factor of 1.4 to CRR to obtain an unbiased (or less conservative) estimate of this parameter.

Although F_S of a soil layer can be estimated by means of several geotechnical parameters, it is not of its own accord a sufficient criterion to assess liquefaction severity. Furthermore, F_S is not a practical parameter to use in liquefaction severity maps. To be more specific, F_S can be used to predict if a layer will liquefy or not, but it cannot be used to represent the severity degree. To overcome these limitations, the liquefaction potential index (LPI) was proposed by Iwasaki et al. (1984):

$$LPI = \int_0^{20} F(10 - 0.5z)dz \tag{3.13}$$

where $F = 1 - F_S$ for a single soil layer.

In this method, the soil profile is sub-divided into several number of layers and the liquefaction potential at the surface-level is predicted by integrating a function of the factor of safety for each soil layer within the top 20m of soil. According to severity categories for the LPI procedure, liquefaction potential is "very low" for $LPI = 0$; "low" for $0 < LPI \leq 5$; "high" for $5 < LPI \leq 15$; and "very high" for $LPI > 15$. Several studies (e.g. Toprak and Holzer, 2003;

Kongar et al., 2017) have used LPI procedure to investigate appropriate thresholds for liquefaction occurrence. In general, based on field observations, they considered $LPI = 4 - 5$ as a threshold value for moderate liquefaction hazard (e.g., sand boils), whereas $LPI = 12 - 15$ was considered as a threshold value for major liquefaction hazard (e.g., lateral spreads).

Data needed for V_s in the CRR calculations (Eqs. (3.8) and (3.9)) are not commonly available from ground investigations for public domain and may not necessarily be available across the entire study area at required resolution. Thus, in many cases, geo-statistical techniques are required for its determination. Therefore, to extend the applicability of the LPI method, two approaches proposed by Kongar et. al (2017) to approximate V_s from more readily available data. The first approach uses V_{s30}, the average shear wave velocity across the top 30m of soil, as a constant proxy for V_s for all soil layers. Global estimates for V_{s30} are available open-access from the web-based US Geological Survey Global V_{s30} Map Server (USGS, 2019), so this parameter is an appealing option for such assessments. The disadvantage of this approach is that the likelihood of liquefaction occurrence in the LPI method is controlled by the presence of soil layers near the surface with low V_s. Furthermore, there is a maximum value of V_s at which liquefaction can occur. Hence, the use of V_{s30} as a proxy for all layers will result in an overestimation of V_s, CRR and F_S at layers closer to the surface, and therefore an underestimation of LPI and liquefaction risk.

As a second approach, empirical equations proposed by Boore et al. (2011) can be used to estimate V_{S10} and V_{S20}, which show the average shear wave velocity across the top 10 m and 20 m of soil, respectively, to calculate CRR using Eq. (3.8):

$$V_{s10} = 10^{\left(\frac{\log V_{s30} - 0.042062}{1.0292}\right)} \tag{3.14}$$

$$V_{s20} = 10^{\left(\frac{\log V_{s30} - 0.025439}{1.0095}\right)} \tag{3.15}$$

From these equations, the average shear wave velocity between the top 10 m and 20 m of soil ($V_{s(10-20)}$) can be obtained as follows:

$$V_{s(10-20)} = \frac{1}{\frac{2}{V_{s20}} - \frac{1}{V_{s10}}} \tag{3.16}$$

The LPI model also requires water table depth and unit weights of soil layers. If such data are not available, engineering judgment needs to be used to estimate these parameters based on information from available sources.

The liquefaction potential can also be assessed in terms of probability of liquefaction, P_L. In many occasions, results of such liquefaction potential assessment can lead to better engineering decisions. Juang and Jiang (2000) extended earlier studies on the Bayesian mapping function, and found that mapping functions could be developed using the distributions of calculated F_S. In another study, Juang et al. (2002) used 225 V_s-based case studies from Andrus and Stokoe (2000) and Andrus et al. (2001) to develop a Bayesian mapping function that relates F_S determined from the V_s-method to P_L. The boundary curve defined by the V_s method was seen to be characterized by a probability of 26%, since $P_L = 0.26$ for $F_S = 1$ according to the derived V_s-based Bayesian mapping function.

The probability of liquefaction using the V_s method proposed by Juang et. al (2002) can be calculated by the following equation:

$$P_L = \frac{1}{1 + \left(\frac{F_S}{0.73}\right)^{3.4}} \tag{3.17}$$

In the P_L method proposed by Juang et. al (2002), liquefaction can occur for a given layer of soil with some probability even for $F_S > 1$, whereas in the procedure proposed by (Iwasaki et al. 1984) it is assumed than no liquefaction can occur if $F_S > 1$. According to Juang et. al (2002), the choice of a particular MSF formula and r_d formulation is not critical to the Bayesian mapping function.

Sonmez and Gokceoglu (2005) replaced F in Eq. (3.13) with P_L to calculate the liquefaction severity index (L_S):

$$L_S = \int_0^{20} P_L(10 - 0.5z)dz \tag{3.18}$$

Table 3.1 shows the severity classification proposed by Sonmez and Gokceoglu (2005), which also includes categories of 'non-susceptible' and 'moderate'. These categories were not included in the original classification proposed by Iwasaki et al. (1984).

The simplified liquefaction assessment methods were developed using post-earthquake field observations supported by in-situ tests. The deterministic procedures can be demonstrated to produce fairly accurate estimates of the liquefaction potential under a given pair of seismic

parameters (a_{max}, M_w), as shown by Kongar et. al (2017) for Christchurch in New Zealand as a case study area.

Table 3.1 Liquefaction severity index L_S classification (Sonmez and Gokceoglu 2005).

L_S	Description
$85 \leq L_S < 100$	Very high
$65 \leq L_S < 85$	High
$35 \leq L_S < 65$	Moderate
$15 \leq L_S < 35$	Low
$0 < L_S < 15$	Very Low
L_S=0	Non-liquefied

3.3 Probabilistic Liquefaction Hazard Analysis

The previously mentioned deterministic methods are applicable to a specific performance level or earthquake scenario; however, they do not estimate liquefaction potential by taking into account all possible earthquake events. To overcome this limitation, probabilistic methods can be adopted to estimate liquefaction hazard. Atkinson et al. (1984) developed a PLHA procedure based on the conventional PSHA proposed by Cornell (1968). The method combines Seed and Idriss (1971) simplified method for assessing liquefaction potential with conventional PSHA method for assessing seismic hazard by modifying the latter to consider the joint probability of magnitude and acceleration. The drawback of this method is that treating uncertainties in conventional PSHA is not a trivial problem and often requires a logic tree, where the choice of weights for branches tends to be subjective. More recent studies by Kramer and Mayfield (2007) and Juang et al. (2008) utilized readily available seismic data such as hazard curves and deaggregation of hazard to perform PLHA. The problem with this approach is that seismic data may not be available for any site of interest or is developed only for specific

return periods of hazard. To address this issue, Goda et al. (2011) proposed the use of an event-based PSHA to perform PLHA. However, in their work four Canadian cities were represented in PLHA calculations with a single location for each city, which is unrealistic for a hazard map. One of the outcomes of their study was that earthquake magnitudes as low as $M = 4.5$ have non-negligible effect on the liquefaction hazard curves, and therefore, should be considered in the PLHA. In a more recent study, Green and Bommer, (2019) suggested that M_{min} to be considered in PLHA for structure sites is $M = 5$, agreeing with the lower limit proposed by Atkinson et al. (1984). Moreover, they suggested that the disparity in M_{min} values can be attributed to the stress reduction (r_d) relationship used in the analysis, as the relationship used by Goda et. al (2011) is independent of earthquake magnitude. The stress reduction (r_d) relationship proposed by Cetin and Seed (2004) will be incorporated in the PLHA study conducted in this work.

3.3.1 Methodology

In general, different stochastic modelling approaches using the MC simulation method can be used in PLHA procedures. In this method synthetic earthquake catalogues are generated by randomizing key parameters in a controlled manner to represent the future seismic behaviour of a region. In both conventional and MC-based PSHA studies, two different types of seismic source models can be used to represent seismicity of an area, including the simple area source zone model, and combining the area source zone model with a fault source zone model. In the former, seismicity is homogenised over source zones, where a future earthquake can occur randomly in the zone area. In this model, seismic events without identified faults are assumed to occur randomly in areal background source zones (BSZs). In the latter model, however, the hazard resulting from active faults with a characteristic magnitude is mainly concentrated in fault source zones (FSZs). In this paper, the latter model is adopted as it is more suitable to regions (such as the Marmara region) with well-defined faults.

Once synthetic catalogues for both BSZs and FSZs are generated, the probability of exceedance of the liquefaction prediction parameter (e.g. LPI, L_S) can be calculated at a site of interest. This can be done by using the distance between site and a given earthquake event to determine the PGA value. Subsequently, by using the obtained PGA-Magnitude pair, the liquefaction prediction parameter can be calculated for a particular year of the synthetic catalogue. For each year of synthetic catalogue, all earthquakes occurring in that year across all source zones are used to identify the largest liquefaction prediction parameter value at the site. In other words, the worst-case scenario from all seismic sources affecting the site of interest is considered as an annual maximum outcome. This step is repeated for all simulations and the results are combined into a single list. The probability of exceedance of certain liquefaction prediction parameter can be then found by sorting annual outcomes in descending order and by selecting the N^{th} value in the sorted list. For the desired return period, N can be calculated using the following equation:

$$N = (\frac{1}{Return\ period} \times Catalogue\ length \times Number\ of\ simulations) + 1 \quad (3.19)$$

Fig. 3.1 shows the detailed procedure for the PLHA based on MC simulations proposed here. In this flowchart, LPI is used as a liquefaction prediction parameter, but any prediction parameter can be used in the procedure.

The previous sections provided an overview of the components of the proposed MC-based PLHA. The following section uses two case study regions to show the accuracy and effectiveness of the developed computational procedure.

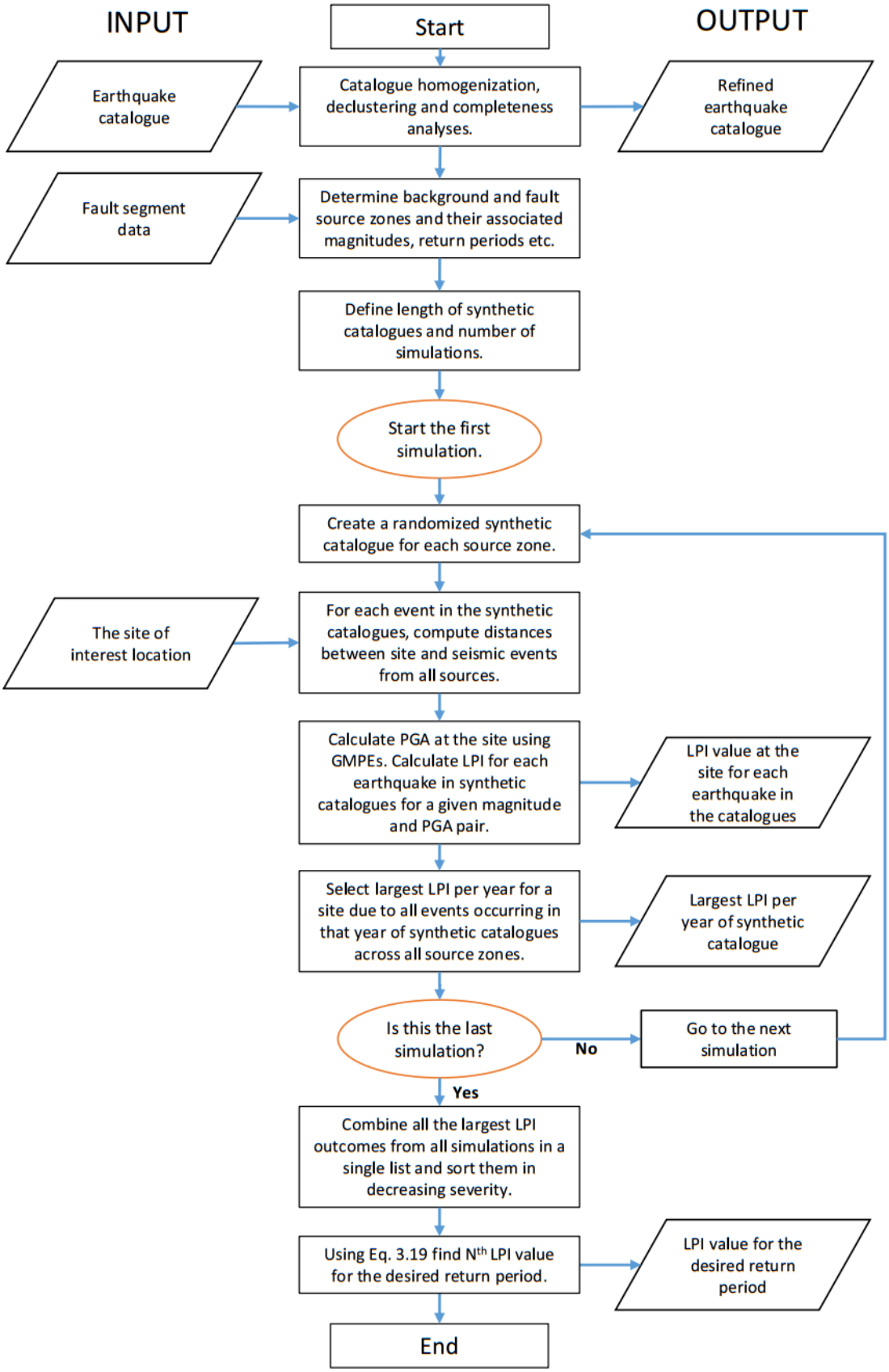

Figure 3.1 The proposed MC-based PLHA procedure using LPI as liquefaction potential prediction parameter.

3.4 Small Scale Case Study: The city of Adapazari

The Marmara region, in north-west of Turkey spanning Europe and Asia, lies in one of the most seismically active zones in the world. The 1999 Kocaeli earthquake with M_w=7.4 hit the region and resulted in significant loss of life (around 20,000 lives) and extensive damage to buildings and infrastructure. It also triggered liquefaction in numerous inland alluvial areas as well as along the coast. Sand boiling, lateral spreading and settlement were widely observed in the city of Adapazari and along the southern coasts of Sapanca Lake and Izmit Bay in the eastern and western parts of the earthquake-affected regions, respectively. Due to the close proximity to the Sakarya river (shown in Fig. 3.2), Adapazari is located on alluvial deposits, consisting of sand and/or silty sand, with potential to liquefy. Moreover, the water table level across the city is very shallow (around 1 meter). These factors played a huge role in triggering liquefaction that caused tilting and settling of numerous buildings in the area during the 1999 Kocaeli earthquake. Adapazari and the Marmara region are highly likely to be hit by an earthquake of M_w>7.3 with a 35-47% probability in the next 30 years (Murru et al., 2016). While Adapazari can be considered as a well-studied area in terms of liquefaction hazard, there is no probabilistic liquefaction hazard map for the city, hence it is selected as the first case study for this proposed procedure.

Figure 3.2 3D topographic map of the city of Adapazari and its surrounding area.

3.4.1 Input parameters

A total of 75 borehole logs located in Adapazari (Fig. 3.3) were collected from different sources including PEER database (U.C. Berkeley et al., 2019) and Adapazari municipality to perform PLHA. Borehole data were used to determine shear wave velocity, the depth of ground water level (GWL), as well as density and fine content of soil layers across the city centre of Adapazari. The available logs vary in depth with most being up to 10 meters. In the presented methodology, three depth ranges are assumed for liquefaction calculations. These are 0-5 meters, 5-10 meters and 10-20 meters. Borehole data up to 10 meters are used directly in the analysis, while data required for the 10-20 meters' range are estimated based on the data up to 10 meters.

While V_{s5} and $V_{s(5-10)}$ are available for some logs, for the rest of them the conversion equation proposed by Akin et al. (2011) is adopted to convert average SPT values to shear wave velocities as follows:

$$\ln V_s = \ln 56.1 + 0.4405 \ln N + \varepsilon \sigma_{\ln V_s}, \qquad \text{where} \qquad \sigma_{\ln V_s} = 0.3231 \quad (3.20)$$

Once V_{s10} is known, V_{s30} is calculated by rearranging Eq. (3.14). Then, Eq. (3.15) is used to find V_{s20} and finally, $V_{s(10-20)}$ is calculated using Eq. (3.16). According to Bray et al. (2004) ground water level (GWL) varies seasonally, but is typically at a depth of 1 to 2 m. In this study GWL from borehole logs is randomized by adding a variable value between -0.5m and 0.5m sampled from uniform distribution to represent this variability. V_s values are randomized using normal distribution with standard deviation provided in the SPT conversion equation. Stress reduction factor r_d is randomized with $\sigma_{\varepsilon_{r_d}}$ calculated from Eqs. (3.4-3.5), and the method proposed by Cetin and Seed (2004) is employed.

The uncertainties of input parameters for the liquefaction hazard calculations used in the MC method, represented by mean values and standard deviations, are shown in Table 3.2. These enable synthetic catalogue generation. By using borehole logs in known locations, it is possible to estimate missing data required for the analysis of the other locations by using interpolation. Fig. 3.4 shows an example of the obtained map for mean $V_{s(0-10)}$.

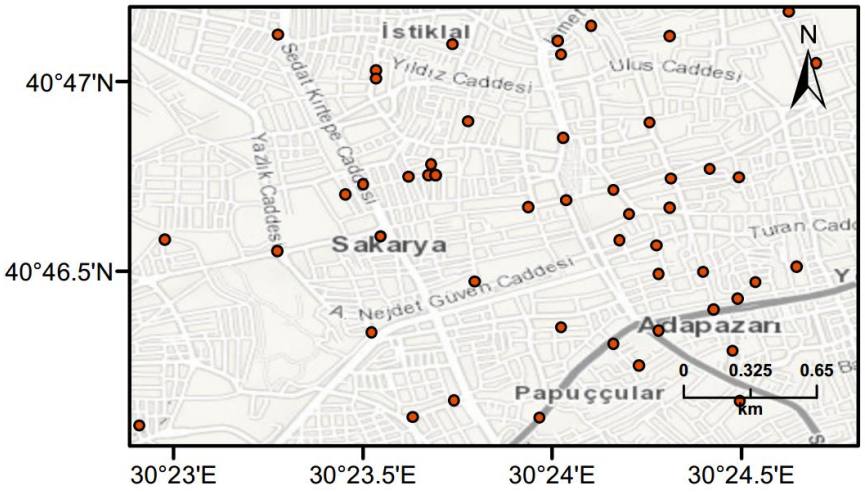

Figure 3.3 Bore logs locations across Adapazari city used in the analysis.

Table 3.2 Parameters randomized in MC simulations for liquefaction hazard calculations.

Parameter	**Type of distribution**	**Randomization value**
V_s	Log-normal distribution	$\sigma_{\ln V_s} = 0.3231$
GWL	Uniform distribution	$\sigma_{GWL} = \pm 0.5$
r_d	Normal distribution	$\sigma_{\varepsilon_{r_d}}$
Soil density	Normal distribution	$\sigma_{soil} = 0.3$
FC	Normal distribution	σ_{fc} =18.9

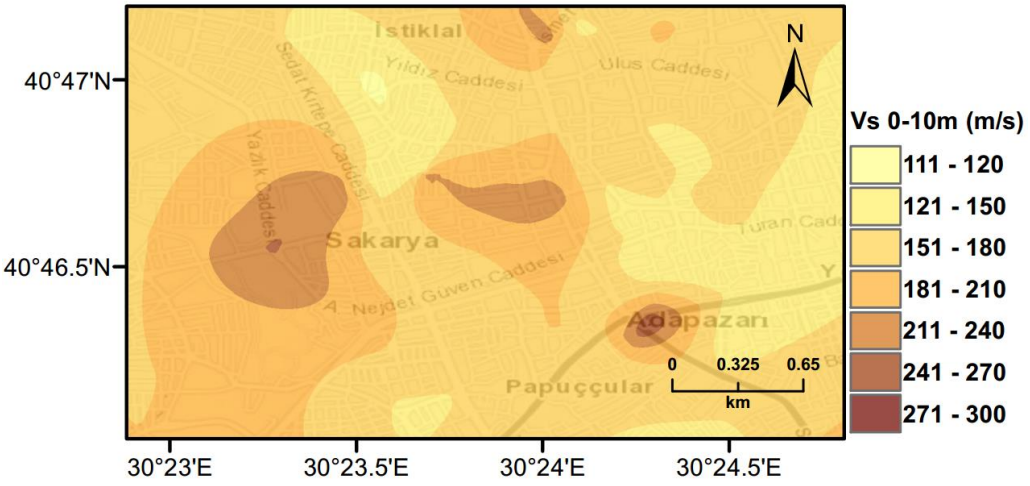

Figure 3.4 V_{s10} map for the city centre of Adapazari used in the PLHA.

The MC based PSHA tool developed by Sianko et al. (2020) is utilised for the PLHA of the case study area due to its practicality and availability of Poisson and time-dependent models. The seismicity of the Marmara region is modelled by considering 25 faults source zones (FSZ) to represent large events occurring on the faults with the assigned characteristic magnitude. There are also 17 background source zones (BSZ) to represent small events occurring in the region. Readers are referred to the paper by Sianko et al. (2020) for more details on the adopted MC-based PSHA.

3.4.2 PLHA for Adapazari

In this study, the *LPI* method based on Eq. (3.13) and the L_S method based on Eq. (3.18) are incorporated in MC-based PLHA procedure for quantifying the liquefaction hazard for the city of Adapazari. r_d methods proposed by Liao and Whitman (1986) and Cetin and Seed (2004) are also integrated into the procedure. Fig. 3.5 shows seismic hazard curves for average V_s profile developed for the city centre of Adapazari using *LPI* and L_S procedures. One can observe from this figure that the r_d method proposed by Liao and Whitman (1986) provides more conservative predictions than that proposed by Cetin and Seed (2004), leading to a higher liquefaction hazard for the corresponding return period. In Fig. 3.6 seismic hazard curves are

presented for low, mean and high V_s profiles for the city centre of Adapazari. The results clearly indicate the high influence of V_s profiles on liquefaction hazard.

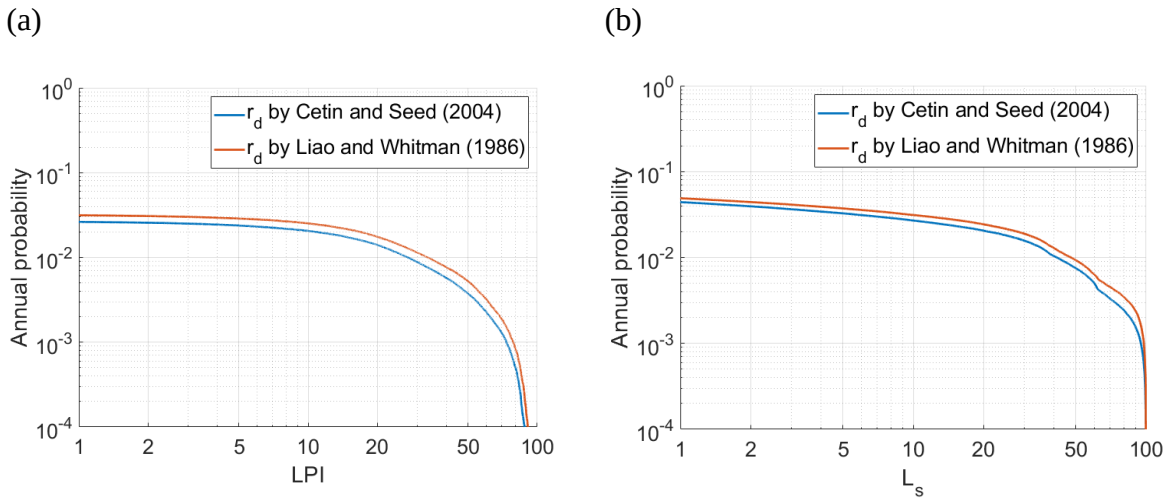

Figure 3.5 The liquefaction hazard curves for the city centre of Adapazari for average V_s profile obtained using (a) LPI and (b) L_S procedures employing r_d methods proposed by Liao and Whitman (1986) and Cetin and Seed (2004).

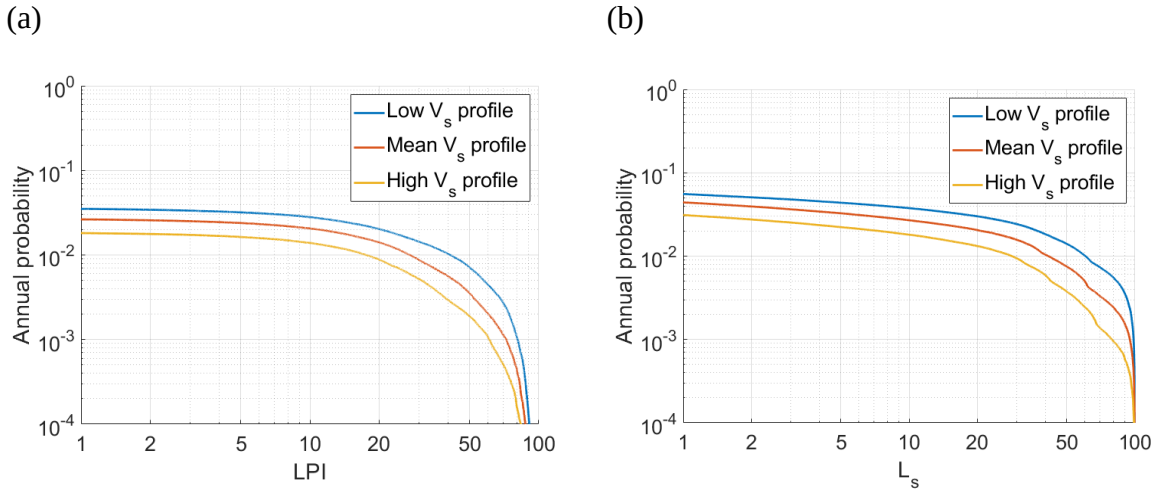

Figure 3.6 The liquefaction hazard curves for the city centre of Adapazari for representative low, mean and high V_s profiles obtained using (a) LPI and (b) L_S procedures employing r_d methods proposed by Liao and Whitman (1986) and Cetin and Seed (2004).

Deaggregation of results is carried out to identify earthquake magnitude and distance values that contribute to the liquefaction hazard in terms of *LPI* at the case study area for a given return period. As opposed to the conventional method, the proposed MC-based PLHA procedure can be used to identify design earthquakes at sites of interest. To achieve this, all

earthquake events that produce the target LPI according to a probability of exceedance (with a plus/minus tolerance level) are extracted from the synthetic catalogues. Then, a 3D surface map with the third dimension showing the probability of the events is created for a range of magnitude and distance combinations. The peaks in the graph identify potential design earthquakes in terms of magnitude and distance. Fig. 3.7 shows deaggregation plots for the return periods of 475 and 2475 years for two different r_d methods. It can be seen that M_w ~7 is the most dominant magnitude for both return periods. This is due to the fact that Adapazari is in close proximity to active fault segments with a similar characteristic magnitude. It can also be noticed that the chosen r_d method has an effect on magnitude-distance distribution and LPI value. For the same return period, LPI values are smaller when r_d is calculated based on the method proposed by Cetin and Seed (2004). Also, this r_d method leads to less contribution of earthquakes with magnitude M_w<6 in liquefaction hazard than that obtained by the Liao and Whitman (1986) method. These results support Green and Bommer (2019) findings that earthquakes of magnitude smaller than M=5 should not be considered in liquefaction hazard calculations, contrary to Musson (1998) who recommended that lower magnitudes should not be excluded from the analysis.

The previous studies by Yoshida et al. (2001) and Mollamahmutoglu et al. (2003) identified liquefied areas following the 1999 Kocaeli earthquake as shown in Fig. 3.8. As one can observe from this figure, the agreement between the two studies in terms of observed liquefaction is relatively poor. This could be attributed to the collapse of a large proportion of buildings in the city during the earthquake, which made it difficult to determine the occurrence of liquefaction.

(a)

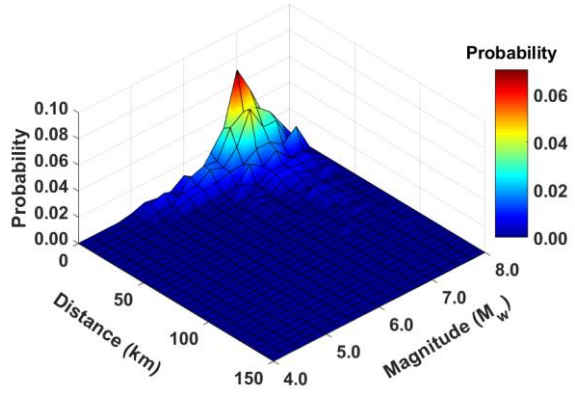

1/475 *LPI*=67.8, Liao and Whitman (1986)

(b)

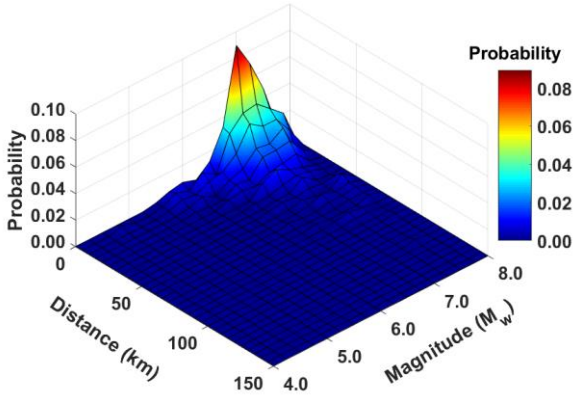

1/475 *LPI*=61.2, Cetin and Seed (2004)

(c)

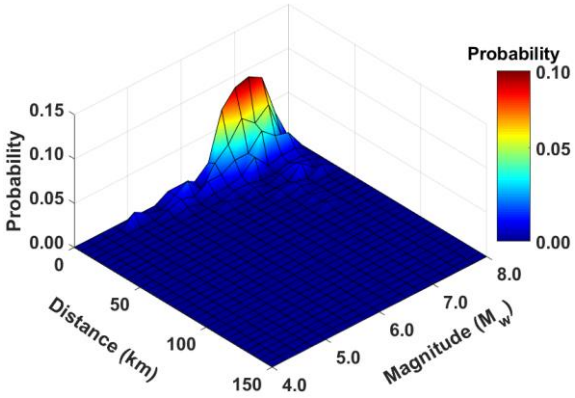

1/2475 *LPI*=85.2, Liao and Whitman (1986)

(d)

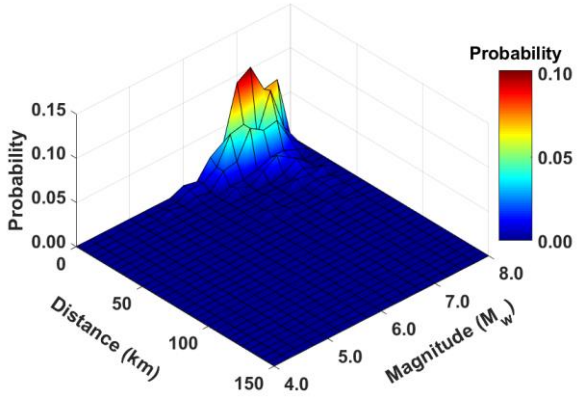

1/2475 *LPI*=81.8, Cetin and Seed (2004)

Figure 3.7 Disaggregation of liquefaction hazard for target LPI for two different return periods and stress reduction factor calculation methods: (a) 1/475, Liao and Whitman (1986), (b) 1/475, Cetin and Seed (2004), (c) 1/2475, Liao and Whitman (1986), and (d) 1/2475, Cetin and Seed (2004).

PLHA maps were prepared for Adapazari using the MC based PLHA procedure developed in this work. Figs. 3.9-3.11 illustrate probabilistic liquefaction hazard maps for probability of exceedance (PoE) of 10% in 50 years (return period of 475 years). These maps can be compared with Fig. 3.8 showing the observed liquefaction areas during the 1999 Kocaeli earthquake, which caused structural damages to buildings in Adapazari. It can be noted that the areas with high liquefaction severity show similar pattern with the areas of observed liquefaction. This is partially due to the fact that the fault ruptured during the 1999 Kocaeli earthquake contributes

the most to the hazard in PSHA disaggregation. In Fig. 3.11, the PLHA hazard map is calculated based on unbiased *LPI* values.

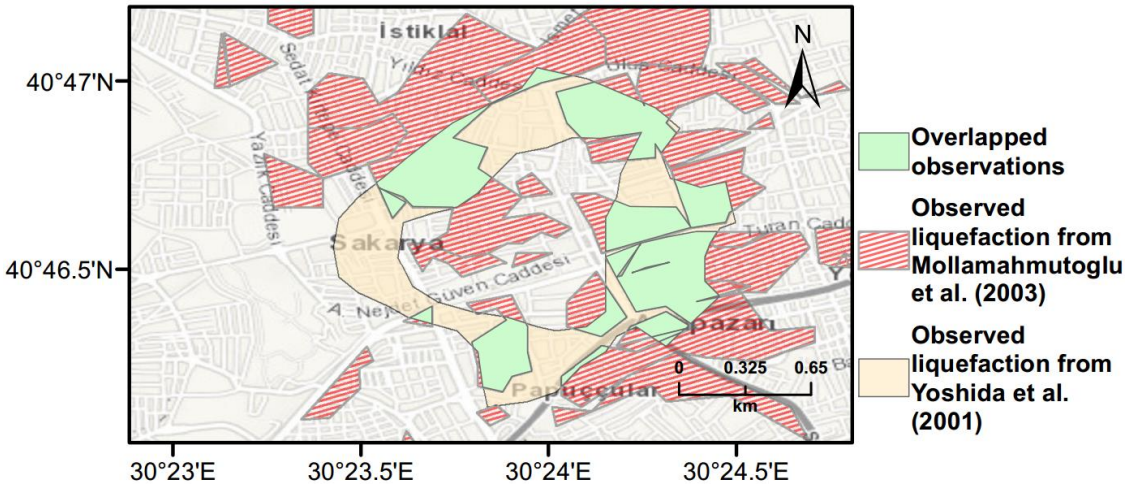

Figure 3.8 Observed liquefaction damage in Adapazari during the 1999 Kocaeli earthquake mapped from Yoshida et al. (2001) and Mollamahmutoglu et al. (2003).

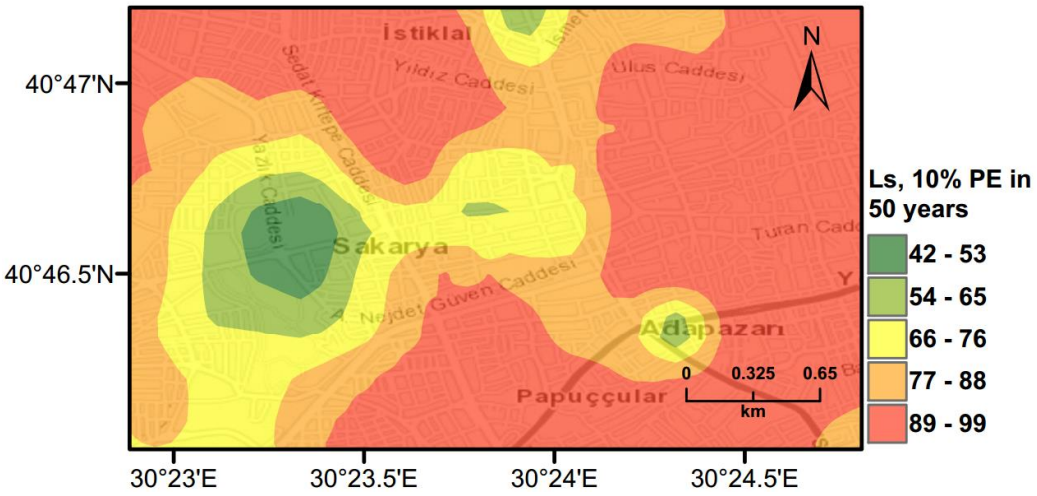

Figure 3.9 Probabilistic liquefaction hazard map in terms of L_S for central part of Adapazari city with return period of 475 years.

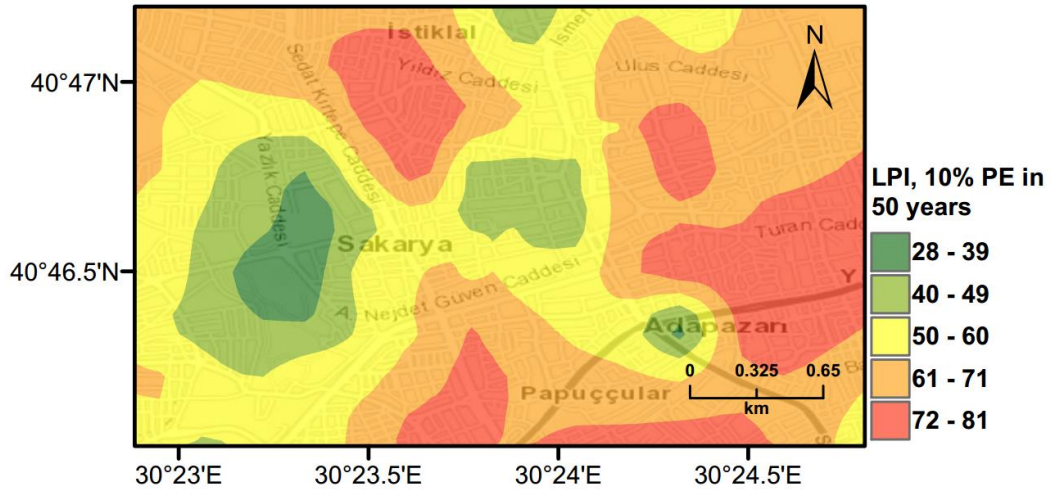

Figure 3.10 Probabilistic liquefaction hazard map in terms of LPI for central part of Adapazari city with return period of 475 years.

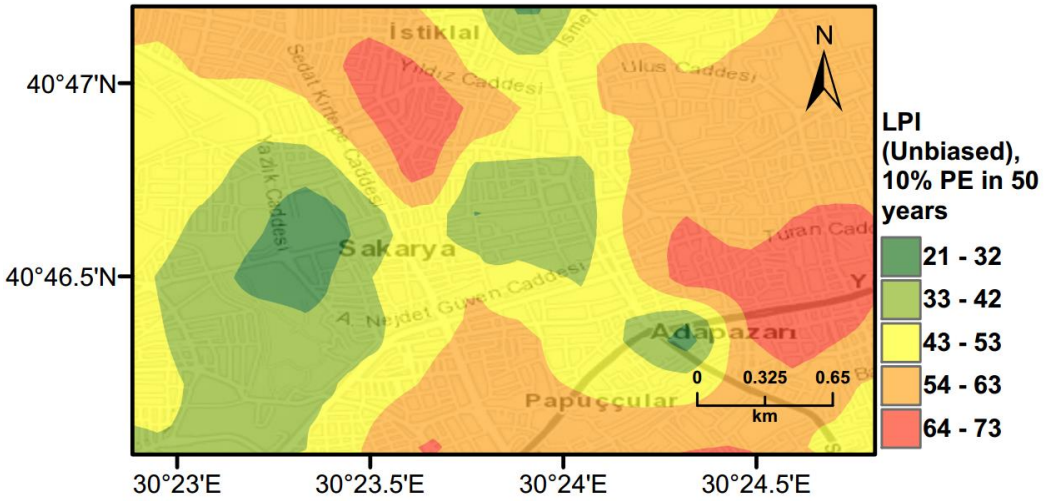

Figure 3.11 Probabilistic liquefaction hazard map in terms of unbiased LPI for central part of Adapazari city with return period of 475 years.

3.4.3 Scenario earthquake for Adapazari (Deterministic method)

To show the accuracy of L_S and LPI hazard assessment procedures, a scenario earthquake is simulated for the city of Adapazari to compare with the liquefaction observed during the 1999 Kocaeli earthquake. An earthquake event with Mw=7.4 and PGA=0.41g is used representing the actual values recorded during this event. Figs. 3.12-3.14 show liquefaction hazard maps in terms of L_S and LPI together with the observed liquefaction from 1999 Kocaeli

earthquake. For the central part of Adapazari, the predictions are well-matched to the observed liquefaction hazard from Yoshida et al. (2001). It should be noted that, Yoshida et al. (2001) investigated the liquefaction occurrence in an area slightly larger than the outer limits of the "ring" given in Figs. 3.12-3.14. Therefore, it is difficult to say from Yoshida et al. (2001) study if the liquefaction actually occurred outside of the area. On the other hand, if liquefaction predictions in Figs. 3.12-3.14 are compared to observations from Mollamahmutoglu et al. (2003), there are additional areas for which liquefaction occurrences match with the predictions of the proposed procedure. By comparing the scenario earthquake hazard maps obtained from L_S and *LPI* methods with those obtained from PLHA for a return period of 475 years, it can be concluded that the probabilistic maps (Figs. 3.9-3.11) are predicting higher hazard due to the selected return period and consideration of numerous earthquake events.

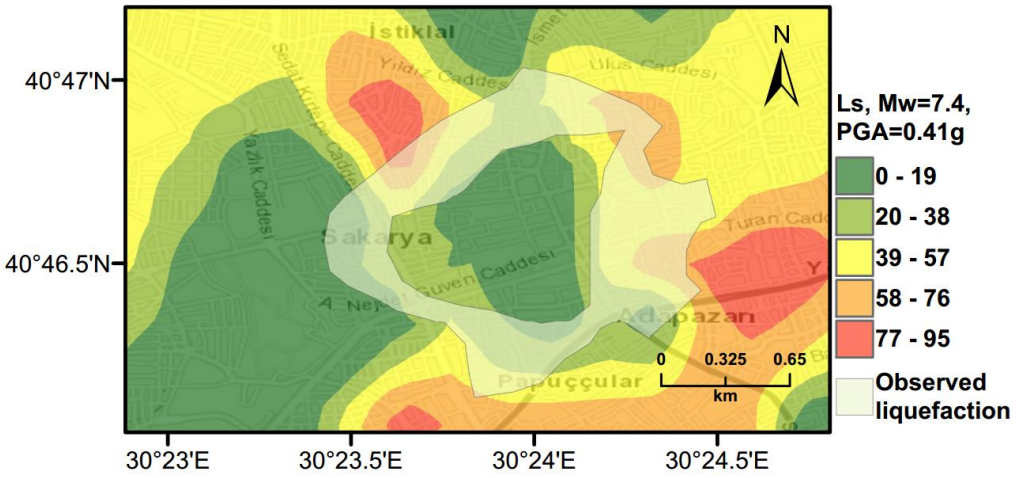

Figure 3.12 Scenario earthquake liquefaction hazard map in terms of L_S for central part of Adapazari city for Mw=7.4 and PGA=0.41g.

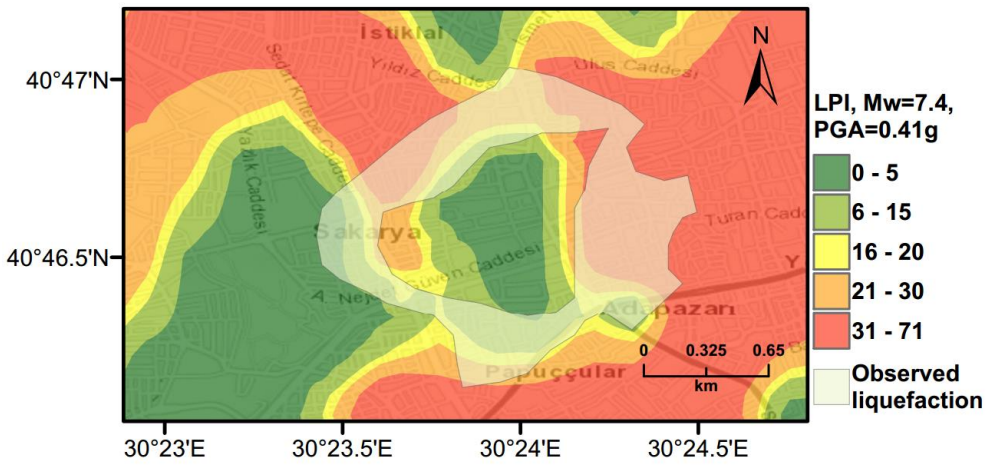

Figure 3.13 Scenario earthquake liquefaction hazard map in terms of LPI for central part of Adapazari city for Mw=7.4 and PGA=0.41g.

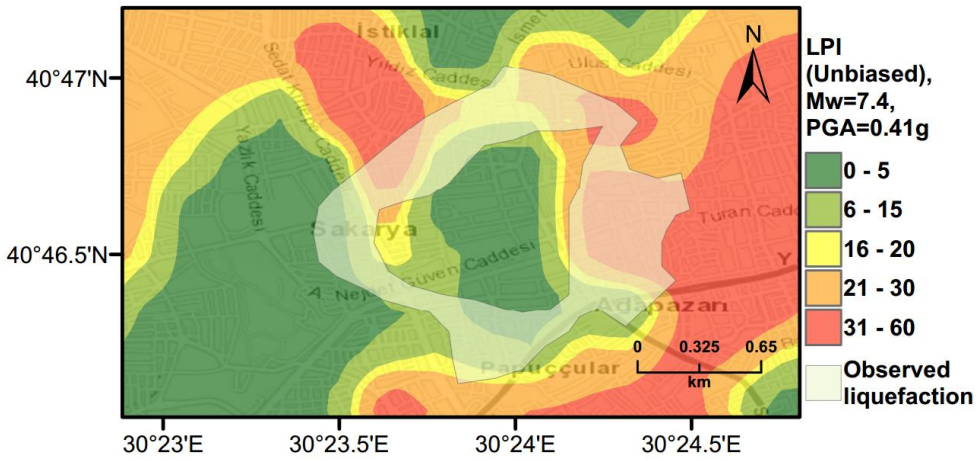

Figure 3.14 Scenario earthquake liquefaction hazard map in terms of unbiased LPI for central part of Adapazari city for Mw=7.4 and PGA=0.41g

3.5 Large Scale Case Study: Marmara region

Currently, there is no liquefaction hazard map available at a regional scale for Turkey and particularly for the Marmara region. To address this need, a set of liquefaction hazard maps for 475 years return period are prepared. Ground water level (GWT) is conservatively assumed around 1 meter across the region, while slope based V_{s30} data from USGS (2019) is utilized to perform PLHA. In Figs. 3.15-3.18, *LPI* and L_S procedures are utilised considering Poisson and time-dependent (Renewal) hazard models. From the obtained hazard maps, additional

liquefaction areas can be observed in the western part of the Marmara region for the time-dependent model. This is due to the fact that the major faults did not rupture in the western part of the Marmara for long period of time, while relatively recent earthquakes have occurred in the eastern part. This lowered the time-dependent seismic hazard and as a consequence slightly reduces the liquefaction hazard in the eastern part of the region.

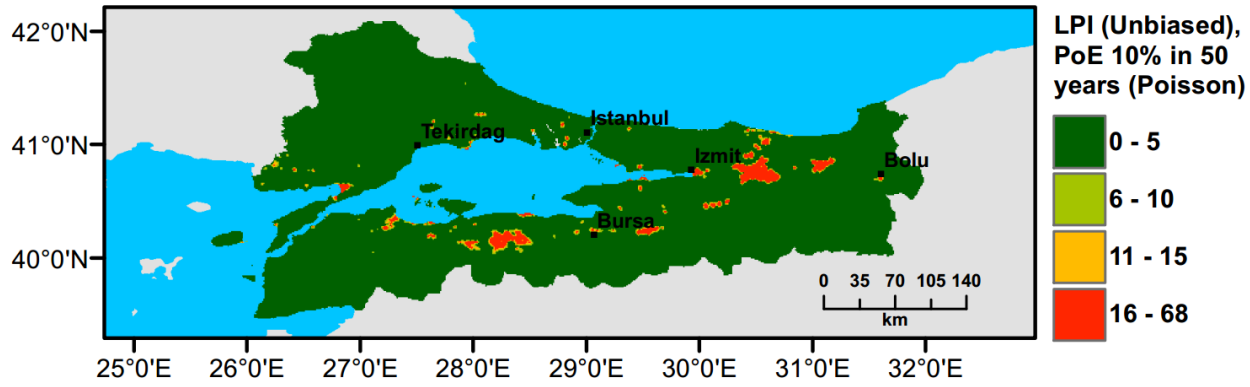

Figure 3.15 PLHA map for the Marmara region in terms of unbiased LPI for 475 years return period based on Poisson model.

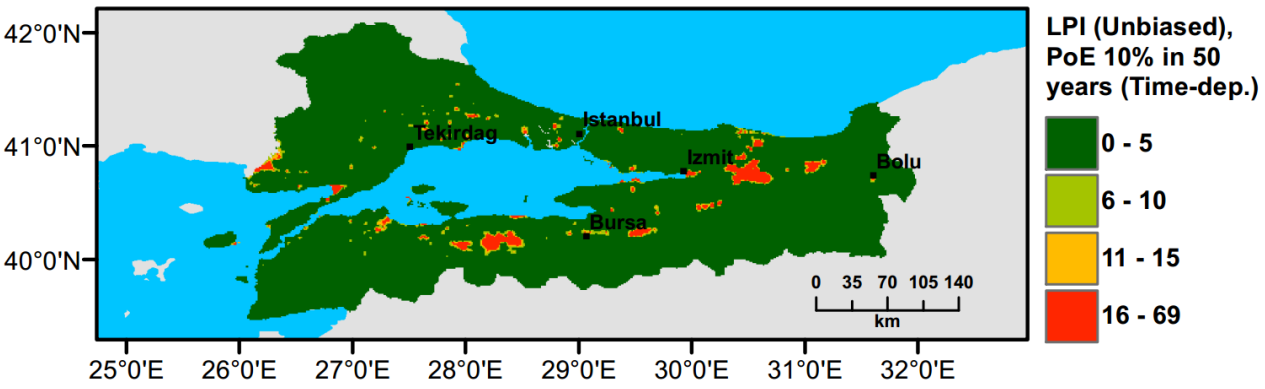

Figure 3.16 PLHA map for the Marmara region in terms of unbiased LPI for 475 years return period based on time-dependent model

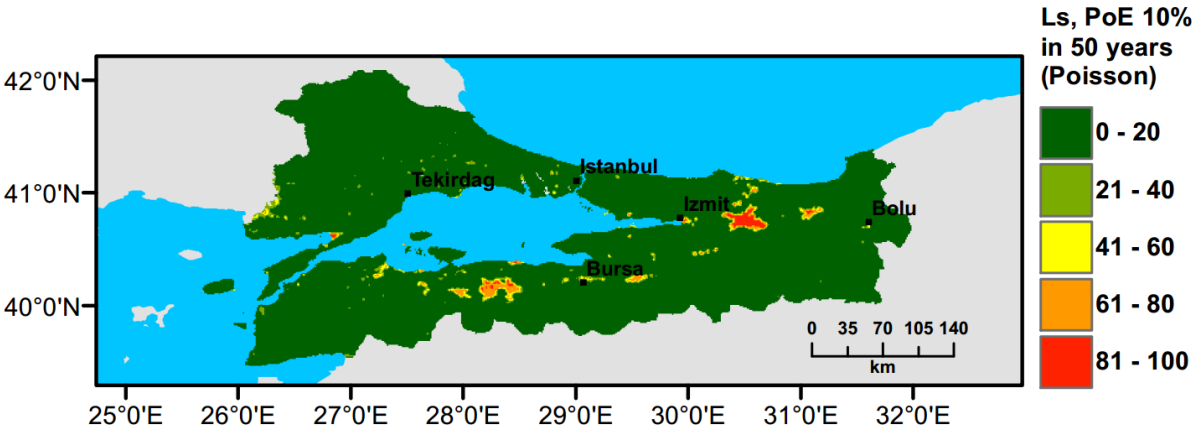

Figure 3.17 PLHA map for the Marmara region in terms of L_S for 475 years return period based on Poisson model.

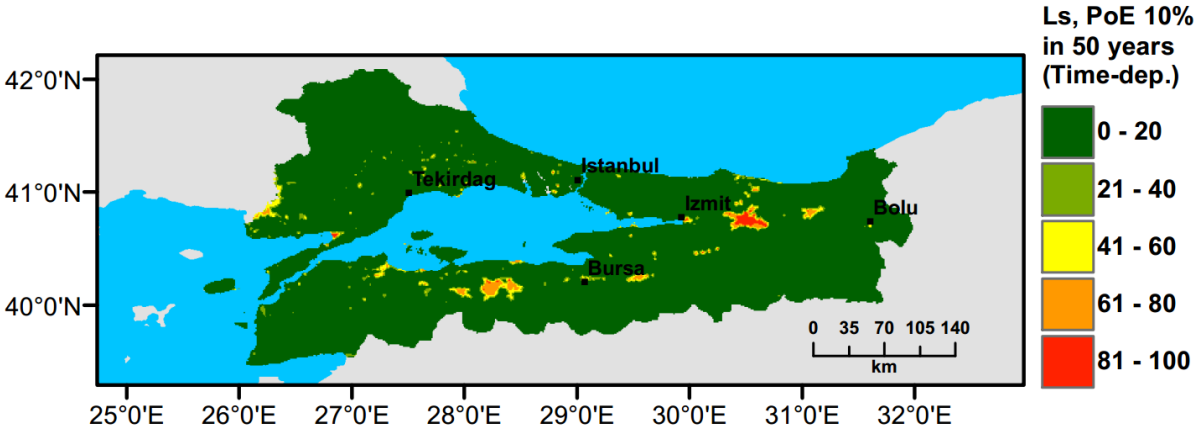

Figure 3.18 PLHA map for the Marmara region in terms of L_S for 475 years return period based on time-dependent model.

It should be noted that the liquefaction hazard maps developed for the Marmara region (Figs. 3.15-3.18) are indicative, rather than precise, due to the lack of detailed soil data and lower resolution (~17000 data points in total) in comparison to detailed micro-zonation studies. There are a number of local liquefaction hazard studies carried out for small areas in the Marmara Region, such as Inegol area studied by Sonmez (2003), Bolu area studied by Ulamis and Kilic (2007), Izmit bay studied by Sonmez (2008) and South of lake Manyas studied by Kürçer et. al. (2017). The results of these studies show good correlation with the liquefaction predictions shown in the PLHA maps developed by this study.

3.6 Conclusions

In this work, a PLHA procedure based on MC simulations is proposed to develop liquefaction hazard curves and PLHA maps for seismic prone regions. The developed procedure is practical and efficient as uncertainties in earthquake and soil related input parameters are randomised in a controlled way using distribution functions. In addition, the proposed procedure can automatically identify peak acceleration and magnitude couples that contribute the most to the liquefaction hazard, and therefore, the disaggregation of PSHA results is not required to perform PLHA. Both LPI and L_S liquefaction prediction methods are integrated into the procedure to quantify liquefaction hazard. Small and large scale case studies are performed for the city of Adapazari and the Marmara region of Turkey, respectively, to demonstrate the efficiency of the developed PLHA tool. A parametric analysis is also carried out to investigate the effect of different stress-reduction factor r_d calculation methods on liquefaction prediction parameters LPI and L_S and the distribution of earthquake magnitudes contributing to the liquefaction hazard. Liquefaction hazard curves and maps are prepared for the city of Adapazari in terms of LPI and L_S. Besides, indicative PLHA maps for the Marmara region are prepared using time-dependent and Poisson models in the PSHA. The following conclusions can be drawn from the present study:

1. The liquefaction hazard maps prepared for the city of Adapazari show good agreement with the observed liquefaction following the 1999 Kocaeli earthquake. The PLHA results show that the liquefaction hazard for Adapazari can be considered as very high.
2. The comparison of PLHA maps developed using the Poisson and time-dependent PSHA models for the Marmara region show that the time-dependent PSHA model identifies additional areas of non-negligible liquefaction hazard in the region.
3. The r_d procedure used in the PLHA affects the magnitude-distance distribution and the

obtained LPI value. Disaggregation of liquefaction hazard shows that the contribution of earthquakes with magnitude M_w<6 to the liquefaction hazard is smaller in the r_d procedure that takes into account earthquake magnitude. The use of more refined r_d procedure by Cetin and Seed (2004) procedure, supports the findings of Green and Bommer (2019) that a lower bound magnitude for probabilistic liquefaction hazard analyses is M_w=5. The selection of lower bound magnitude is important for sites where the seismic hazard is dominated by lower magnitude events as it will have influence on the computed return period of liquefaction.

To conclude, the MC-based PLHA procedure proposed in this work can serve as an efficient tool for the development of liquefaction hazard curves and PLHA maps to use in performance-based design applications and for a better prediction of future hazard in loss estimation studies. The developed PLHA maps for Adapazari and the Marmara region will allow designers and decision-makers to assess the expected liquefaction hazard in these areas in more complete way due to consideration of numerous potential earthquake events considered in the proposed PLHA framework.

References

Akin, M. K., Kramer, S. L. & Topal, T. 2011. Empirical correlations of shear wave velocity (Vs) and penetration resistance (SPT-N) for different soils in an earthquake-prone area (Erbaa-Turkey). *Engineering geology,* 119**,** 1-17.

Andrus, R. D. & Stokoe, K. H. 2000. Liquefaction resistance of soils from shear-wave velocity. *Journal of Geotechnical and Geoenvironmental Engineering,* 126**,** 1015-1025.

Atkinson, G. M., Finn, W. D. L. & Charlwood, R. G. 1984. Simple computation of liquefaction probability for seismic hazard applications. *Earthquake Spectra,* 1**,** 107-123.

Bird, J. F., Bommer, J. J., Crowley, H. & Pinho, R. 2006. Modelling liquefaction-induced building damage in earthquake loss estimation. *Soil Dynamics and Earthquake Engineering,* 26**,** 15-30.

Boore, D. M., Thompson, E. M. & Cadet, H. 2011. Regional Correlations of VS30 and Velocities Averaged Over Depths Less Than and Greater Than 30 Meters. *Bulletin of*

the Seismological Society of America, 101**,** 3046-3059.

Bray, J. D., Sancio, R. B., Youd, L. F., Christensen, C., Cetin, K. O., Onalp, A., Durgunoglu, T., Stewart, J. P. C., Seed, R. B., Baturay, M. B. & Karadayilar, T. 2001. *Documenting Incidents of Ground Failure Resulting from the August 17, 1999 Kocaeli, Turkey Earthquake*. https://apps.peer.berkeley.edu/publications/turkey/adapazari/index.html: Pacific Earthquake Engineering Research Center. [Accessed 21/09 2019].

Bray, J. D., Sancio, R. B., Durgunoglu, T., Onalp, A., Youd, T. L., Stewart, J. P., Seed, R. B., Cetin, O. K., Bol, E. & Baturay, M. B. 2004. Subsurface characterization at ground failure sites in Adapazari, Turkey. *Journal of Geotechnical and Geoenvironmental Engineering*, 130, 673-685.

Cetin, K. O. & Seed, R. B. 2004. Nonlinear shear mass participation factor (rd) for cyclic shear stress ratio evaluation. *Soil Dynamics and Earthquake Engineering,* 24**,** 103-113.

Cornell, C. A. 1968. ENGINEERING SEISMIC RISK ANALYSIS. *Bulletin of the Seismological Society of America,* 58**,** 1583-1606.

Finn, W. D. L. & Wightman, A. Logical evaluation of liquefaction potential using NBCC 2005 probabilistic ground accelerations. Proc. of the 9th Canadian Conf. on Earthquake Eng, 2007. 1984-1993.

Franke, K. W., Ulmer, K. J., Ekstrom, L. T. & Meneses, J. F. 2016. Clarifying the differences between traditional liquefaction hazard maps and probabilistic liquefaction reference parameter maps. *Soil Dynamics and Earthquake Engineering,* 90**,** 240-249.

Goda, K., Atkinson, G. M., Hunter, J. A., Crow, H. & Motazedian, D. 2011. Probabilistic liquefaction hazard analysis for four Canadian cities. *Bulletin of the Seismological Society of America,* 101**,** 190-201.

Green, R. A. & Bommer, J. J. 2019. What is the smallest earthquake magnitude that needs to be considered in assessing liquefaction hazard? *Earthquake Spectra,* 35**,** 1441-1464.

Iwasaki, T. 1986. Soil liquefaction studies in Japan: state-of-the-art. *Soil Dynamics and Earthquake Engineering,* 5**,** 2-68.

Iwasaki, T., Arakawa, T. & Tokida, K.-I. 1984. Simplified procedures for assessing soil liquefaction during earthquakes. 3(1)**,** 49-58.

Iwasaki, T., Tokida, K. I., Tatsuoka, F., Watanabe, S., Yasuda, S. & Sato, H. Microzonation for soil liquefaction potential using simplified methods. Proceedings of the 3rd international conference on microzonation, Seattle, 1982. 1310-1330.

Juang, C. H., Chen, C. J. & Jiang, T. 2001. Probabilistic framework for liquefaction potential by shear wave velocity. *Journal of geotechnical and geoenvironmental engineering,* 127**,** 670-678.

Juang, C. H. & Jiang, T. 2000. Assessing probabilistic methods for liquefaction potential

evaluation. *Soil dynamics and liquefaction 2000,* 148-162.

Juang, C. H., Jiang, T. & Andrus, R. D. 2002. Assessing probability-based methods for liquefaction potential evaluation. *Journal of Geotechnical and Geoenvironmental Engineering,* 128**,** 580-589.

Juang, C. H., Liu, C.-N., Chen, C.-H., Hwang, J.-H. & Lu, C.-C. 2008. Calibration of liquefaction potential index: A re-visit focusing on a new CPTU model. *Engineering Geology,* 102**,** 19-30.

Juang, C. H., Yang, S. H. & Yuan, H. 2005. Model uncertainty of shear wave velocity-based method for liquefaction potential evaluation. *Journal of geotechnical and geoenvironmental engineering,* 131**,** 1274-1282.

Kc, S., Bhochhibhoya, S., Adhikari, P., Adhikari, P. & Gautam, D. 2020. Probabilistic seismic liquefaction hazard assessment of Kathmandu valley, Nepal. *Geomatics, Natural Hazards and Risk,* 11**,** 259-271.

Kongar, I., Rossetto, T. & Giovinazzi, S. 2017. Evaluating simplified methods for liquefaction assessment for loss estimation. *Natural Hazards and Earth System Sciences Discussions,* 17**,** 781-800.

Kramer, S. L. & Elgamal, A.-W. M. 2001. *Modeling soil liquefaction hazards for performance-based earthquake engineering,* University of California, Berkeley, Pacific Earthquake Engineering Research Center, College of Engineering.

Kramer, S. L. & Mayfield, R. T. 2007. Return period of soil liquefaction. *Journal of Geotechnical and Geoenvironmental Engineering,* 133**,** 802-813.

Kürçer, A., Özaksoy, V., Özalp, S., Güldoğan, Ç. U., Özdemir, E. & Duman, T. Y. 2017. The Manyas fault zone (southern Marmara region, NW Turkey): active tectonics and paleoseismology. *Geodinamica Acta,* 29**,** 42-61.

Liao, S. S. C. & Whitman, R. V. 1986. *A catalog of liquefaction and non-liquefaction occurrences during earthquakes,* Department of Civil Engineering, MIT.

Maurer, B. W., Green, R. A., Cubrinovski, M. & Bradley, B. A. 2014. Evaluation of the liquefaction potential index for assessing liquefaction hazard in Christchurch, New Zealand. *Journal of Geotechnical and Geoenvironmental Engineering,* 140**,** 04014032.

Mollamahmutoglu, M., Kayabali, K., Beyaz, T. & Kolay, E. 2003. Liquefaction-related building damage in Adapazari during the Turkey earthquake of August 17, 1999. *Engineering Geology,* 67**,** 297-307.

Murru, M., Akinci, A., Falcone, G., Pucci, S., Console, R. & Parsons, T. 2016. M≥ 7 earthquake rupture forecast and time-dependent probability for the Sea of Marmara region, Turkey. *Journal of Geophysical Research: Solid Earth,* 121**,** 2679-2707.

Musson, R. M. W. 1998. The Barrow-in-Furness earthquake of 15 February 1865: liquefaction from a very small magnitude event. *pure and applied geophysics,* 152**,** 733-745.

Putti, S. P. & Satyam, N. 2018. Ground response analysis and liquefaction hazard assessment for Vishakhapatnam city. *Innovative Infrastructure Solutions,* 3**,** 12.

Rahman, M. Z., Siddiqua, S. & Kamal, A. M. 2015. Liquefaction hazard mapping by liquefaction potential index for Dhaka City, Bangladesh. *Engineering geology,* 188**,** 137-147.

Salloum, T. 2008. *Probabilistic assessments of soil liquefaction hazard.* Carleton University.

Seed, H. B. & Idriss, I. M. 1971. Simplified procedure for evaluating soil liquefaction potential. *Journal of Soil Mechanics & Foundations Div*.

Sianko, I., Ozdemir, Z., Khoshkholghi, S., Garcia, R., Hajirasouliha, I., Yazgan, U. & Pilakoutas, K. 2020. A practical probabilistic earthquake hazard analysis tool: case study Marmara region. *Bulletin of Earthquake Engineering*, 18, 2523-2555

Sonmez, B. & Ulusay, R. 2008. Liquefaction potential at Izmit Bay: comparison of predicted and observed soil liquefaction during the Kocaeli earthquake. *Bulletin of Engineering Geology and the Environment,* 67**,** 1-9.

Sonmez, H. 2003. Modification of the liquefaction potential index and liquefaction susceptibility mapping for a liquefaction-prone area (Inegol, Turkey). *Environmental Geology,* 44**,** 862-871.

Sonmez, H. & Gokceoglu, C. 2005. A liquefaction severity index suggested for engineering practice. *Environmental Geology,* 48**,** 81-91.

Toprak, S. & Holzer, T. L. 2003. Liquefaction potential index: field assessment. *Journal of Geotechnical and Geoenvironmental Engineering,* 129**,** 315-322.

Ulamis, K. & Kilic, R. 2008. Liquefaction potential of Quaternary alluvium in Bolu settlement area, Turkey. *Environmental geology,* 55**,** 1029-1038.

Yoshida, N., Tokimatsu, K., Yasuda, S., Kokusho, T. & Okimura, T. 2001. Geotechnical aspects of damage in Adapazari city during 1999 Kocaeli, Turkey earthquake. *Soils and foundations,* 41**,** 25-45.

Youd, T. L. & Idriss, I. M. 1997. Proceedings of the NCEER workshop on evaluation of liquefaction resistance of soils.

Chapter 4: Probabilistic Seismic Risk Assessment Framework: case study Adapazari, Turkey

Sianko I**, Ozdemir Z, Khoshkholghi S, Hajirasouliha I, Pilakoutas K. Probabilistic Seismic Risk Assessment Framework: case study Adapazari, Turkey.* ***Ready for publication.

ABSTRACT

Earthquake disasters have a significant impact on economic growth and social welfare of earthquake prone regions. A probabilistic seismic risk assessment can be employed to assess and mitigate the risks from future destructive events. The development of a seismic risk model is a challenging process for loss estimation due to numerous parameters and their uncertainties involved in the process. In a previous study, a probabilistic seismic hazard analysis (PSHA) tool based on the Monte-Carlo approach was developed to predict the seismic hazard for high seismicity areas. In this study, a seismic risk assessment framework is developed by incorporating the previously developed PSHA tool, with vulnerability functions based on various damage criteria, exposure and casualty models. Epistemic uncertainty is addressed by the employment of logic trees and distribution functions for input parameters. The developed seismic risk assessment framework can estimate human and economic losses for particular return periods using an event-based stochastic procedure. The proposed framework is applied to a case study area, the city of Adapazari in Turkey, by utilising readily available data. Seismic hazard and risk maps for different return periods are developed to identify the most vulnerable areas of the city. The verification of the developed seismic risk framework is performed by comparing the predicted seismic losses to those observed during the past 1999 Kocaeli earthquake that severely affected the city of Adapazari. The results of the study indicate that while overall predictions for extensive and complete damage states demonstrate strong correlation with the observed data, accurate risk predictions at the district level are not achievable with conventional procedures.

4.1 Introduction

Earthquakes may have a huge negative impact on economic welfare and resilience of communities, particularly in developing countries. Destructive social and economic consequences of earthquakes on structures and society have been seen following several major events (such as Haiti (2010), Tohoku (2011) and Nepal (2015) earthquakes). The rapid urbanisation of earthquake prone areas makes seismic risk assessment more important than previous decades. The development of a seismic risk model for loss estimation in earthquake prone regions is a challenging process due to numerous parameters involved in the process and their uncertainties.

There are commercial risk assessment tools that are normally used by insurance and reinsurance industries. Often these tools are presented as "black boxes" and the user is limited to the pre-defined procedures and input parameters (Bommer et al., 2006). As a result, region specific modifications to the hazard and vulnerability models are difficult to implement. Moreover, the assumptions and uncertainties adopted in these commercial tools are not controlled by the user (Bommer et al., 2006) and the processes of the conversion of input to output are not transparent (Musson and Winter, 2012). Also, there are existing probabilistic seismic hazard models available to the public at the regional or country level, that can be used in seismic risk calculations. However, these models only provide data for specific return periods or soil conditions (e.g. SHARE project and Unified Hazard Tool by USGS). The hazard results from these models are available for a limited number of regions or countries for which they were developed and cannot be easily implemented in the risk calculations.

An open access unified European Seismic Risk Model (ESRM20) is under development as part of the Horizon 2020 SERA project (Silva et al., 2020). The open-source earthquake risk software OpenQuake is used in ESRM20, which is also using event-based hazard and risk calculations similar to this work. State-of-art seismic risk studies are required to verify and

calibrate the seismic risk models developed within ESRM20. The estimation of damage or losses from past events can provide opportunity to compare the estimated and observed impacts, hence providing valuable cross-check for ESRM20 developers.

This work aims to develop a practical yet comprehensive seismic risk assessment framework for the areas with limited information on hazard, vulnerability and exposure. The proposed framework is based on a stochastic Monte-Carlo procedure, that generates synthetic earthquake catalogues by randomizing key input parameters. The main advantage of this procedure is that uncertainties in input parameters can be addressed with distribution functions with its means and standard deviations in an efficient manner (Musson, 2000). Moreover, logic trees with weightings for each branch can be easily employed within the procedure when required. The main drawback of the procedure is that it can become computationally expensive with both increasing complexity of the model and desired level of accuracy. In the developed framework, fault source zones and background seismicity are considered in the seismic hazard model. Appropriate fragility functions based on various damage criteria and ground motion intensity measures are selected and converted to vulnerability functions using a consequence model to find mean damage ratios (MDRs). While exposure model is generally obtained from the detailed census data, a practical procedure is proposed to collect building stock information by mapping building footprints from satellite images and gathering data from remote street view survey when census data is not available.

To demonstrate the capability of the developed seismic risk assessment framework, the city of Adapazari in Marmara region (Turkey) is selected as a case study area. The city is located in a high seismicity area and was previously hard hit by earthquakes events in the 20th century. This work contributes to the development of country-specific disaster risk profiles which helps to achieve targets identified within the Sendai Framework for Disaster Risk Reduction. The results of the study are presented in form of seismic loss curves and seismic risk maps for

Adapazari. A scenario earthquake similar to the 1999 Kocaeli earthquake is used to compare predicted damage with observed damage after that event.

4.2 Probabilistic seismic risk procedure

Seismic Risk analysis entails a set of earthquakes, the associated consequences (e.g. damage and loss) and the probabilities of occurrence of these consequences over different time periods (Erdik, 2017). There are numerous seismic risk studies performed that are based on available engines or frameworks (e.g. Chaulagain et al., 2015; Silva et al., 2015). In this work, new seismic risk framework is proposed with general procedure for calculating mean damage ratio using Monte-Carlo simulations described in detail. Seismic risk calculation is based on three main parts (Fig. 4.1): seismic hazard, vulnerability and exposure models., To address each of the components, a brief discussion on seismic hazard, fragility functions, consequence and exposure models are presented in this section.

Figure 4.1 Probabilistic Graphical representation of the risk components.

4.2.1 Seismic hazard model

Assessment of seismic hazard is an essential component of seismic risk analysis. In a previous study, Monte-Carlo based PSHA was developed as part of the seismic risk assessment framework proposed in this work. Monte-Carlo simulations are used to generate synthetic earthquake catalogues to represent future seismicity. One of the main advantages of the Monte-

Carlo procedure over conventional PSHA is the capability of taking into account the spatial variability with intra-event residuals and the efficient way of treating aleatory uncertainties. Conventional PSHA pioneered by Cornell (1968) lacks this advantage and as a result underestimates the total loss value at high return periods (Jayaram and Baker, 2009). This is due to ground motions considered perfectly correlated and the intra-event component of the aleatory variability is treated as inter-event variability, which results in ground motions to be log-normally distributed about the median motion (Bommer and Crowley, 2006). The detailed information on the Monte-Carlo based seismic hazard procedure employed in this work can be found in Sianko et al. (2020).

4.2.2 Fragility/Vulnerability models

Fragility curves can be used to predict the probability of exceedance of certain limit/damage states for a given intensity measure value. It is common for structures to use four damage states as follows: slight, moderate, extensive and complete damage (e.g. FEMA (2003)). Consequence models, which are defined as the cost of loss to the rebuilding cost for a given damage state, can be used to convert a set of fragility curves into vulnerability curves (Erdik, 2017; Kohrangi et al., 2021a). Vulnerability models are generally defined as mean damage ratio (MDR) conditioned on ground motion intensity level. MDR for a given ground motion intensity level can be calculated by summing products of damage ratios and proportions of the buildings that correspond to each damage state.

4.2.3 Exposure model

A reliable exposure model for buildings is essential to perform a realistic earthquake risk analysis. Exposure models provide useful information on the location, replacement costs, occupants numbers of the building, in addition to its vulnerability class. Up-to-date data that can be used in exposure models is often unavailable, particularly in developing countries where

built environment altering rapidly and gathered data becomes outdated quickly. Normally the exposure models heavily rely on the national housing census of a country. These censuses are usually repeated every 10 years and performed at administrative division resolution. The quality of the data collected by each country is not consistent, which makes the development of an exposure model a challenging part of the risk analysis (Silva et al., 2018).

The main goal of the exposure model is to obtain a layer of uniform resolution across the study area with spatially distributed structures that are classified according to selected building taxonomy. The taxonomy for the characterization of the exposed building stock and the description of its damage should be compatible with the fragility/vulnerability relationships that will be considered in the risk assessment process (Erdik, 2017). For estimating economic and social losses, an exposure model might need to contain additional information about the estimated replacement cost of the structures and expected number of occupants depending on the time of a day as it can affect number of casualties. Rapid survey procedures can be performed such as utilisation of satellite imagery and from volunteered data in cases where the census data is outdated or missing vital information that is required for building exposure model (Wieland et al., 2015).

In addition to housing censuses, there are publicly available sources of data about housing in different countries e.g. UN Housing database, UN Statistical Database on Global Housing and the World Housing Encyclopedia. Moreover, there are ongoing projects such as Prompt Assessment of Global Earthquakes for Response (PAGER) and Global Earthquake Model (GEM), that have an objective to develop global building inventory databases.

4.2.4 Casualty assessment

The large number of casualties in earthquake events is caused by the fact that most of the buildings are located in highly populated urban areas where severe earthquakes are responsible for high degree of destruction to the buildings (Tong et al., 2012). This is particularly important

as the number of fatalities caused by an earthquake is strongly dependent on the number of buildings that collapsed or were extensively damaged (Coburn et al., 1992; Feng et al., 2013; So and Spence, 2013). There are two main approaches for estimating casualties after an earthquake event. The first approach is empirical, where fatality rate is estimated based on ground motion intensity level and population exposed (Jaiswal et al., 2009). The casualty estimates using this approach are not satisfactory (Ranjbar et al., 2017), as shaking intensity is not directly linked to the number of deaths and also depends on vulnerability of the building stock. The second approach is semi-empirical and based on relationship between the buildings damage and the number of casualties. In this work, casualty models based on the second approach will be employed.

The casualty model proposed by So and Spence (2013) is a semi-empirical model that was tested against actual casualty data from previous events. The model is capable of considering different building classes (structural systems) to alter lethality rates for extensively damaged and collapsed buildings. In this casualty model, the number of people killed due to collapse or extensive damage of buildings K for a given building class is defined as:

$$K = O * P * (d5 * L5 + d4 * L4) \tag{4.1}$$

where, O is occupancy rate at the time of earthquake and P is the average number of people normally reside in a building. $d5$ and $d4$ are the number of the buildings that collapse and extensive damaged respectively. $L5$ and $L4$ are the lethality rates representing the proportion of occupants killed, for buildings that collapse ($d5$) and extensively damaged ($d4$) respectively.

The second model used in analysis is proposed by Coburn et al. (1992), and considers only collapse damage state for casualty estimations. On the other hand, this model has additional parameters as occupants trapped by collapse and mortality post-collapse. The number of fatalities in this model K is expressed as follows:

$$K = D5 * (M1 * M2 * M3 * (M4 + M5 * (1 - M4)) \quad (4.2)$$

where, $D5$ is the number of collapsed buildings, $M1$ represents the population per building, $M2$ is the occupancy rate at the time of earthquake, $M3$ is the number of occupants trapped by collapse, $M4$ and $M5$ are lethality rates for collapse and post-collapse respectively.

4.2.5 Mean damage ratio

Mean damage ratio (MDR) represents the ratio of the cost of repairing a structure to its replacement cost. It can be used to estimate loss by multiplying the ratio by the economic value of the structure. In the proposed framework, MDR can be found by utilising synthetic earthquake catalogues generated within Monte-Carlo simulations, where each earthquake source zone has as separate synthetic catalogue. Then, for each earthquake in synthetic catalogue MDR at the site is calculated for a given ground motion intensity and vulnerability model. Largest MDR value is identified across all source zones for each year of catalogues length. In other words, the worst-case scenario from all seismic sources affecting the site of interest is considered as an annual maximum outcome. This step is applied for all simulations and the results are merged in a single list. The probability of exceedance of certain MDR value can be found by sorting all annual outcomes in descending order and by finding the N^{th} MDR value in the sorted list. For the desired return period, N can be calculated using the following equation:

$$N = (\frac{1}{Return\ period} \times\ Catalogue\ length \times Number\ of\ simulations) + 1 \quad (4.3)$$

The sorted list of obtained MDR can be plotted against its annual frequency of exceedance to result in a loss curve. Fig. 4.2 shows the flowchart of the procedure for finding probability of exceedance of MDR using Monte-Carlo simulations procedure.

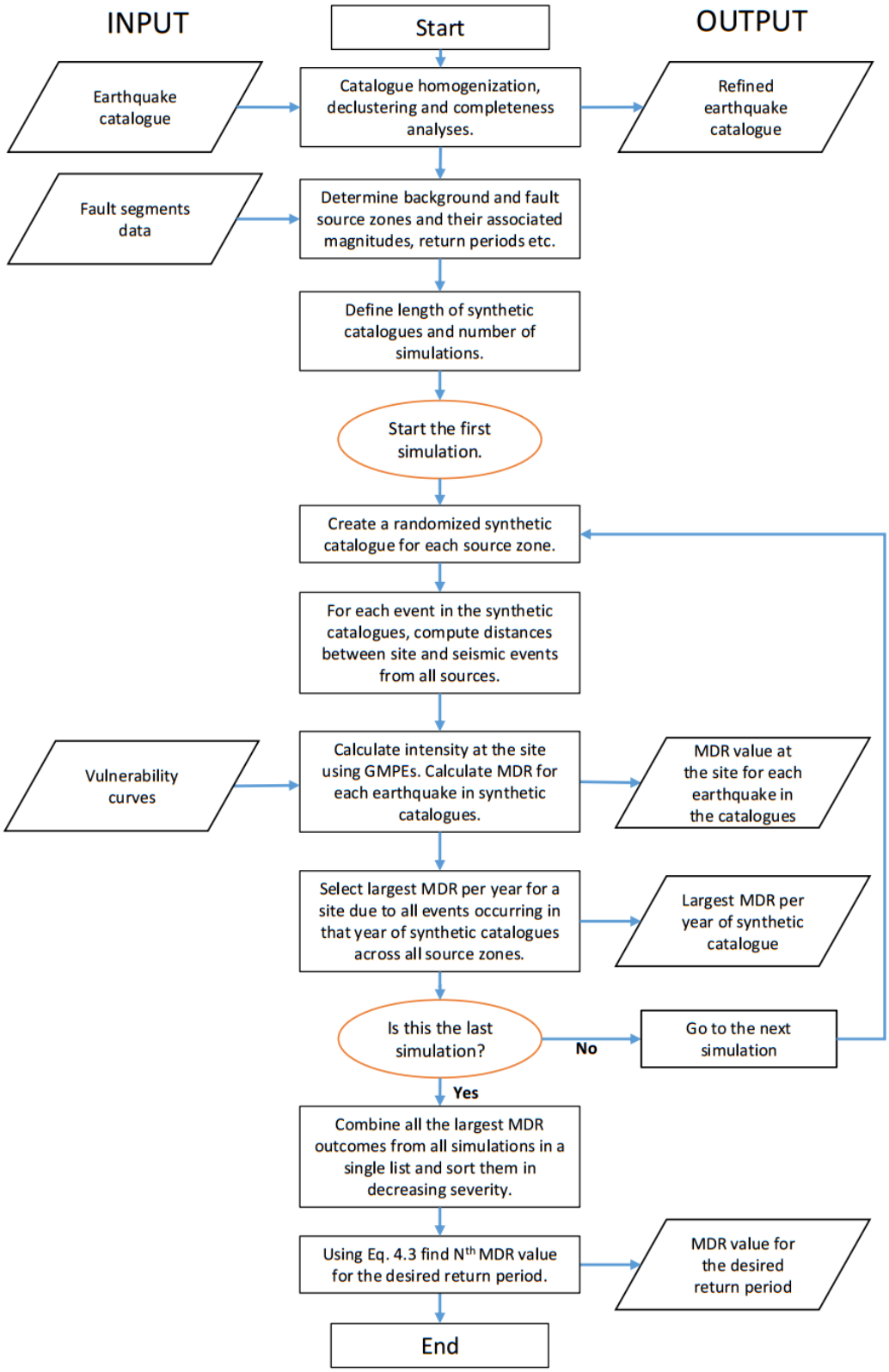

Figure 4.2 The proposed MC-based earthquake risk assessment procedure to calculate mean damage ratio (MDR).

The previous sections provided a general overview of the main components used in the

proposed framework. To verify the effectiveness and integrity of the framework, the following section uses the city of Adapazari in Turkey as a case study area.

4.3 Seismic hazard model for Adapazari

To test the capability of the developed seismic risk assessment framework, the city of Adapazari in Marmara region (Turkey) is selected as a case study area. The Marmara region is located in one of the most seismically active regions in the world and was subjected to multiple earthquakes during the 20th century. The North Anatolian Fault (NAF) lies across northern Turkey for more than 1,500 km starting from Karliova in the east and extending to the Gulf of Saros in the west. The western portion of the NAF zone dominates the tectonic regime of the Marmara Sea area.

The 1999 Kocaeli earthquake was the latest major earthquake event that ruptured the North Anatolian fault in the Marmara region. Due to its close proximity to the fault, Adapazari was one of the most severely damaged cities during this earthquake. Enormous economic losses, extensive structural damage to structures and a high fatality rate were observed in the city after the earthquake. There is a high probability of another devastating seismic event that might occur in the Marmara region in the foreseeable future (Erdik et al., 2004; Murru et al., 2016). Although, Adapazari can be potentially affected by this future event, there are no probabilistic seismic risk studies performed for the city. This highlights the need of a seismic risk assessment for Adapazari, as it is a vital resource for earthquake preparedness and risk mitigation (Erdik, 2017).

4.3.1 Earthquake source zones

In this work, the earthquake source zones model is adopted from Sianko et al. (2020) and consists of background source zones (BSZs) and fault source zones (FSZs) used to generate synthetic earthquake catalogues. In total there are 17 BSZs (Fig. 4.3) and 25 FSZs (Fig. 4.4)

with unique earthquake recurrence parameters. BSZs are based on Gutenberg-Richter relationship, while FSZs are utilising characteristic magnitude M_{char}. Aleatory uncertainty is taken into account by randomizing key earthquake parameters with distribution functions during generation of synthetic catalogues.

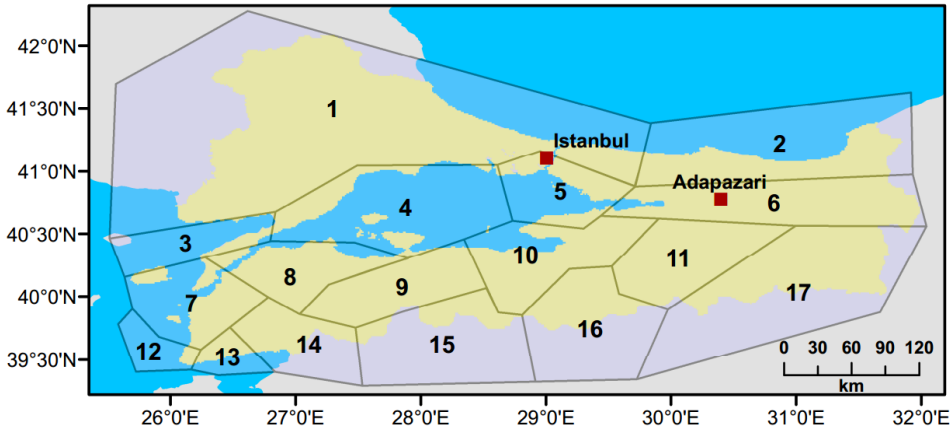

Figure 4.3 BSZs model used in the PSHA for this study (Sianko et al. 2020).

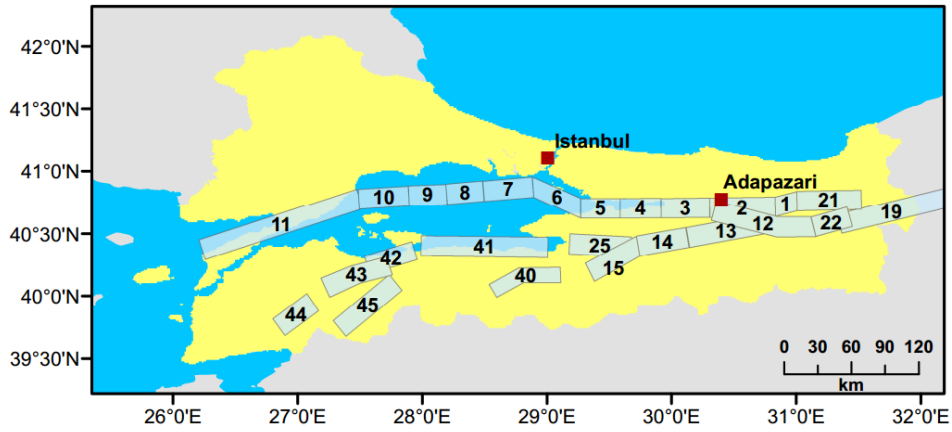

Figure 4.4 FSZs model used in the PSHA for this study (Sianko et al. 2020).

4.3.2 Ground motion prediction equations (GMPEs)

Ground motion prediction equations have a big impact on both seismic hazard and seismic risk predictions (Silva et al., 2015). In this study, the GMPEs proposed by Akkar et al. (2014) and Boore et al. (2014) are used to predict ground motion intensities in terms of PGV, Sa(T) and Sd(T). The GMPE provided by Akkar et al. (2014) mainly consists of earthquake records from Italy, Turkey and Greece and the majority of records for strike-slip mechanism events with M>7 are obtained from earthquakes occurred in the Marmara region. The GMPE provided

by Boore et al. (2014) has a correction coefficient for different countries in the world including Turkey. In Boore et al. (2014), inter-event and intra-event variabilities are determined for various magnitudes considering period, distance and soil conditions. Both GMPEs have a model for PGV, which is commonly used as ground motion intensity parameter in fragility functions for structures. Also both GMPEs are capable of considering various fault mechanisms and can utilise finite-fault (R_{JB}) distance metric, which can be considered more accurate for earthquakes occurring on the faults than point-source (R_{epi}). Local site effects can be estimated with relative ease as mentioned GMPEs are utilising widely available 30 m shear-wave velocity data, V_{s30}. This is particularly important as considerable part of the city of Adapazari is located in the areas prone to ground motion amplification. Epistemic uncertainty is addressed through employment of the logic tree, where 70% weight is given to Akkar et al. (2014) and 30% weight to Boore et al. (2014). Higher weight is given to the GMPE developed by Akkar et al. (2014) because such model contains a large proportion of recordings from Turkey. Both GMPEs are capable of estimating Sa(T) for wide range of periods and satisfy the criteria specified by Bommer et al. (2010) to be used in PSHA.

4.3.3 Site conditions

Most of the area of the city of Adapazari is located over deep alluvial sediments deposited by the Sakarya River (Bray et al., 2004). The sub-surface soil is heterogeneous with big variations in soil layers. The soil generally consists of silty clays, silty sands, clean fine sands and gravels. The groundwater level is changing with seasons but on average 1–2 m below the ground surface. Shallow groundwater level contributed to the occurrence of extensive liquefactions during the 1999 Kocaeli earthquake.

It is important to consider site effects in seismic hazard calculations for Adapazari due to the presence of soft soil and possible site amplification effects. The V_{s30} is a widely used parameter to characterize seismic site conditions due to its relative availability and generally

acceptable performance. Moreover, many recent GMPEs have site amplification functions based on V_{s30} values to take into account site conditions. The estimated topographic slope-based V_{s30} values are available globally through the web-based open-access USGS map server. The use of V_{s30} values obtained from topographic slope data can be used for large scale studies as shown by Riga et al. (2021). In this research the shear-wave velocities (V_{s30}) map shown in Fig. 4.5 is used in the PSHA performed for the city of Adapazari.

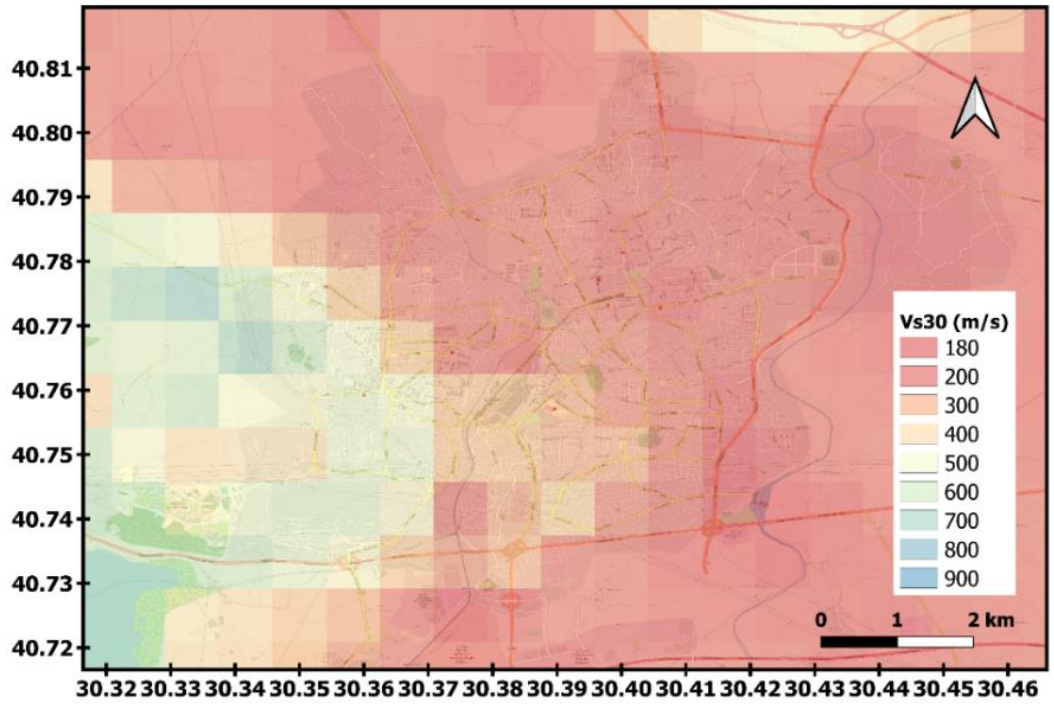

Figure 4.5 Shear-wave velocities (V_{s30}) map for the city of Adapazari used in the PSHA.

4.4 Exposure model for Adapazari

The development of an exposure model is a challenging process as the model needs to include data about the location, fragility and value of the structures. In this work, different sources of data are utilized to build the exposure model. The latest Building Census for Turkey was conducted in 2000, which makes it relatively outdated and considering rapid development of Adapazari it is not advised to fully rely on it. To address this problem, aerial and satellite images are used to perform building footprints mapping to quantify the number and area of the

buildings in Adapazari. In addition, satellite images from past decades are examined to track the expansion of the city. This allows to approximate construction period of the structures in different parts of the city. The 2011 Population and Housing Census is used to determine average household size, average number of floors as well as proportion of buildings constructed before and after 1980.

4.4.1 Building stock data

In this work, a novel method based on building footprint mapping is used to find the number of buildings and their locations in Adapazari. The study area is divided in a grid consisting of 58 cells as shown in Fig. 4.6. Cell dimension is 0.01x0.01 degrees and all the data collected is at the cell level. The total number of buildings considered in the analysis is 47283, where 31067 found from manual mapping (red coloured hatched area in Fig 4.6) and 16216 from assumed areas (green polygons in Fig. 4.6). In assumed areas, number of buildings is found by using density of buildings from adjacent mapped buildings areas. In this work, only residential buildings are used, thus public infrastructures, solely commercial or industrial buildings are not mapped or quantified, due to lack of the reliable fragility curves for such structures.

Adapazari is the capital of the Sakarya province for which the 2011 Population and Housing Census provides extra information about the building stock. From that census it is found that in the Sakarya province there are ~80% of low rise (1-3 stories) buildings and ~20% are mid-rise (4-6 stories), with 2.5 being an average number of floors. There are 23% of the buildings that are dated before 1980, 60.7% dated after 1980 and 16.3% are of unknown date of construction. According to 2000 Building Census, in Sakarya province ~63% of the buildings were RC frames and ~35% bearing wall construction. The data from Building Census is for a whole province including smaller town centers, where usually the higher proportion of buildings is bearing wall construction. Hence, it is safe to assume that the proportion of RC buildings in the city of Adapazari should be larger in comparison to the province data. In this

research it is assumed that 80% of the building stock is RC buildings and 20% are masonry with this ratio randomized within ±10% using uniform distribution in the Monte-Carlo simulations.

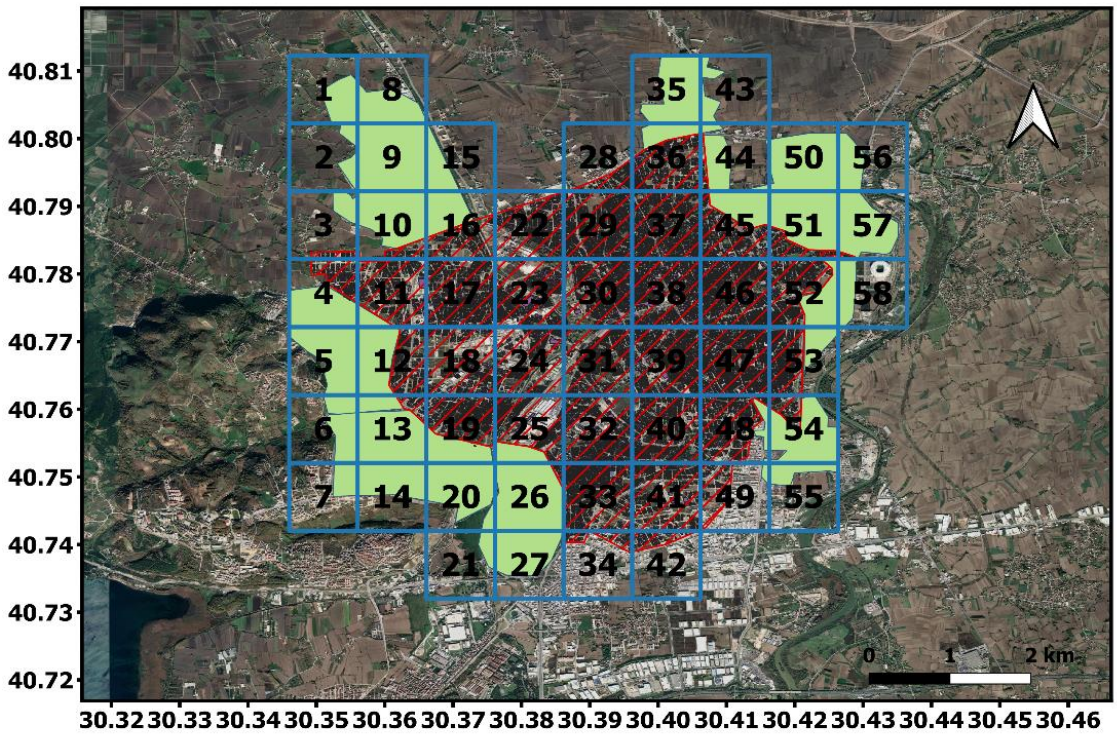

Figure 4.6 Cells structure, mapped buildings (red hatched area) and assumed areas (green polygons) for Adapazari.

The construction year of the buildings can be a useful parameter for selection of fragility curves, which in turn have an impact on seismic risk estimates. Seismic design guidelines in Turkey became more comprehensive after 1975 (Erdik et al., 2003), therefore in this study to reflect seismic resistance of the buildings, they are classified as pre-1980 (Low-Code) and post-1980 (High-Code). Satellite and aerial images from 1984, 1987, 1992, 1997 and 2005 are used to track development of the city and to assess age of the buildings inside of each cell. Fig. 4.7 shows example of images with substantial time difference that were used for visual inspection. It can be noticed from these images that the city expanded almost in all directions over the time period of 1984-2020.

a)

b)

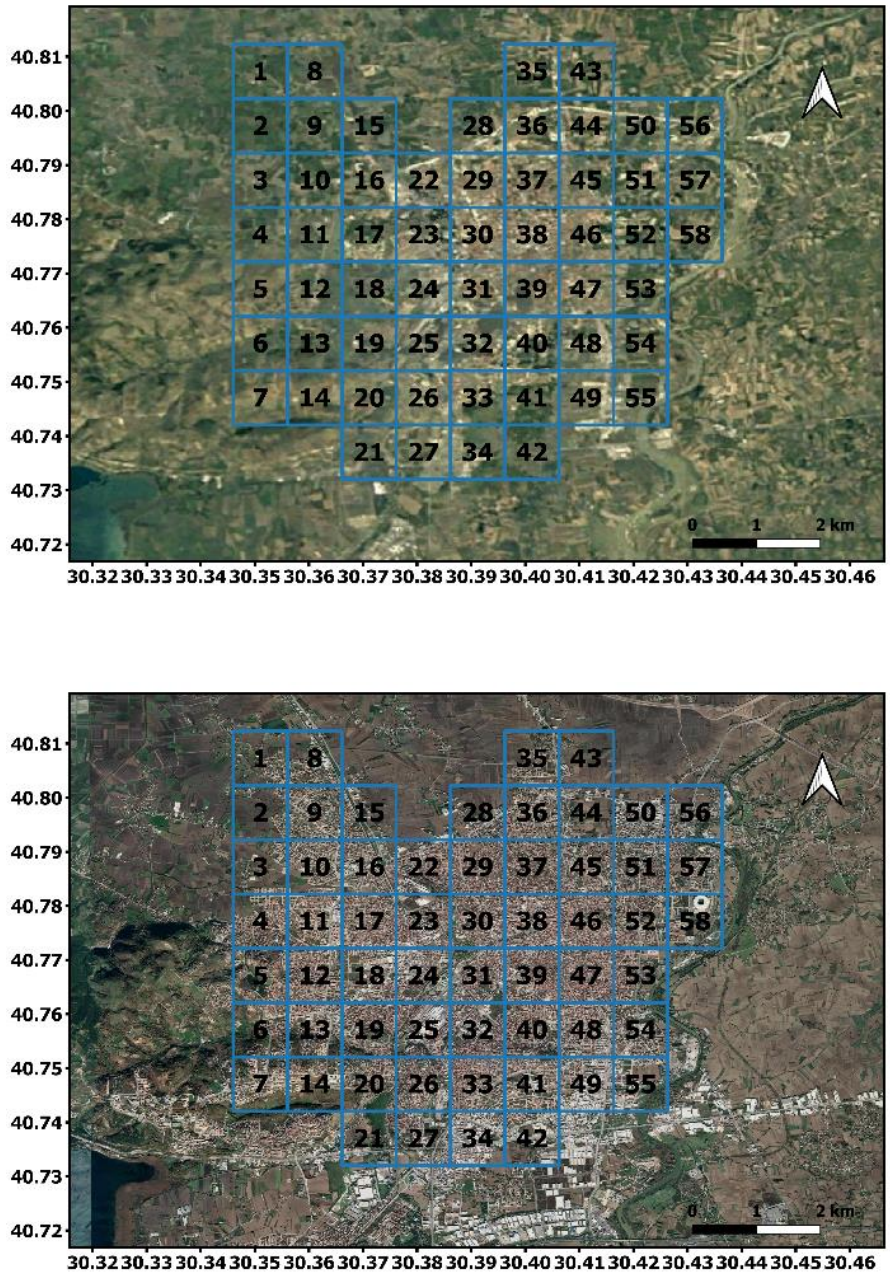

Figure 4.7 Images of Adapazari and suburb areas in 1984 (a) and 2020 (b).

Fig. 4.8 shows the result of visual inspection of satellite images represented with assigned code values, where 1 stands for high-code buildings and 2 is used for low-code buildings in the cell. This information will be used later in fragility functions capable of distinguishing low-code and high-code buildings.

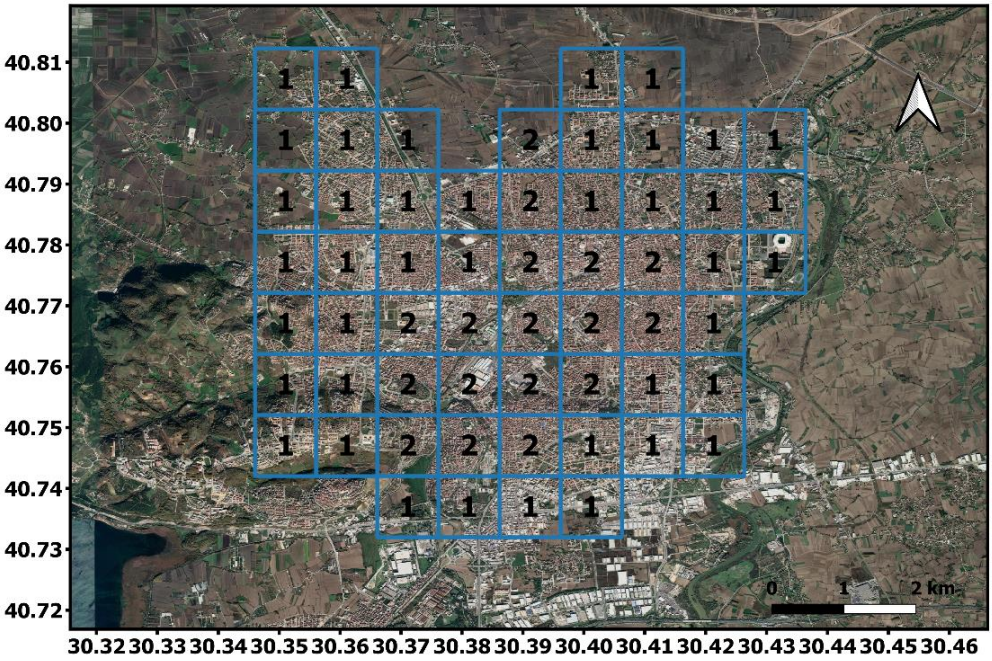

Figure 4.8 Grid developed for Adapazari with assigned 1 and 2 code values, which represent high-code and low-code buildings in the cell respectively.

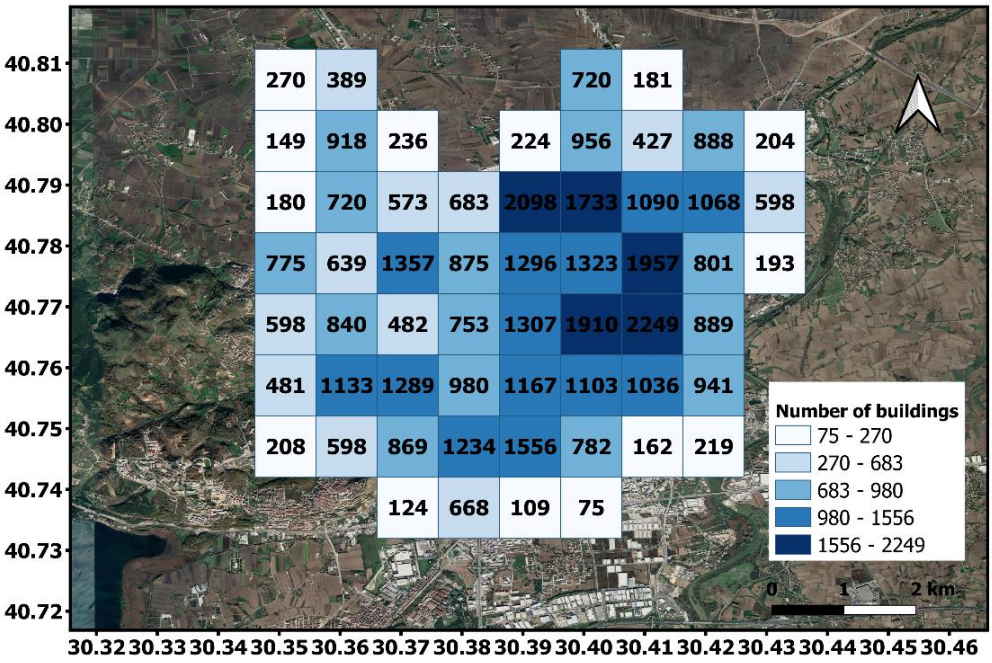

Figure 4.9 Total number of buildings in each cell.

Ground motion intensities from PSHA and scenario earthquake are calculated in the centres of the cells. For simplicity, buildings locations inside the cell are represented by the centroid of the cell, which is common assumption in seismic risk studies (e.g. Bommer et al., 2002;

Erdik et al., 2003). The total number of buildings in each cell is given in the Fig. 4.9.

New procedure of remote street survey (Google street view) is utilized at the nodes of the cell to determine the average floor height and verify the age of construction estimated from satellite images for each cell. In total 40 buildings are surveyed per cell (10 buildings surveyed per node of the cell).

4.4.2 Economic value and population

Once the spatial distribution of buildings is determined, the economic and population values need to be estimated to perform earthquake risk assessment. To find the roof area of buildings in the assumed areas (green polygons in Fig. 4.6) the distribution of the roof area across manually mapped buildings is utilised (Figure 4.10). The total roof area is the sum of the roof area of the mapped buildings and the roof area estimated from the assumed areas for each cell. From the total roof area, total floor area is predicted by multiplying roof area by the average storey number in the cell. Finally, cost of the buildings is found by multiplying total floor area by average cost of construction per sq. meter. According to Turkish Revenue Administration, the average cost of construction of RC residential buildings is ranging from 1330 TL for first class buildings to 2130 TL for premium class buildings. The average cost of construction per sq. meter is 1083 TL for first class masonry buildings and is 1671 TL for premium class masonry buildings. In this study, the average cost of construction per sq. meter is assumed to be 1730 TL (230 USD) and 1377 TL (180 USD) for RC buildings and masonry buildings, respectively (conversion rate 7.5 TL to 1 USD in March 2021). Following the calculations explained above, the total value of the building stock in the study area is estimated to be 5 850 977 411 USD.

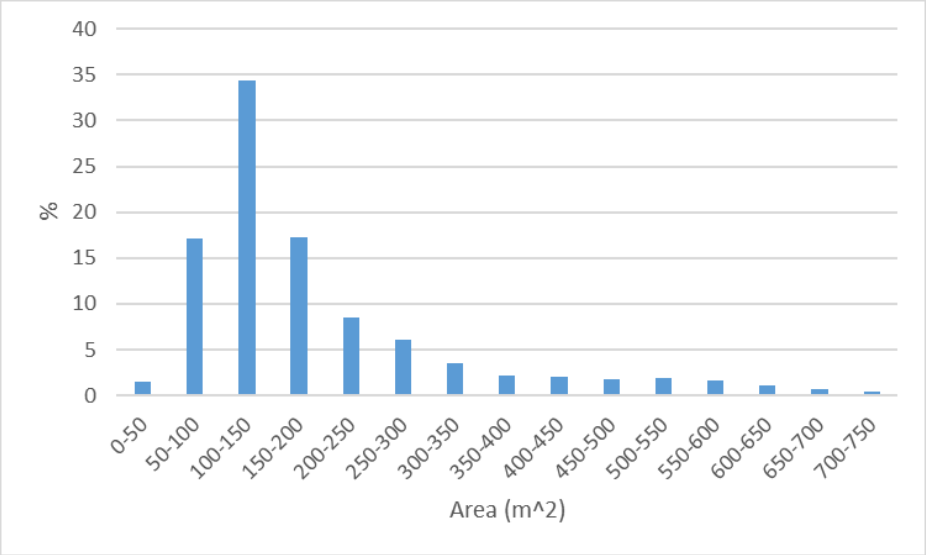

Figure 4.10 Roof area distribution from the mapped buildings.

According to 2011 Population and Housing Census data, the average household size is found to be 3.9 in Sakarya province. Population per cell is calculated with the floor area in the cell multiplied by 70% (to exclude commercial buildings), then multiplied by the average household size and divided by average dwelling area (130 sq. meters. in Adapazari). By summing the population of cells, the total population for the study area is found to be 538 178. This value is relatively close to the one provided on the Turkish statistics website (https://www.tuik.gov.tr/). In 2020, the city had a population of 517 000 when Adapazarı city center (279 000), Serdivan (148 802) and Erenler (90 855) districts are combined to represent the study area in this research.

4.5 Vulnerability model

The fragility and vulnerability models are the main sources of uncertainty in a seismic risk assessment procedure (Riga et al., 2017). Therefore, rigorous selection of these models is very important for accurate predictions of a seismic risk. In this study, fragility models developed for Turkish building stock are considered.

4.5.1 Fragility curves

This section of the paper provides an overview of the fragility curves that were considered for the seismic risk analysis in the case study area. Most of the analytical fragility curves, that are widely used in common practice, are not benchmarked against past earthquake events (Villar-Vega and Silva, 2017). Contrary, the fragility curves by Erdik et al. (2003), were obtained from post-earthquake damage data collected from Turkish building stock. These fragility curves are based on MSK-81 intensity and spectral displacement (Sd(T)) for damage states slight, moderate, extensive and complete. The spectral displacement demand is calculated from spectral accelerations and use using the displacement coefficient method given in FEMA356 (2000). Also, the fragility curves classification considers construction age by providing fragility curves for pre-1980 and post-1980 buildings, which can be useful for vulnerability model refinement in the areas where construction date is known. Moreover, Erdik et al. (2003) fragility curves classification includes buildings construction type (RC and masonry) and buildings with various number of heights (low-rise, mid-rise, high-rise). Fig. 4.11 shows an example of these fragility curves based on spectral displacement.

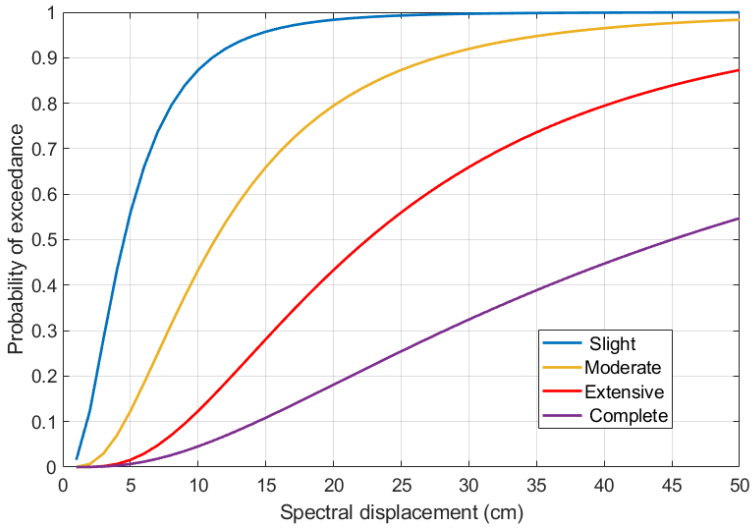

Figure 4.11 Fragility curves based on spectral displacement for post-1980 mid-rise RC frame buildings proposed by (Erdik et al. 2003).

Analytical fragility curves developed by Erberik (2008) are also used in this work. These

curves are based on PGV and derived from 28 RC buildings extracted from a building database of approximately 500 buildings in Duzce, Turkey, which were constructed between 1962 and 1999. The fragility curves were verified by comparing the predicted damage distributions to the actual damage data. The example of the fragility curves developed by Erberik (2008) for low-rise RC buildings, which use LS1 - serviceability, LS2 - damage control and LS3 - collapse prevention limit states are shown in Fig. 4.12.

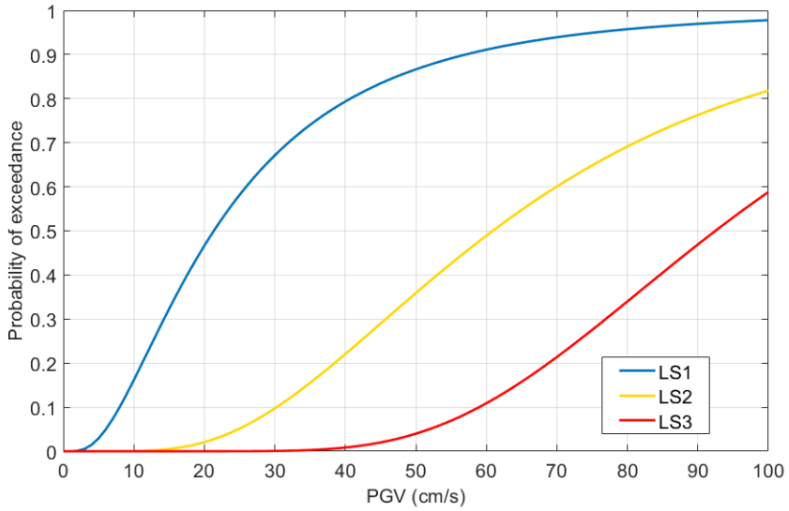

Figure 4.12 Fragility curves based on PGV for low-rise RC buildings (Erberik 2008).

Similar to Erberik (2008), Akkar et al. (2005) used a building database consisting of 32 low- rise and mid-rise typical RC buildings from Duzce (Turkey) to develop fragility curves based on PGV. Fig. 4.13 shows the fragility curve for 3-storey RC buildings with slight, moderate and severe damage states. Comparison of Figs. 4.12 and 4.13 shows that the fragility curves developed by Erberik (2008) and Akkar et al. (2005) are quite similar and the main difference comes from low PGV values in curves representing LS1, LS2 and light, moderate damage states respectively. For example, the fragility curves developed by Akkar et al. (2005) predict no moderate damage for PGV values less than or equal to 30 cm/s, while Erberik (2008) curves predict a probability of exceedance of ~10% for LS2. It can be concluded that the fragility curves developed by Akkar et al. (2005) are less conservative in terms of moderate damage in comparison to those developed by Erberik (2008).

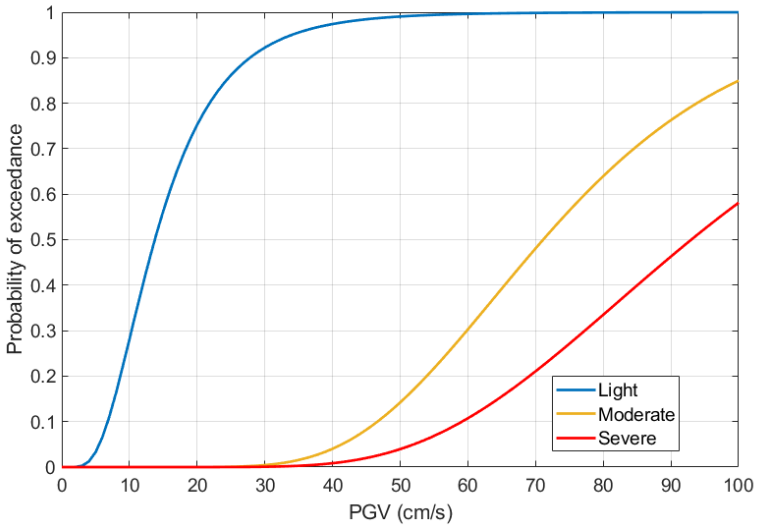

Figure 4.13 Fragility curves based on PGV for ordinary 3-storey RC buildings (Akkar et al. 2005).

Kirçil and Polat (2006) developed analytical fragility curves based on Sa(T), Sd(T) and PGA for RC frame buildings designed according to the Turkish seismic code published in 1975. They also proposed fragility curves for two different steel grades (S220 and S420), but often there is no data available on the proportion of buildings constructed with each type of reinforcement. Hence, it can be more practical to combine fragility curves of two steel grades. One of the shortcomings of fragility curves proposed by Kirçil and Polat (2006) is that only two limit states are considered: yielding and collapse. Moderate and extensive damage are missing, which makes fragility curves difficult to be applied in seismic risk calculations. Also, low-rise buildings are only represented with the fragility curves for 3-storey buildings, which might lead to overestimation of damage if they are used for 1-2 storey buildings. Fig. 4.14 shows the combined material fragility curves for 3-storey RC buildings for yielding and collapse damage states.

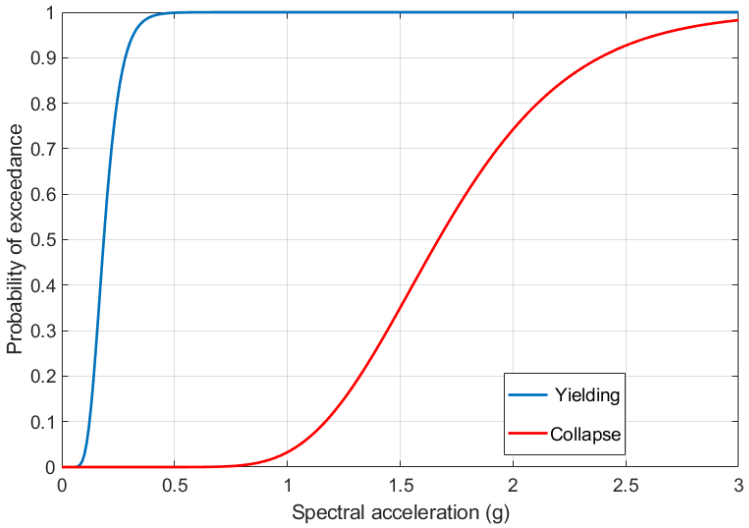

Figure 4.14 Sa(T) fragility curves proposed by Kirçil and Polat (2006) for 3-storey RC buildings.

In the present study, fragility curves based on PGA are not preferred due to some shortcomings of such curves. At short distances, PGA values observed during the 1999 Kocaeli earthquake were under-predicted by most of GMPEs due to the smoothness of rupture and fairly low stress drop in 1999 Kocaeli earthquake (Erdik 2001). On the other hand, the PGV estimates of GMPEs were similar to values observed in similar past events. This is particularly important as the case study area is located in a close proximity to the fault ruptured in that earthquake. The other reason is that PGA and PGV do not consider frequency content on the structural response, while by choosing Sa(T) as ground motion intensity parameter the influence of the frequency content is taken into account (Ferreira et al., 2013).

4.5.2 Consequence model and vulnerability curves

There are direct and indirect losses that can be caused by earthquake events. While direct losses are mostly associated with earthquake damage to the buildings, indirect losses can be caused by business and industry downtime due to recovery. In this study only direct losses associated with structural damage are considered. Direct seismic losses can be evaluated with the help of vulnerability curves and consequence models through finding mean damage ratios

(MDR) of the affected structures for a given ground motion intensity. The MDR represents the ratio of the repair cost to the cost of replacement. Consequence models developed for Turkish building stock (e.g. Smyth et al., 2004; Crowley et al., 2005; Bal et al., 2008) are shown in Table 4.1 in addition to suggested values in HAZUS (FEMA, 2003) for US building stock. It can be noticed that consequence models Turkish building stocks provide higher damage ratios than that proposed in HAZUS (FEMA, 2003). According to the legal requirements in Turkey, buildings with extensive damages need to be demolished after the earthquake (Bal et al. 2008). Consequence models for Turkish building stock take this into consideration, by providing 100-105% of replacement cost for extensive damage, while HAZUS considers 50% replacement cost for the same damage state. In the present study, the consequence model developed by Bal et al. (2008) is utilized for seismic risk calculations as it also includes demolition cost for extensive and complete damage states.

Table 4.1 Comparison of consequence models developed for Turkish and US building stocks.

Damage state	Smyth et al. (2004)	Crowley et al. (2005)	Bal et al. (2008)	HAZUS (US)
Slight	1%	10%	16%	2%
Moderate	10%	30%	33%	10%
Extensive	100%	100%	105%	50%
Complete	100%	100%	104%	100%

Fig. 4.15 shows the comparison of vulnerability curves obtained with the convolution of fragility curves developed by Erdik et al. (2003) and consequence models proposed by Bal et al. (2008) and HAZUS. The effect of consequence models on the developed vulnerability curves can be observed from this figure. In Fig. 4.16 vulnerability curves for RC buildings with various number of storeys are obtained with Bal et al. (2008) consequence model and Akkar et al. (2005) fragility curves. The plateau for PGV values between 10-40 cm/s is due to low contribution of moderate and severe damage fragility curves to MDR for this PGV range.

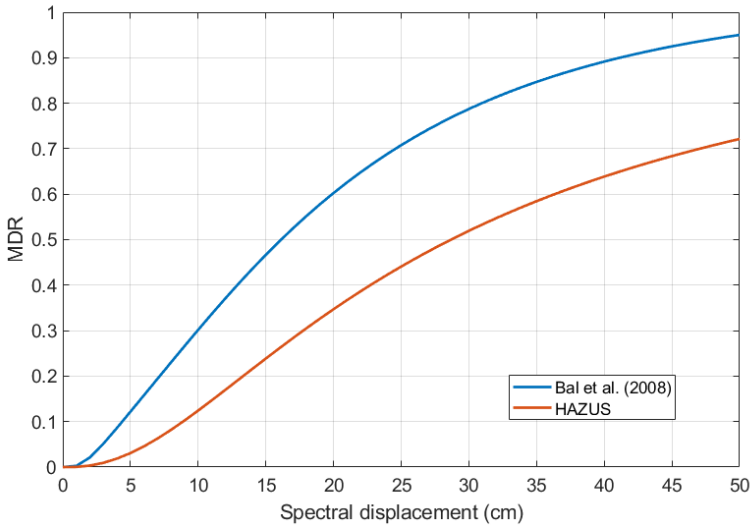

Figure 4.15 Comparison of vulnerability curves obtained by the convolving fragility curves developed by Erdik et al. (2003) for post-1980 mid-rise RC frame buildings with the consequence models developed by Bal et al. (2008) and given in HAZUS.

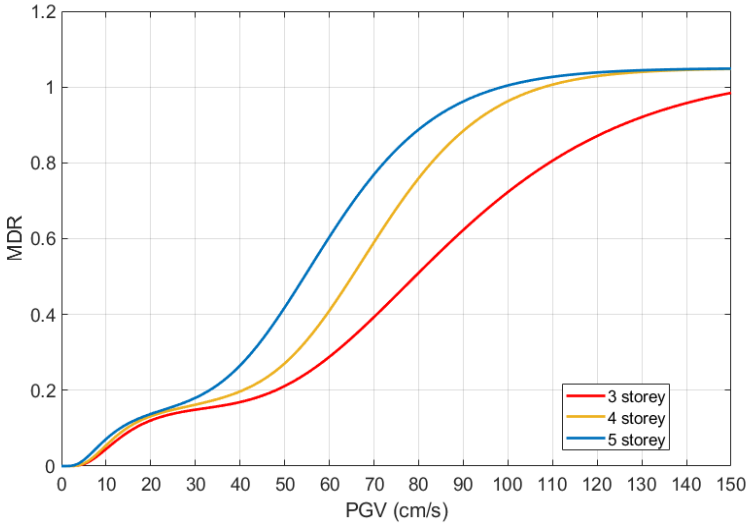

Figure 4.16 Comparison of vulnerability curves obtained by convolving the consequence model developed by on Bal et al. (2008) with the fragility curves developed by Akkar et al. (2005) for ordinary 3,4,5-storey RC buildings.

4.6 Seismic Risk Analysis Results for Adapazari

Monte-Carlo-based probabilistic seismic risk analysis is performed for the city of Adapazari and results are presented in this section. In addition, a scenario earthquake similar to 1999 Kocaeli earthquake is modelled and a risk analysis is performed using the scenario earthquake to compare these results with observed damage and casualties.

4.6.1 Seismic hazard

An event-based PSHA is performed for the case study area using background and faults source zones as explained in Section 4.3.1. Ground motion intensities (such as PGA, PGV and Sa(T)) are calculated from GMPEs considering soil amplification with intra-event and inter-event variabilities. Hazard maps for Adapazari are developed for probability of exceedances 50%, 10% and 2% in 50 years (return periods of 72, 475 and 2475 years, respectively). Figs. 4.17 and 4.18 present PGA and PGV values obtained from hazard analysis at the centre of each cell for the specified return periods. The results of this work shows that the PGA values for Adapazari range between 0.65g and 0.83g with an average value of 0.74g, for a 475-year return period; and the PGA values range between 1.06g and 1.44g with an average value of 1.23g, for 2475-year return period. Erdik et al. (2004), who performed a seismic hazard study in terms of PGA for the Marmara region, predicted PGA values for Adapazari to be in a range between 0.6g and 0.8g and in a range between 1.0 and 1.5g for 475 and 2475 years return periods, respectively. These values are in line with PGA values predicted in this work. In a more recent study performed for the eastern part of the Marmara region, Gülerce and Ocak (2013) predicted PGA values for Adapazari to be between 0.6-0.8g and 1.0-1.2g for 475 and 2475 years return period respectively. The PGV values for Adapazari range between 61 cm/s and 89 cm/s with an average value of 79 cm/s, for a 475-year return period; and the PGV values range between 100 cm/s and 141 cm/s with an average value of 128 cm/s, for 2475-year return period.

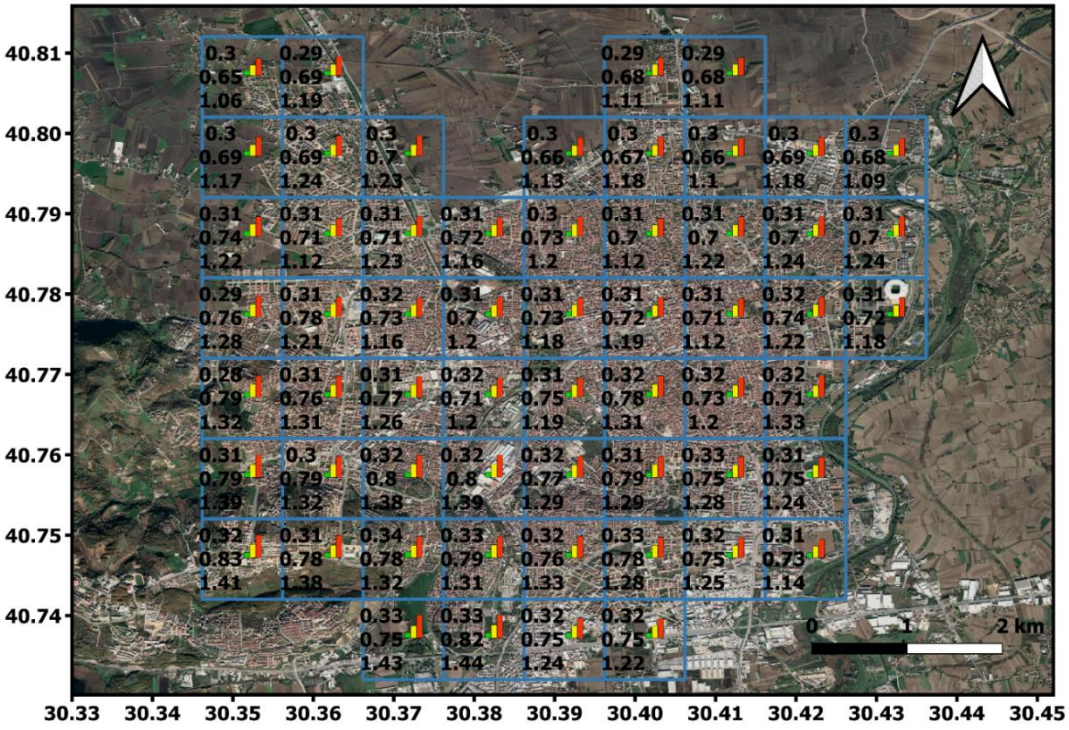

Figure 4.17 PGA (g) hazard map for: 72-year return period (top value in a cell), 475-year return period (middle value in a cell) and 2475-year return period (bottom value in a cell).

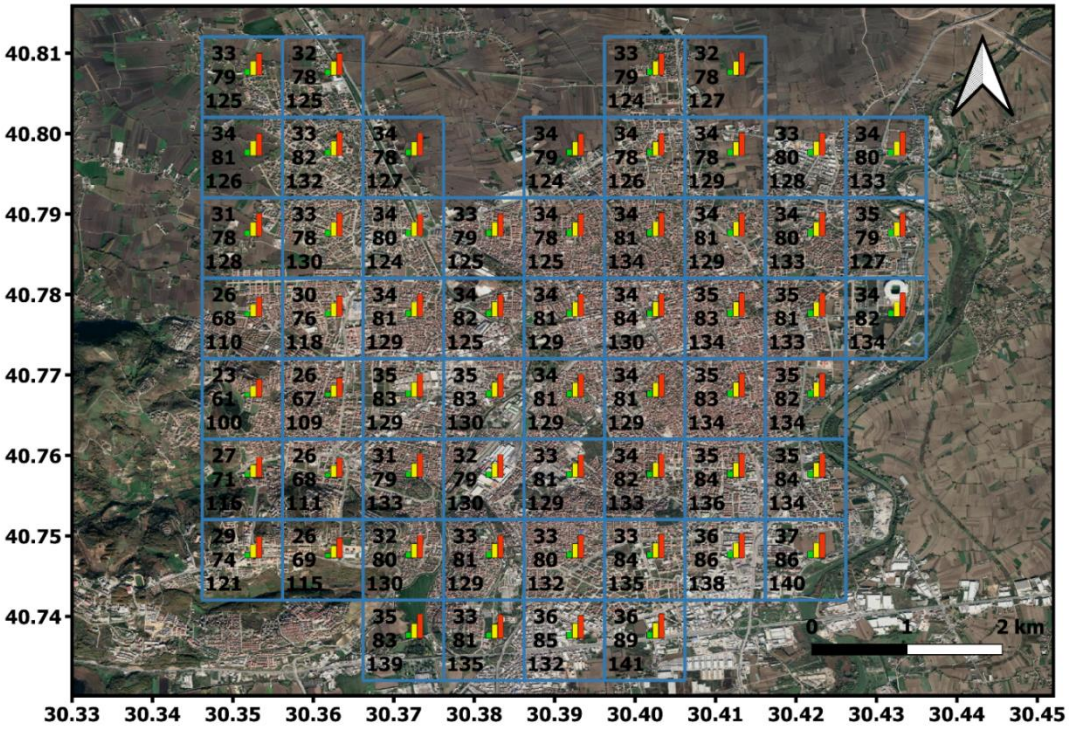

Figure 4.18 PGV (cm/s) hazard map for: 72-year return period (top value in a cell), 475-year return period (middle value in a cell) and 2475-year return period (bottom value in a cell).

Relatively high PGA and PGV values obtained in PSHA are due to the fact that Adapazari is located in close proximity to the active fault segments, which are capable of producing earthquakes with characteristic magnitude of M_w=7.2 at relatively low mean recurrence period of 140 years or annual rate of 0.0071 (Erdik et al., 2004). In addition, the city of Adapazari is mostly situated on a stiff soil (180<V_{s30}<360 m/s), which can amplify the spectral acceleration components at short periods and long periods (Silva et al., 2014).

4.6.2 Seismic risk

An event-based probabilistic seismic risk analysis is performed for the case study area following the procedure explained in Section 4.4.2 and results of this analysis are presented in this section. Fig. 4.19-4.20 shows the loss curves in terms of MDR and USD for the city of Adapazari, which are developed using the fragility curves proposed by Erdik et al. (2003) and Erberik (2008).

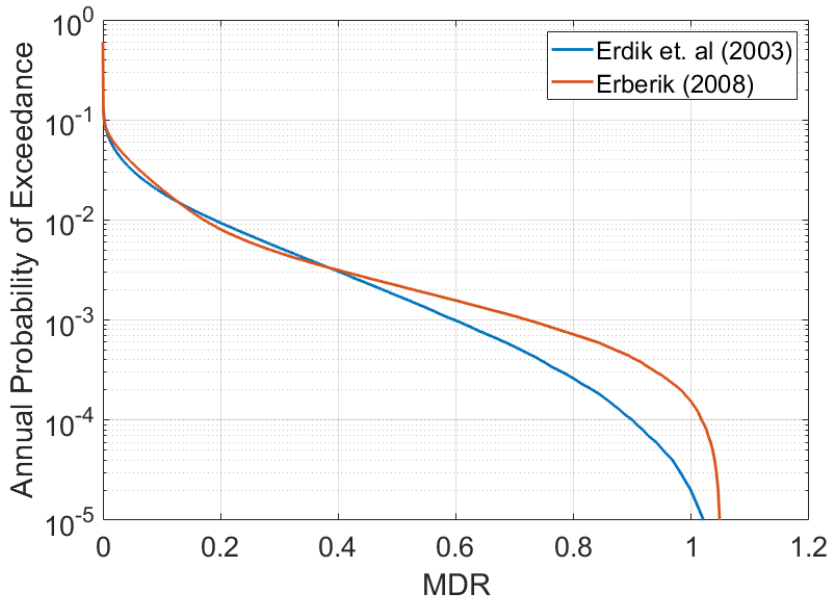

Figure 4.19 Loss curves in terms of MDR for Adapazari based on fragility curves developed by Erdik et al. (2003) and Erberik (2008).

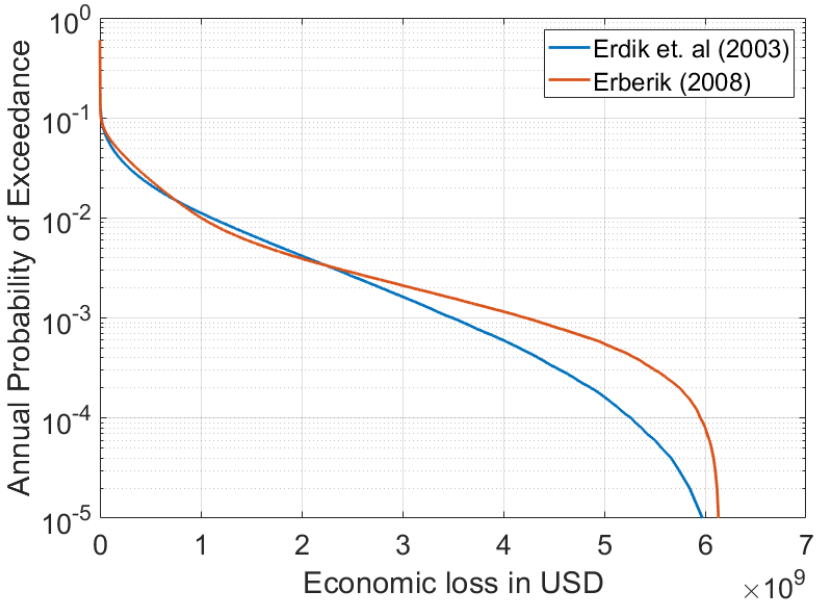

Figure 4.20 Loss curves in terms of USD for Adapazari based on fragility curves developed by Erdik et al. (2003) and Erberik (2008).

In the development of the latter curve, all buildings in the study area were assumed to be RC, as fragility curves proposed by Erberik (2008) are for RC buildings only. It can be seen from Fig. 4.19 that similar mean damage ratio (MDR) values are obtained from two fragility curves at smaller return periods. The MDR values based on the fragility curve developed by Erberik (2008) are more conservative at larger return periods than those based on the fragility curve developed by Erdik et al. (2003). Figs. 4.21 and 4.22 show the MDR values obtained from loss analysis at the centre of each cell for return periods of 72, 475 and 2475 years. As expected, the MDR values are the lowest for recently constructed areas of the city, while those values are the highest for old areas of the city.

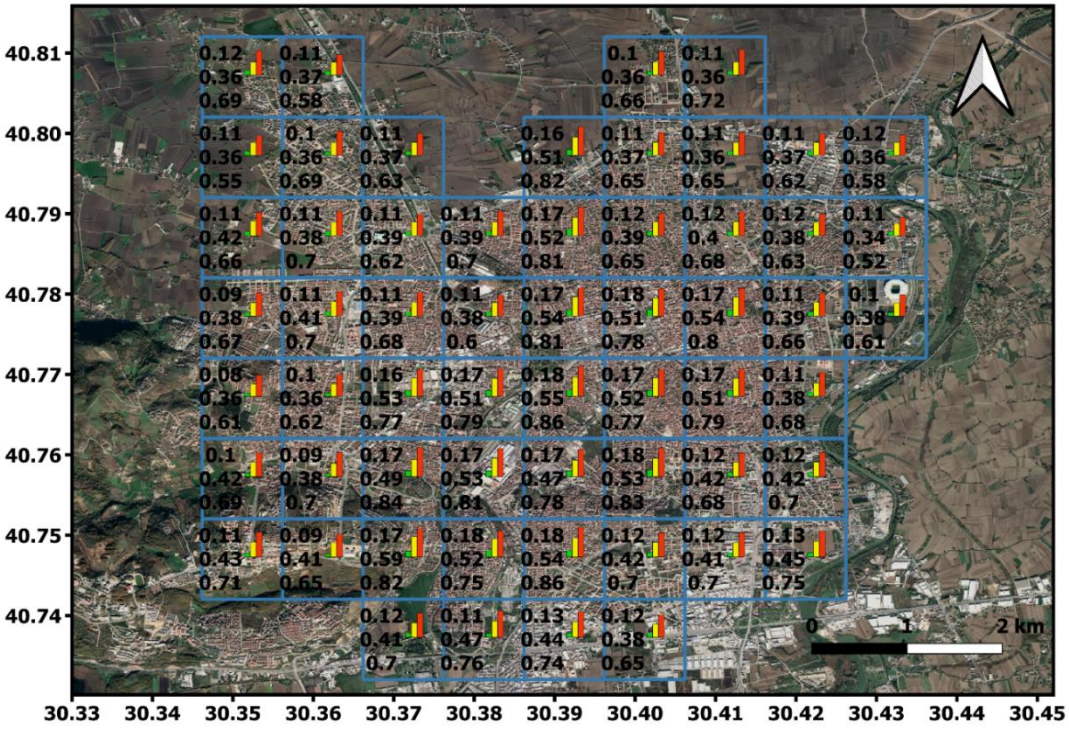

Figure 4.21 MDR map based on fragility curves developed by Erdik et al. (2003) for 72-year return period (top value in a cell), 475-year return period (middle value in a cell) and 2475-year return period (bottom value in a cell).

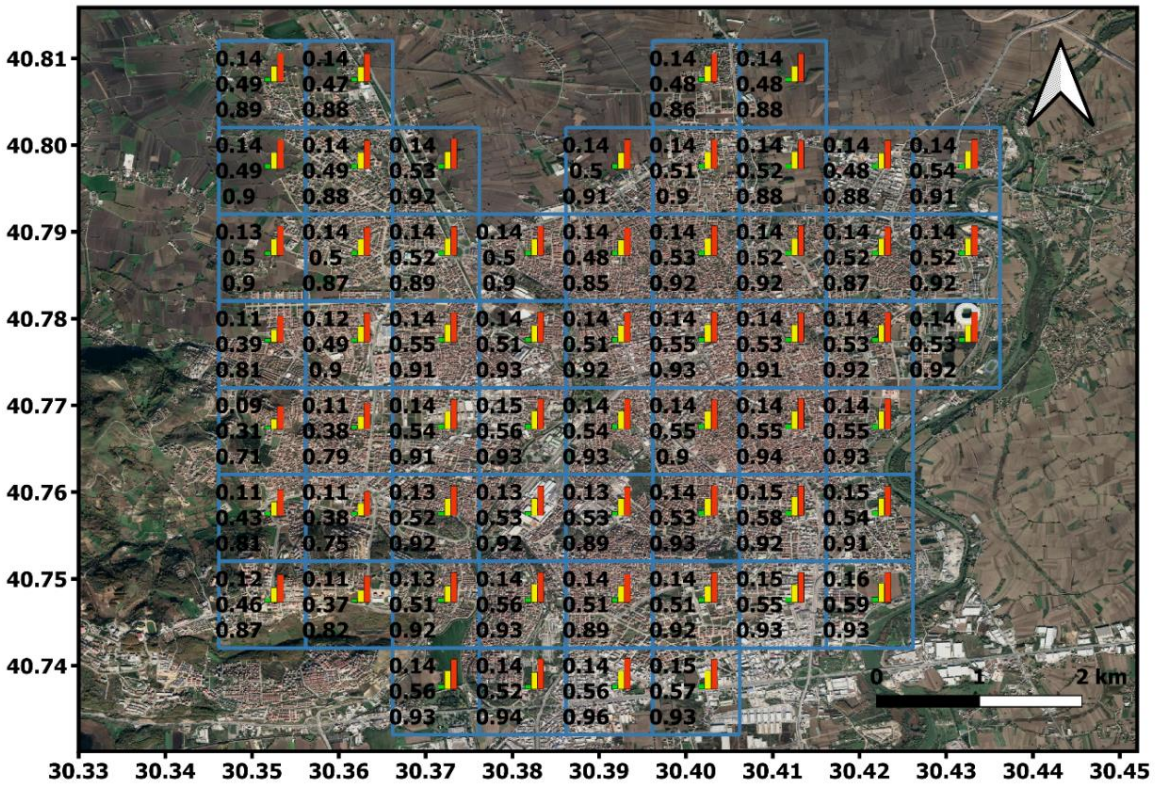

Figure 4.22 MDR map based on fragility curves developed by Erberik (2008) for 72-year return period (top value in a cell), 475-year return period (middle value in a cell) and 2475-year return period (bottom value in a cell).

Lethality analysis results for Adapazari are presented in Fig. 4.23. Number of death at the center of each cell are calculated for return periods of 72, 475 and 2475 years using fragility curves developed by Erdik et al. (2003) and casualty model proposed by So and Spence (2013). Occupancy rate in the casualty model is assumed to be 0.9 as proposed by So and Spence (2013), which is typical for night time.

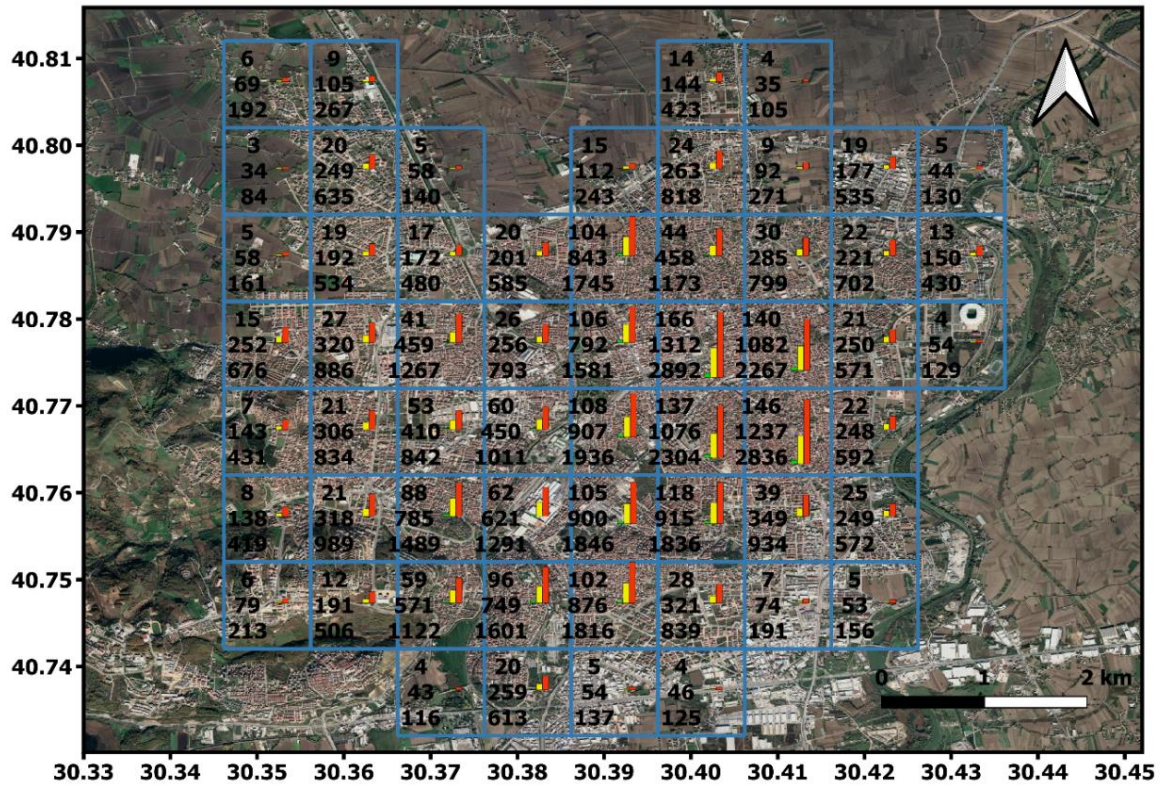

Figure 4.23 Lethality map based on Erdik et al. (2003) fragility curves and So and Spence (2013) casualty model for: 72-year return period (top value in a cell), 475-year return period (middle value in a cell) and 2475-year return period (bottom value in a cell).

Table 4.2 shows total lethality predictions for the city of Adapazarı based on casualty models proposed by So and Spence (2013) and Coburn et al. (1992) for return periods of 72, 475, 2475 years.

Table 4.2 Lethality estimates for Adapazari based on So and Spence (2013) and Coburn et al. (1992) casualty models for day and night time earthquake events for various return periods.

	So and Spence (2013)		**Coburn et al. (1992)**	
Return period	**Night**	**Day**	**Night**	**Day**
72 years	2326	811	3253	960
475 years	21112	7448	35921	11045
2475 years	49110	17435	92924	31457

4.6.3 Scenario earthquake and comparison with 1999 Kocaeli earthquake

A scenario earthquake, which has characteristics similar to 1999 Kocaeli earthquake, is generated using the hazard analysis tool developed in a previous study (Sianko et al., 2020). Fault rupture model is represented as a single rectangular plane with magnitude of M_w=7.4. The GMPEs mentioned in Section 3.2 are used for the generation of the scenario earthquake. To verify the developed framework, a seismic risk assessment is performed for Adapazari using the generated scenario earthquake. The importance of scenario earthquake risk assessment is to predict the damage distribution of the buildings portfolio caused by the modelled earthquake (Kohrangi et al., 2021b). Fig. 4.24 shows the spatial distribution of median PGA values obtained from the scenario earthquake. The PGA ranges from 0.31g in the northern part of the city and gradually increasing to 0.52g towards the fault in the south. The PGA recorded during 1999 Kocaeli earthquake at Sakarya station was 0.41g, but according to Kudo et al. (2002) the station is located on very stiff soil and ground intensities in the alluvial basin, at the central part of Adapazari, could be substantially different from those recorded by the station. As a result, the station does not represent the site conditions at the city center, where most of the damage was observed (Bakir et al., 2002). In the hazard analysis, the PGA values in the city center of Adapazari is estimated to be in the order of 0.3–0.4g as suggested by previous studies (e.g. Sancio et al., 2002, Yakut et al., 2005).

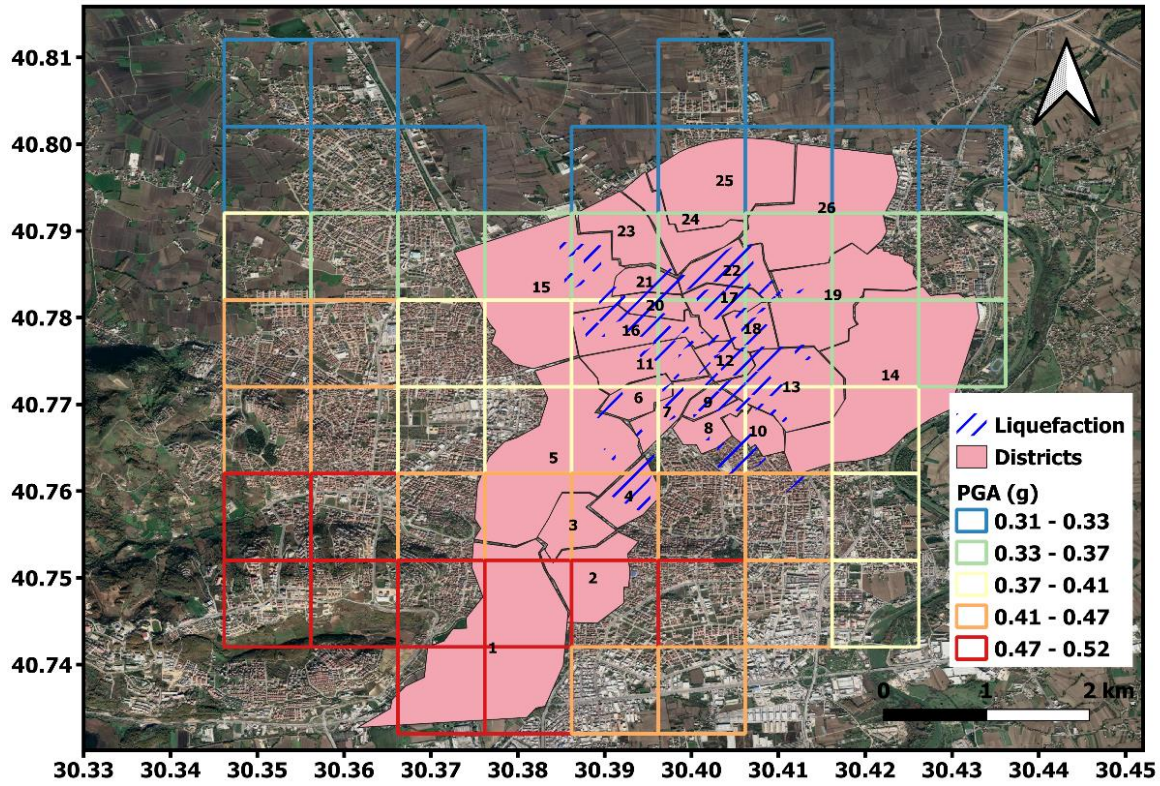

Figure 4.24 PGA (g) distribution from scenario earthquake and areas with observed damage from liquefaction after 1999 Kocaeli earthquake adopted from Mollamahmutoglu et al. (2003).

Following the 1999 Kocaeli earthquake, the municipality of the Adapazari performed a damage assessment for the buildings in the city (Yakut et al., 2005). The total number of buildings assessed by municipality was 23914 and these buildings are categorised into two damage groups. The first group represents buildings that can be repaired (light and moderate damage) and the second group is for buildings that are required to be demolished (extensive and complete damage). Table 4.3 provides comparison of percentage of buildings with extensive and complete damage at district level obtained from the scenario earthquake and the survey performed by the Adapazari municipality following the 1999 Kocaeli earthquake. It can be observed from this table that the results of the scenario earthquake hugely overestimate damage for districts located in the south of the study area (e.g. districts 1-4). This is an unexpected finding as those districts are located closer to the fault rupture and GMPEs are predicting high ground motion intensities in these areas considering soil conditions. Therefore,

observed damage in these areas is expected to be higher. On the other hand, the seismic risk analysis performed using the scenario earthquake underestimates the observed damage at the central districts (e.g. districts 20-22). This can be partially explained with the severe liquefaction observed in these areas (Fig. 4.24). Large proportion of buildings located in these areas suffered extensive and complete damage due to liquefaction instead of strong ground motion itself. In addition, according to Mollamahmutoglu et al. (2003) even buildings designed according to the seismic regulations suffered from severe displacements. Poor predictions for central districts might be due to GMPEs not being able to predict soil amplification correctly as occurred in 1999 Kocaeli earthquake. Nevertheless, Bakır et al. (2005) predicted higher ground motion intensity for the north and central parts of the city using microzonation and soil response analysis than presented in the current study with GMPEs. Disagreement in the results can be also due to the fact that seismic risk procedures do not consider damage due to liquefaction. It can be concluded that it is not possible to predict damage patterns observed during the 1999 Kocaeli earthquake using conventional methods that are developed for large scale studies. Similar conclusion for scenario earthquakes for Adapazari was drawn by Yakut et al. (2005).

Table 4.3 Comparison of the extensive and complete damage at the district level obtained from the scenario earthquake and the survey data from Adapazari municipality.

ID	District	Extensive and complete damage (%)		ID	District	Extensive and complete damage (%)	
		Scenario	Municipality			Scenario	Municipality
1	Maltepe	11.4	0.0	14	Tepekum	4.5	1.7
2	Hızırtepe	15.0	0.6	15	Seker	4.5	12.5
3	Sirinevler	14.1	3.7	16	Cumhuriyet	9.6	15.4
4	Güllük	13.7	3.3	17	Orta	8.4	13.8
5	Mithatpasa	11.7	5.3	18	Yahyalar	8.8	8.3
6	Yenidogan	11.0	24.6	19	Yagcılar	4.7	7.1
7	Pabuççular	11.0	28.8	20	Kurtulus	9.2	10.7
8	Akıncılar	11.1	20.3	21	Istiklal	8.5	40.8
9	Yenicami	11.3	25.4	22	Karaosman	6.3	30.0
10	Çukurahmediye	10.6	18.6	23	Ozanlar	8.3	8.6
11	Semerciler	9.6	24.2	24	Sakarya	7.8	8.6
12	Tıgcılar	9.3	11.4	25	Tekeler	3.2	8.0
13	Yenigün	9.1	16.5	26	Tuzla	2.8	8.6

Table 4.4 shows overall comparison between scenario earthquake and survey data in terms of % of total number of building. As one can see from this table, predictions for extensive and complete damage states obtained from the proposed risk analysis for the scenario earthquake are correlated well with the damage data collected following the 1999 Kocaeli earthquake. On the other hand, the number of buildings with slight and moderate damage states are highly overestimated by the proposed risk analysis method in comparison to the survey data. During the 1999 Kocaeli earthquake, numerous surface manifestations of liquefaction, in the form of sand boils and lateral spreading, were observed in Adapazari. The softened and/or liquefied soil acted as an isolator dissipating the energy at the foundation level and reduced shaking damage to the buildings (Bakir et al., 2002). Where there is no or slight structural damage caused by ground shaking to the tilted or settled buildings, they still might be considered to be damaged due to liquefaction, where damage affects future structural performance. For extreme cases of rotation or settlement of the building the damage state is complete, as such building are only suitable for demolition. Moreover, the cost of the replacement of such building can be potentially be higher than that due to complete structural collapse, since demolition of the tilted or settled building will be required. This highlights an urgent need for the integration of the effect of liquefaction susceptible soil conditions for buildings located on such soils into the risk analysis. This can be done by following comprehensive procedure suggested by Bird et al. (2006). In their work the interaction of ground shaking and liquefaction in is considered in two different models. In the first model, the ground shaking and liquefaction do not interact, therefore, any group of buildings has a probability $P(X)$ of being affected by liquefaction, and a probability of 1-$P(X)$ of being damaged by ground shaking. In the second model, the two hazards do interact and the damage state of building depends on both the initial damage caused by ground shaking and following damage caused by liquefaction. In addition, the procedure by Bird et al. (2006) is capable of distinguishing between stiff (structure moves without significant

internal deformation) and flexible (unrestrained) foundations, which will have different response to the ground failure. Due to the relative complexity of the procedure, limitations and lack of the detailed data on foundation types used in buildings in the Adapazari, it is not possible to include liquefaction damage in the risk calculations in the current study.

Table 4.4 Comparison of the overall predicted damage from the scenario earthquake and the survey data from Adapazari municipality.

	Number of buildings	
Damage group	**Scenario earthquake**	**Adapazari municipality**
Slight and moderate	23881 (50.5%)	2076 (8.7%)
Extensive and complete	3841 (8.1%)	2844 (11.9%)

Fig. 4.25 shows the damage distribution in Adapazari obtained from risk analysis using the fragility curves developed by Erdik et al. (2003).

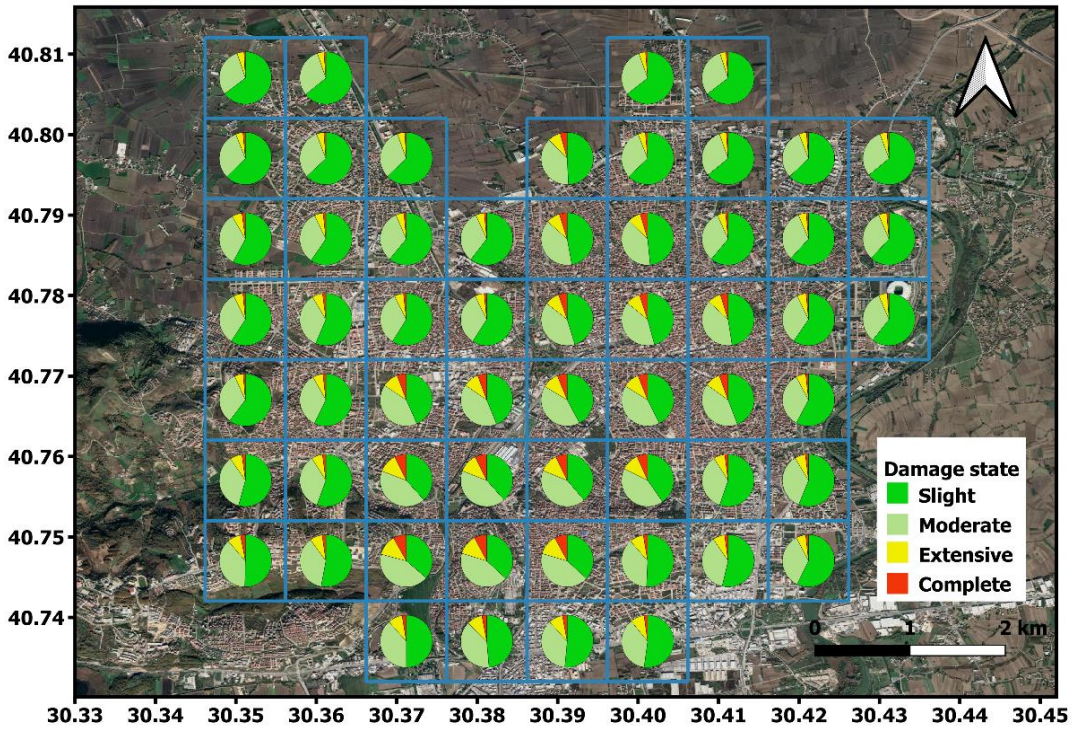

Figure 4.25 Damage distribution from scenario earthquake using Erdik et al. (2003) fragility curves.

The lethality predictions for the scenario earthquake gives 3817 and 5298 deaths using So and Spence (2013) and Coburn et al. (1992) casualty models respectively. The occupancy rate

at the time of the earthquake is assumed to be 0.9 (as the Kocaeli earthquake occurred at night time). Bar-Dayan et al. (2000) and Margalit et al. (2002) stated that the 1999 Kocaeli earthquake killed 2680 people and approximately 5300 injuries in Adapazari. However, Bakir et al. (2002) reported fatalities as 3684 for the same earthquake. The population of Adapazari was 283,752 according to the census taken in the 2000s. In this work, the population of Adapazari is estimated as 517,000. It can be concluded that both casualty models used in this work give reasonable results.

4.7 Conclusions

In this work, a probabilistic seismic risk assessment framework based on MC-simulations is developed, that is capable to produce seismic risk maps and loss curves. The uncertainty of input parameters in seismic risk is treated by employing logic tree and randomization process in Monte-Carlo simulations. An exposure model for the study area is obtained with building footprints mapped from aerial and satellite images and remote street survey. The developed earthquake risk assessment framework is applied to the city of Adapazari in Turkey using readily available data. The results for Adapazari are presented with PGA and PGV hazard maps, MDR distributions for various return periods and loss curves.

One of the biggest challenges in the development of a reliable seismic risk framework is the verification of obtained results against post-earthquake data, which are not very common. The developed framework was verified by comparing the building damage predicted for a scenario earthquake with those observed after the 1999 Kocaeli earthquake. In addition, casualty models are employed in the earthquake risk analysis for the estimation of fatalities in the city of Adapazari due to the scenario earthquake. Risk analysis results demonstrated that the developed earthquake risk assessment framework can predict extensive and complete damage states in Adapazari very reasonably for the scenario event in comparison to damage

observed after the real event. However, slight and moderate damage states are overestimated by the developed procedure. This could be partially explained with the soil conditions of Adapazari, which lies over liquefiable silts and sands. During the 1999 Kocaeli earthquake, the liquefied soil should have dissipated the energy acting as an isolator and reduced the shaking damage to the buildings.

To conclude, the developed framework can serve as an efficient tool for the assessment of seismic risk, but it should be used with caution in areas with complex geological conditions and which are prone to liquefaction. There is an urgent need for the integration of soft soil and liquefaction effects into the risk analysis for buildings located on such soil conditions.

References

Akkar, S., Sandıkkaya, M. & Bommer, J. 2014. Empirical ground- motion models for point- and extended- source crustal earthquake scenarios in Europe and the Middle East. *Official Publication of the European Association for Earthquake Engineering*, 12, 359-387.

Akkar, S., Sucuoğlu, H. & Yakut, A. 2005. Displacement-based fragility functions for low-and mid-rise ordinary concrete buildings. *Earthquake Spectra*, 21, 901-927.

Bakir, B. S., Sucuoglu, H. & Yilmaz, T. 2002. An overview of local site effects and the associated building damage in Adapazari during the 17 August 1999 Izmit earthquake. *Bulletin of the Seismological Society of America*, 92, 509-526.

Bakır, B. S., Yılmaz, M. T., Yakut, A. & Gülkan, P. 2005. Re-examination of damage distribution in Adapazarı: Geotechnical considerations. *Engineering Structures*, 27, 1002-1013.

Bal, İ. E., Crowley, H., Pinho, R. & Gülay, F. G. 2008. Detailed assessment of structural characteristics of Turkish RC building stock for loss assessment models. *Soil Dynamics and Earthquake Engineering*, 28, 914-932.

Bar-Dayan, Y., Mankuta, D., Wolf, Y., Levy, Y., Vanrooyen, M., Beard, P., Finestone, A., Gruzman, C., Benedek, P. & Martonovits, G. 2000. An earthquake disaster in Turkey: an overview of the experience of the Israeli Defence Forces Field Hospital in Adapazari. *Disasters*, 24, 262-270.

Bird, J.F., Bommer, J.J., Crowley, H. & Pinho, R. 2006. Modelling liquefaction-induced building damage in earthquake loss estimation. *Soil Dynamics and Earthquake Engineering*, 26(1), 15-30.

Bommer, J. & Crowley, H. 2006. The influence of ground-motion variability in earthquake loss modelling. *Bulletin of Earthquake Engineering*, 4, 231-248.

Bommer, J., Spence, R., Erdik, M., Tabuchi, S., Aydinoglu, N., Booth, E., Del Re, D. & Peterken, O. 2002. Development of an earthquake loss model for Turkish catastrophe insurance. *Journal of Seismology*, 6, 431-446.

Bommer, J., Spence, R. & Pinho, R. Earthquake loss estimation models: time to open the black boxes. *First European Conference on Earthquake Engineering and Seismology*. Geneva, 2006.

Bommer, J., Douglas, J., Scherbaum, F., Cotton, F., Bungum, H. & FäH, D. 2010. On the selection of ground-motion prediction equations for seismic hazard analysis. *Seismological Research Letters*, 81, 783-793.

Boore, D. M., Stewart, J. P., Seyhan, E. & Atkinson, G. M. 2014. NGA-West2 equations for predicting PGA, PGV, and 5% damped PSA for shallow crustal earthquakes. *Earthquake Spectra*, 30, 1057-1085.

Bray, J. D., Sancio, R. B., Durgunoglu, T., Onalp, A., Youd, T. L., Stewart, J. P., Seed, R. B., Cetin, O. K., Bol, E. & Baturay, M. B. 2004. Subsurface characterization at ground failure sites in Adapazari, Turkey. *Journal of Geotechnical and Geoenvironmental Engineering*, 130, 673-685.

Chaulagain, H., Rodrigues, H., Silva, V., Spacone, E. & Varum, H. 2015. Seismic risk assessment and hazard mapping in Nepal. *Natural Hazards*, 78, 583-602.

Coburn, A. W., Spence, R. J. & Pomonis, A. Factors determining human casualty levels in earthquakes: mortality prediction in building collapse. *Proceedings of the tenth world conference on earthquake engineering*, 1992. Balkema Rotterdam, 5989-5994.

Cornell, C. A. 1968. Engineering Seismic Risk Analysis. *Bulletin of the Seismological Society of America*, 58, 1583-1606.

Crowley, H., Bommer, J. J., Pinho, R. & Bird, J. 2005. The impact of epistemic uncertainty on an earthquake loss model. *Earthquake engineering & structural dynamics*, 34, 1653-1685.

Erberik, M. A. 2008. Fragility- based assessment of typical mid- rise and low- rise RC buildings in Turkey. Engineering Structures, 30, 1360-1374.

Erdik, M. 2001. Report on 1999 Kocaeli and Duzce (Turkey) Earthquakes. *Structural control for civil and infrastructure engineering: World Scientific*, 149-186.

Erdik, M. 2017. Earthquake risk assessment. *Bulletin of Earthquake Engineering*, 15, 5055-5092.

Erdik, M., Aydinoglu, N., Fahjan, Y., Sesetyan, K., Demircioglu, M., Siyahi, B., Durukal, E., Ozbey, C., Biro, Y., Akman, H. & Yuzugullu, O. 2003. Earthquake risk assessment for Istanbul metropolitan area. *Earthq. Eng. Vib.*, 2, 1-23.

Erdik, M., Demircioglu, M., Sesetyan, K., Durukal, E. & Siyahi, B. 2004. Earthquake hazard in Marmara Region, Turkey. *Soil Dynamics and Earthquake Engineering*, 24, 605-631.

FEMA356. 2000. Federal Emergency Management Agency, Prestandard and Commentary for the Seismic Rehabilitation of Building. 356.

FEMA 2003. Technical Manual, Vol. Earthquake Model. Federal Emergency Management Agency, Washington DC.

Feng, T., Hong, Z., Wu, H., Fu, Q., Wang, C., Jiang, C. & Tong, X. 2013. Estimation of earthquake casualties using high-resolution remote sensing: a case study of Dujiangyan city in the May 2008 Wenchuan earthquake. *Natural hazards*, 69, 1577-1595.

Ferreira, T. M., Vicente, R., Da Silva, J. M., Varum, H. & Costa, A. 2013. Seismic vulnerability assessment of historical urban centres: case study of the old city centre in Seixal, Portugal. *Bulletin of Earthquake Engineering*, 11, 1753-1773.

Gülerce, Z. & Ocak, S. 2013. Probabilistic seismic hazard assessment of Eastern Marmara Region. *Bulletin of Earthquake Engineering*, 11, 1259-1277.

Jaiswal, K., Wald, D. J. & Hearne, M. 2009. Estimating casualties for large earthquakes worldwide using an empirical approach, US Geological Survey Denver, CO.

Jayaram, N. & Baker, J. W. 2009. Correlation model for spatially distributed ground-motion intensities. *Earthquake Engineering & Structural Dynamics*, 38, 1687-1708.

Kirçil, M. S. & Polat, Z. 2006. Fragility analysis of mid-rise R/C frame buildings. *Engineering Structures*, 28, 1335-1345.

Kohrangi, M., Bazzurro, P. & Vamvatsikos, D. 2021a. Seismic risk and loss estimation for the building stock in Isfahan. Part I: exposure and vulnerability. *Bulletin of Earthquake Engineering*, 1-29.

Kohrangi, M., Bazzurro, P. & Vamvatsikos, D. 2021b. Seismic risk and loss estimation for the building stock in Isfahan: part II—hazard analysis and risk assessment. *Bulletin of Earthquake Engineering*, 1-25.

Kudo, K., Kanno, T., Okada, H., ÖZel, O., Erdik, M., Sasatani, T., Higashi, S., Takahashi, M. & Yoshida, K. 2002. Site-specific issues for strong ground motions during the Kocaeli, Turkey, earthquake of 17 August 1999, as inferred from array observations of microtremors and aftershocks. *Bulletin of the Seismological Society of America*, 92, 448-465.

Margalit, G., Rosen, Y., Tekes-Manova, D., Golan, M., Benedek, P., Levy, Y., Martonovits, G. & Bar-Dayan, Y. 2002. Recommendations for nursing requirements at a field hospital, based on the Israel Defense Forces field hospital at the earthquake disaster in Turkey—August 1999. *Accident and emergency nursing*, 10, 217-220.

Mollamahmutoglu, M., Kayabali, K., Beyaz, T. & Kolay, E. 2003. Liquefaction-related

building damage in Adapazari during the Turkey earthquake of August 17, 1999. *Engineering Geology*, 67, 297-307.

Murru, M., Akinci, A., Falcone, G., Pucci, S., Console, R. & Parsons, T. 2016. M≥ 7 earthquake rupture forecast and time-dependent probability for the Sea of Marmara region, Turkey. *Journal of Geophysical Research: Solid Earth*, 121, 2679-2707.

Musson, R. M. W. 2000. The use of Monte Carlo simulations for seismic hazard assessment in the U.K. *Annals of Geophysics*, 43.

Musson, R. M. W. & Winter, P. 2012. Objective assessment of source models for seismic hazard studies: with a worked example from UK data. *Bulletin of Earthquake Engineering*, 10, 367-378.

Ranjbar, H. R., Dehghani, H., Ardalan, A. R. A. & Saradjian, M. R. 2017. A GIS-based approach for earthquake loss estimation based on the immediate extraction of damaged buildings. *Geomatics, Natural Hazards and Risk*, 8, 772-791.

Riga, E., Karatzetzou, A., Apostolaki, S., Crowley, H. & Pitilakis, K. 2021. Verification of seismic risk models using observed damages from past earthquake events. *Bulletin of Earthquake Engineering*, 19, 713-744.

Riga, E., Karatzetzou, A., Mara, A. & Pitilakis, K. 2017. Studying the uncertainties in the seismic risk assessment at urban scale applying the Capacity Spectrum Method: The case of Thessaloniki. *Soil dynamics and earthquake engineering*, 92, 9-24.

Sancio, R., Bray, J., Stewart, J., Youd, T., Durgunoğlu, H., Önalp, A., Seed, R., Christensen, C., Baturay, M. & Karadayılar, T. 2002. Correlation between ground failure and soil conditions in Adapazari, Turkey. *Soil Dynamics and Earthquake Engineering*, 22, 1093-1102.

Sianko, I., Ozdemir, Z., Khoshkholghi, S., Garcia, R., Hajirasouliha, I., Yazgan, U. & Pilakoutas, K. 2020. A practical probabilistic earthquake hazard analysis tool: case study Marmara region. *Bulletin of Earthquake Engineering*, 18, 2523–2555.

Silva, V., Amo-Oduro, D., Calderon, A., Costa, C., Dabbeek, J., Despotaki, V., Martins, L., Pagani, M., Rao, A. & Simionato, M. 2020. Development of a global seismic risk model. *Earthquake Spectra*, 36, 372-394.

Silva, V., Crowley, H., Jaiswal, K., Acevedo, A. B., Pittore, M. & Journey, M. Developing a global earthquake risk model. *16th European Conference on Earthquake Engineering*, 2018. 18-21.

Silva, V., Crowley, H., Pagani, M., Monelli, D. & Pinho, R. 2014. Development of the OpenQuake engine, the Global Earthquake Model's open-source software for seismic risk assessment. *Natural Hazards*, 72, 1409-1427.

Silva, V., Crowley, H., Varum, H. & Pinho, R. 2015. Seismic risk assessment for mainland Portugal. *Bulletin of Earthquake Engineering*, 13, 429-457.

Smyth, A. W., Altay, G., Deodatis, G., Erdik, M., Franco, G., Gülkan, P., Kunreuther, H., Luş, H., Mete, E. & Seeber, N. 2004. Probabilistic benefit-cost analysis for earthquake damage mitigation: Evaluating measures for apartment houses in Turkey. *Earthquake Spectra*, 20, 171-203.

So, E. & Spence, R. 2013. Estimating shaking-induced casualties and building damage for global earthquake events: a proposed modelling approach. *Bulletin of Earthquake Engineering*, 11, 347-363.

Tong, X., Hong, Z., Liu, S., Zhang, X., Xie, H., Li, Z., Yang, S., Wang, W. & Bao, F. 2012. Building-damage detection using pre-and post-seismic high-resolution satellite stereo imagery: A case study of the May 2008 Wenchuan earthquake. *ISPRS Journal of Photogrammetry and Remote Sensing*, 68, 13-27.

Villar-Vega, M. & Silva, V. 2017. Assessment of earthquake damage considering the characteristics of past events in South America. *Soil Dynamics and Earthquake Engineering*, 99, 86-96.

Wieland, M., Pittore, M., Parolai, S., Begaliev, U., Yasunov, P., Tyagunov, S., Moldobekov, B., Saidiy, S., Ilyasov, I. & Abakanov, T. 2015. A multiscale exposure model for seismic risk assessment in Central Asia. *Seismological Research Letters*, 86, 210-222.

Yakut, A., Gülkan, P., Bakır, B. S. & Yılmaz, M. T. 2005. Re-examination of damage distribution in Adapazarı: Structural considerations. *Engineering structures*, 27, 990-1001.

Chapter 5: Conclusions and Recommendations for Future Work

5.1 Introduction

The aim of this study is to develop ERA framework, which can take into account secondary hazards. Currently, probabilistic liquefaction hazard assessment is incorporated into the framework. But, other secondary hazards can also be integrated into the framework relatively easily in a future work (e.g. landslides, fires). The developed framework is based on Monte-Carlo simulations and consists of three main modules: PSHA, PLHA and earthquake risk. The seismic hazard part of the framework is capable of performing both Poisson and time-dependent PSHA as well as consider pulse-like ground motions in the analysis. The Marmara region (Turkey) is selected as a case study area to verify the developed PSHA module by comparing it with the existing PSHA studies. The liquefaction hazard is assessed with PLHA module, which provides output in terms of LPI (Liquefaction potential index) and LS (Liquefaction severity). The developed liquefaction hazard assessment procedure is practical for large scale studies as it uses publicly available V_{s30} parameter to represent soil conditions. The seismic risk module of the framework employs satellite images and remote street surveys for the development of a building exposure model when detailed up-to-date census data is not publicly available. Social and economic losses are calculated by employing different vulnerability and casualty models in the framework. The developed risk framework is applied to the city of Adapazari (Turkey).

5.2 Outcomes and Conclusions

The main conclusions of this study are divided into (a) PSHA, (b) PLHA and (c) seismic risk assessment and are presented in the following sub-sections.

5.2.1 Probabilistic Seismic Hazard Analysis (PSHA)

- Practical MC-based PSHA tool is developed which utilises synthetic earthquake catalogues by using readily available information on the seismo-tectonic structure, seismicity and geology of a region.
- New background seismicity model is proposed in this study to represent seismicity of the Marmara region for earthquakes below M_w=7.0.
- The chi-squared test is incorporated into the framework to verify proposed background zones if they can replicate the past seismicity in the study area. The results of the tests suggest that zones boundaries are drawn appropriately and activity rates are correctly derived.
- Poisson and time-dependent (renewal) seismic hazard maps are developed for the Marmara region. The hazard level for the Istanbul area is considerably higher in the time-dependent model than that obtained using the Poisson model due to an unruptured seismic gap in the Marmara Sea.
- Novel procedure for inclusion of near-field rupture directivity model in MC-based PSHA is proposed. Amplification and de-amplification factors are used to modify GMPEs to account for pulselike and non-pulselike behaviour, which in turn will have impact on seismic hazard results.
- Hazards maps with consideration of near-field rupture directivity effects are proposed for the Marmara region. The results indicate that the directivity effect can have an impact on the predicted PSHA results by up to 20%, as can be observed for Izmit.
- The obtained hazard maps compare well with the results from other recent PSHA studies (AFAD and SHARE).
- The disaggregation of hazard procedure is developed and incorporated into the framework. The design earthquake of M_w=7.25 at 10km for Istanbul is identified.

- The developed hazard module serves as a foundation for PLHA and risk assessment modules of the framework.

5.2.2 Probabilistic Liquefaction Hazard Analysis (PLHA)

- In this work, a novel PLHA module is developed that can utilise both LPI and L_S liquefaction assessment parameters to predict liquefaction hazard by using generated synthetic catalogues from Monte-Carlo simulations. The module is capable of producing probabilistic liquefaction hazard maps without relying on previously derived seismic data such as hazard curves and deaggregation of hazard in order to perform PLHA.
- The methodology employed in the PLHA module is practical and efficient as uncertainties in earthquake and soil related input parameters are randomised in a controlled way using distribution functions during MC simulations process.
- Employed MC-based PLHA methodology is capable of identifying worst cases that contribute the most to the liquefaction hazard, and therefore can help to select appropriate earthquake parameters such as distance and magnitude to be used in scenario earthquake.
- Probabilistic liquefaction hazard maps are developed for the city of Adapazari and the Marmara region of Turkey, respectively.
- A parametric analysis is also carried out to investigate the effect of different stress-reduction factor r_d calculation methods on liquefaction prediction parameters such as LPI and L_S. The r_d procedure used in the PLHA affects the magnitude-distance distribution and the obtained LPI value. Disaggregation of liquefaction hazard shows that the contribution of earthquakes with magnitude M_w<6 to the liquefaction hazard is smaller when earthquake magnitude dependent r_d is used.

- Disaggregation of liquefaction hazard is performed to identify magnitude-distance couples contributing to the liquefaction hazard. From disaggregation M_w ~7 at 5km is the most dominant couple for 475 and 2475 return periods. This is due to the fact that Adapazari is in a close proximity to active fault segments with a similar characteristic magnitude.
- The liquefaction hazard maps prepared for the city of Adapazari show good agreement with the observed liquefaction following the 1999 Kocaeli earthquake. The PLHA results show that the liquefaction hazard for Adapazari can be considered as very high.
- The comparison of PLHA maps developed using the Poisson and time-dependent PSHA models for the Marmara region show that the time-dependent PSHA model identifies additional areas of non-negligible liquefaction hazard in the region.
- Since the PLHA module is utilising V_{s30} approximations, it is recommended to only use it for regional scale analysis and not for site-specific analysis. On the other hand, the framework can easily adopt SPT measurements for more accurate predictions in the areas where such data is available.

5.2.3 Seismic Risk Assessment

- A probabilistic seismic risk assessment framework based on MC-simulations is developed and applied to the city of Adapazari in Turkey. The seismic hazard module of the framework is used to develop PSHA maps for the city of Adapazari. The obtained PGA values are in line with previous studies conducted for study area.
- The framework utilises readily available data such as census data, global shear-wave velocity maps and satellite images. Therefore, it may be used in developing countries and areas with limited data available.
- A building exposure model for the study area is developed by mapping building footprints from aerial and satellite images and using remote street survey.

- Loss curves and probabilistic MDR maps are obtained for the study area considering various return periods and vulnerability models.
- The developed framework was verified through comparison of predicted buildings damage from scenario earthquake and with those observed after the 1999 Kocaeli earthquake. While for extensive and complete damage states the overall results (for all buildings considered) can be considered satisfactory, the damage predictions for slight and moderate damage states are overestimated.
- Casualty models are incorporated into the framework for estimation of fatalities associated with earthquakes in the city of Adapazari. The results are obtained using probabilistic analysis for various return periods. In addition, models are verified with a scenario earthquake similar to the 1999 Kocaeli earthquake. It can be concluded that models are making adequate predictions when results are compared to observed values from that past event.
- The developed framework can serve as an efficient tool for assessment of seismic risk, but should be applied with caution in areas with complex geological conditions and prone to liquefaction.

5.3 Future work recommendations

Whilst this study successfully achieved initially set aims and objectives, it also identifies areas that require future work and opened new topics for investigation such as:

- The PLHA module proposed in this work can serve as a foundation for further development of liquefaction risk procedure, which can be further integrated into the seismic risk calculations.
- While PLHA module was developed in this work, it was not used for seismic risk calculations, due to complexity of integration of liquefaction damage in seismic risk

calculations. Further investigations should be made for calculating the combined damage, in the event liquefaction and ground shaking are interacting at a site of interest.

- The ERA framework can be extended by inclusion of earthquake induced landslides and fires.
- Vulnerability models for industrial facilities and other infrastructure such as dams, power plants, etc. needs to be included into the framework. This will help to extend the applicability of the ERA framework.
- The methodology for building inventory assessment needs to be further developed to utilize more sophisticated and automated image processing procedures such as image recognition based on artificial neural networks and deep learning.
- More GMPEs need to be incorporated into the ERA framework to make it more suitable for a global use.
- Inclusion of vulnerability curves for seismically strengthened/retrofitted structures should be also considered.

Appendix A

This appendix presents the earthquake data set used for PSHA in Chapter 2, showing events with magnitude equal to or bigger than 4.0 in any magnitude scale reported.

ID	Year	Month	Day	M type	Magnitude	Latitude	Longitude
1	1509	9	10	Mw	7.2	40.9	28.7
2	1556	5	10	Mw	6.7	40.6	28
3	1625	5	18	Mw	6.6	40.3	26
4	1659	2	17	Mw	6.7	40.5	26.4
5	1672	2	14	Mw	7	39.5	26
6	1719	5	25	Mw	7.4	40.7	29.8
7	1737	3	6	Mw	7	40	27
8	1766	5	22	Mw	7.1	40.8	29
9	1766	8	5	Mw	7.6	40.6	27
10	1855	2	28	Mw	7.1	40.1	28.6
11	1894	7	10	Mw	7.3	40.7	29.6
12	1900	1	24	MS	5.2	39.54	26.14
13	1900	2	7	MS	4.3	40.5	26.6
14	1900	4	10	MS	4.7	39.85	27.36
15	1900	5	16	MS	4.7	39.8	30.3
16	1900	6	18	MS	4.8	40.43	29.26
17	1900	7	12	MS	4.2	40.5	26.3
18	1900	8	1	MS	4.7	40.44	30.1
19	1900	8	4	MS	4.4	39.85	27.36
20	1900	8	9	MS	4.2	40.44	30.1
21	1900	8	11	MS	4	39.59	30.24
22	1900	9	7	MS	4	40.63	30.56
23	1900	12	2	MS	4.2	40.44	28.98
24	1901	4	20	MS	4.9	40.61	30.32
25	1901	5	12	MS	5	39.8	30.5
26	1901	9	7	MS	4.1	39.84	28.14
27	1901	12	18	MS	5.9	39.4	26.7
28	1902	7	13	MS	4	40.3	28.75
29	1902	7	14	MS	5.3	40.7	27.8
30	1902	7	15	MS	5.4	40.7	27.8
31	1902	7	15	MS	5.5	40.7	27.8
32	1903	5	26	MS	5.9	40.65	29
33	1903	11	18	MS	4	41.7	26.8
34	1904	9	19	MS	4.8	40.63	26.88
35	1905	1	11	MS	5	39.6	27.9
36	1905	4	15	MS	5.6	40.2	29

37	1905	4	30	MS	5.4	39.8	30.5
38	1905	10	22	MS	5.2	41	31
39	1905	10	22	MS	5.9	40.6	28.3
40	1905	11	18	MS	4.3	41.23	26.43
41	1907	1	22	MS	4.8	41.5	28.5
42	1907	1	22	MS	4.5	41	29
43	1907	4	17	MS	4.5	40.72	30.48
44	1907	8	21	MS	5.5	40.7	30.1
45	1908	7	7	MS	4.1	41.04	26.62
46	1908	11	16	MS	4.5	41.5	26.5
47	1909	2	18	MS	4.4	41.8	27
48	1909	7	19	MS	5.1	40.5	26.15
49	1909	8	14	MS	4.7	41	28.2
50	1909	10	29	MS	5.8	40.26	29.64
51	1911	3	18	MS	4	40.7	30.35
52	1911	5	13	MS	5.4	40.14	26.4
53	1912	8	9	MS	7.4	40.75	27.2
54	1912	8	9	MS	4.3	40.75	27.2
55	1912	8	10	MS	6.2	40.75	27.2
56	1912	8	10	MS	5.3	40.75	27.2
57	1912	8	11	MS	4.8	40.75	27.2
58	1912	8	11	MS	5	40.6	27.2
59	1912	9	13	MS	6.2	40.7	27
60	1912	9	16	MS	5.2	40.7	27
61	1912	10	21	MS	4.4	40.7	27.08
62	1912	10	21	MS	4.8	40.5	27
63	1913	4	24	MS	4.8	40.8	27.55
64	1913	5	8	MS	4.8	40.05	30.13
65	1914	3	22	MS	4.5	40	26
66	1917	4	10	MS	5.3	40.6	27.1
67	1917	12	27	MS	5	40.5	26
68	1919	10	13	MS	4.5	41.5	28
69	1920	1	9	MS	5.2	41.8	26.2
70	1922	6	19	MS	4.9	40.5	26
71	1923	5	29	MS	5.5	41	30
72	1923	10	26	MS	5	41.2	28.6
73	1924	1	22	MS	5.3	39.51	28.4
74	1924	9	1	MS	4.3	40.9	29.2
75	1924	12	22	MS	5.4	39.6	27.7
76	1925	4	29	MS	4.6	39.6	27.7
77	1925	6	10	MS	4.4	41	29
78	1925	6	24	MS	4.6	40.88	30.39
79	1926	12	16	MS	5.7	40.13	30.72
80	1928	1	24	MS	5.3	40.99	30.86

81	1928	5	2	MS	6.1	39.64	29.14
82	1928	5	3	MS	4.3	40.8	26.8
83	1928	5	6	MS	5	39.8	30.5
84	1929	4	5	MS	4.8	41.5	31.5
85	1929	4	27	MS	4.8	40.51	31.43
86	1929	10	10	MS	4.5	41.11	27.46
87	1931	7	12	MS	5.6	39.5	26
88	1932	10	15	MS	4.5	40.9	30.6
89	1933	2	5	MS	4.4	41.5	31.5
90	1933	5	15	MS	4.7	41.26	31.09
91	1934	7	14	MS	4.3	39.5	26
92	1935	1	4	MS	6.2	40.25	27.5
93	1935	1	4	MS	4.6	40.5	27.5
94	1935	1	4	MS	4.5	40.5	27.5
95	1935	1	4	MS	6	40.25	27.5
96	1935	10	22	MS	5.2	40.31	27.21
97	1938	7	2	MS	5	40.17	27.88
98	1939	7	25	MS	5.2	39.75	29.52
99	1939	7	31	MS	4.8	39.8	29.6
100	1939	8	2	MS	5.3	39.75	29.48
101	1939	8	3	MS	5.5	39.75	29.68
102	1939	8	9	MS	5.1	39.91	29.81
103	1939	9	15	MS	5.6	39.75	30.25
104	1939	10	19	MS	5.3	39.82	29.5
105	1940	6	13	MS	4.6	41.34	30.17
106	1940	8	19	MS	4.5	40.13	30.09
107	1941	2	9	MS	4.6	40.13	28.27
108	1942	6	16	MS	5.6	40.8	27.8
109	1942	10	28	MS	5.5	39.46	27.79
110	1942	11	15	MS	6.1	39.55	28.58
111	1943	3	26	MS	4.5	41.7	25.7
112	1943	4	14	MS	5	39.62	29.64
113	1943	6	20	MS	6.6	40.85	30.51
114	1943	6	20	MS	5.5	40.84	30.73
115	1943	9	6	MS	4.9	40.21	31.35
116	1943	9	8	MS	4	40.7	30.4
117	1944	2	1	MS	5	40.7	31.27
118	1944	2	2	MS	5.1	40.74	31.44
119	1944	4	5	MS	5.5	40.84	31.12
120	1944	10	6	MS	6.8	39.48	26.56
121	1945	2	9	MS	4.9	40.5	31.2
122	1948	11	9	MS	4.7	40.1	26.4
123	1948	11	13	MS	5.6	40.23	29.02
124	1948	12	13	MS	4.2	41	30

125	1949	2	5	MS	5	39.89	29.35
126	1949	11	28	MS	4.7	40.98	30.74
127	1950	11	28	MS	5.1	39.73	28.05
128	1951	9	15	MS	5	40.15	28.02
129	1951	12	13	MS	4.9	40.06	26.2
130	1952	1	22	MS	4.3	40.8	30.4
131	1952	2	3	MS	4.7	40.36	25.82
132	1952	3	13	MS	4.9	41.02	28.14
133	1952	3	19	MS	5.4	39.6	28.64
134	1953	3	18	MS	7.2	39.99	27.36
135	1953	3	18	MS	5	40	27.4
136	1953	3	18	MS	4.6	40.02	27.83
137	1953	3	18	MS	5.4	39.96	27.59
138	1953	3	18	MS	4.8	40	27.4
139	1953	3	18	MS	4.5	40	27.4
140	1953	3	19	MS	4.8	40.1	27.3
141	1953	3	19	MS	5	39.88	27.35
142	1953	3	22	MS	4.2	40	27.3
143	1953	3	24	MS	4.9	40	27.4
144	1953	3	26	MS	4.7	39.94	27.48
145	1953	3	31	MS	4.5	40.1	27.3
146	1953	4	1	MS	4.9	39.97	27.45
147	1953	6	3	MS	5.3	40.28	28.53
148	1953	6	18	MS	5.1	41.8	26.55
149	1954	3	23	MS	5.1	40.58	27.12
150	1954	10	24	MS	4.8	40.46	27.53
151	1954	10	26	MS	4.6	40.56	27.52
152	1955	6	2	MS	5.3	40.35	25.71
153	1956	1	6	MS	5.5	40.39	26.29
154	1956	1	6	MS	4.9	41	30.2
155	1956	2	20	MS	6.4	39.89	30.49
156	1956	2	23	MS	5.2	39.76	30.17
157	1956	7	14	MS	4.6	40.32	30.9
158	1956	7	18	MS	4.5	39.96	27.3
159	1956	8	28	MS	4.6	41.08	29.93
160	1956	8	30	MS	4	41	30.2
161	1957	5	26	MS	7.1	40.67	31
162	1957	5	26	MS	5.4	40.6	30.74
163	1957	5	26	MS	5.1	41.34	30.7
164	1957	5	26	MS	4.9	41.42	31.09
165	1957	5	26	MS	5.9	40.76	30.81
166	1957	5	27	MS	4.2	41.14	31.19
167	1957	5	27	MS	4.7	40.84	31.17
168	1957	5	27	MS	4.6	41.13	30.65

169	1957	5	27	MS	5.8	40.73	30.95
170	1957	5	28	MS	4.8	40.58	30.53
171	1957	5	28	MS	4.7	40.57	31.02
172	1957	5	29	MS	4.7	40.72	31.04
173	1957	5	29	MS	4.9	40.83	30.77
174	1957	5	30	MS	4.2	40.65	31.24
175	1957	6	1	MS	5	40.75	30.86
176	1957	6	1	MS	4.8	40.68	30.84
177	1957	6	2	MS	4.8	40.71	30.78
178	1957	10	24	MS	4.7	40.06	29.75
179	1957	12	26	MS	5.2	40.83	29.72
180	1958	11	23	MS	4.4	40.49	30.69
181	1959	4	2	MS	4.6	40.5	29.41
182	1959	7	26	MS	5.4	40.91	27.54
183	1959	8	6	MS	4.1	40.4	29.2
184	1960	3	6	MS	4.1	41.3	26.5
185	1960	3	9	MS	4.1	40.5	26.5
186	1961	3	28	MS	5	39.82	30.19
187	1961	11	28	MS	5.2	39.99	26.1
188	1962	4	19	MS	4.3	40.75	28.84
189	1962	9	14	MS	4.5	39.57	28.17
190	1963	3	29	MS	5.1	40.29	26.15
191	1963	9	18	MS	6.3	40.77	29.12
192	1963	9	24	MS	4.8	40.84	28.9
193	1964	4	18	mb	4.2	41.1	29
194	1964	10	6	mb	5.4	40.186	28.153
195	1964	10	6	MS	7	40.3	28.23
196	1964	10	7	mb	4.4	40.19	28.36
197	1964	10	20	MS	4.8	40	28.6
198	1964	11	20	mb	4.4	40.2	28.06
199	1964	12	15	mb	4.7	40.02	28.79
200	1964	12	21	mb	4.6	40.5	27.5
201	1965	8	23	mb	5.2	40.436	26.136
202	1965	8	24	mb	4.2	40.39	26.2
203	1965	9	2	MS	4.2	39.7	27.1
204	1965	9	8	MS	4.1	40.2	26.2
205	1965	9	15	mb	4.1	39.5	30
206	1965	10	4	MS	4.1	39.6	26.5
207	1966	8	21	mb	4.8	40.312	27.436
208	1966	12	30	mb	4.2	40.74	30.74
209	1967	2	12	mb	4.2	40.14	28.1
210	1967	4	4	mb	4.5	40.32	26.2
211	1967	4	4	mb	4.4	40.31	26
212	1967	4	7	MS	4.4	40	31

213	1967	5	9	mb	4.6	39.61	27.15
214	1967	6	1	MS	4	40.93	28.9
215	1967	7	22	MS	6.8	40.67	30.69
216	1967	7	22	mb	5.2	40.7	30.8
217	1967	7	22	MS	4.2	40.7	30.8
218	1967	7	22	mb	4.8	40.73	30.53
219	1967	7	22	MS	5.1	40.66	30.62
220	1967	7	22	mb	4	40.7	30.8
221	1967	7	22	MS	4.7	41	30
222	1967	7	22	mb	4.7	40.7	30.8
223	1967	7	22	mb	5.1	40.748	30.555
224	1967	7	22	mb	4.7	40.7	30.8
225	1967	7	22	mb	4.6	41.07	30.59
226	1967	7	22	mb	4.7	40.79	30.42
227	1967	7	22	mb	4.6	41	30.45
228	1967	7	22	mb	4.5	40.8	30.52
229	1967	7	22	mb	4.8	40.655	30.544
230	1967	7	23	mb	4.2	40.7	30.57
231	1967	7	23	mb	4.1	40.7	30.57
232	1967	7	23	mb	4.5	40.61	30.35
233	1967	7	23	mb	4.6	40.63	30.36
234	1967	7	23	mb	4.1	40.74	30.36
235	1967	7	23	mb	4.3	40.98	30
236	1967	7	23	mb	4.2	40.4	30.3
237	1967	7	23	mb	4	40.7	30.8
238	1967	7	23	mb	4.4	40.63	30.59
239	1967	7	23	mb	4.2	40.78	30.45
240	1967	7	23	mb	4.3	40.61	30.63
241	1967	7	24	mb	4.3	40.64	30.52
242	1967	7	24	mb	4.3	40.58	30.7
243	1967	7	24	mb	4.3	40.7	30.8
244	1967	7	25	mb	4.3	40.7	30.8
245	1967	7	26	mb	4.2	41.1	30.5
246	1967	7	26	MS	4	40.7	30.8
247	1967	7	26	mb	4.5	40.61	30.67
248	1967	7	30	mb	4.6	40.71	30.58
249	1967	7	30	mb	5.4	40.697	30.549
250	1967	7	30	mb	4.4	40.7	30.58
251	1967	7	30	mb	4.4	40.77	30.56
252	1967	7	30	mb	4.5	40.75	30.46
253	1967	7	30	mb	4.4	40.7	30.8
254	1967	7	31	mb	4.2	40.6	27.62
255	1967	8	1	mb	4.6	40.72	30.52
256	1967	8	1	mb	4.4	40.4	30.4

257	1967	8	2	mb	4.2	40.7	27.2
258	1967	8	2	mb	4.4	40.67	30.46
259	1967	8	3	mb	4	41	30.3
260	1967	8	6	mb	4.3	41	28.8
261	1967	8	8	mb	4.2	40.47	30.61
262	1967	8	14	mb	4.4	40.75	30.38
263	1967	8	14	mb	4.4	40.68	30.27
264	1967	8	14	mb	4.7	40.74	30.37
265	1967	8	18	mb	4.7	41.2	30.1
266	1967	9	18	mb	4.4	40.86	30.3
267	1968	1	31	MS	4	40.5	30.75
268	1968	2	19	mb	5.2	39.8	26.4
269	1968	2	21	MS	4.3	39.5	25.75
270	1968	2	22	mb	4.5	39.66	25.72
271	1968	2	29	MS	4.5	39.5	26
272	1968	3	4	mb	4.1	39.53	25.9
273	1968	3	18	mb	4.4	40.83	30.53
274	1968	3	23	mb	4.6	39.78	25.64
275	1968	3	28	mb	4.5	40.5	31.34
276	1968	5	6	mb	4.3	40.33	28.63
277	1968	5	9	mb	4.2	40.07	29.26
278	1968	7	1	mb	4.1	40.1	30.8
279	1968	7	22	mb	4.3	39.67	25.66
280	1968	9	28	mb	4.4	40.49	26.38
281	1968	11	8	mb	4.1	39.74	25.64
282	1968	11	9	mb	4.2	40.15	28.35
283	1969	1	14	mb	4.4	39.4	30.1
284	1969	2	12	mb	4.5	40.7	30.29
285	1969	3	3	MS	5.3	40.048	27.536
286	1969	3	5	mb	4.7	40.038	27.565
287	1969	8	9	MS	4	40.53	25.97
288	1969	8	14	mb	4.7	39.52	27.87
289	1969	8	19	MS	4.2	39.7	27.8
290	1969	12	24	MS	4.3	40.5	28.4
291	1970	3	28	MS	5.3	39.5	30.3
292	1970	3	30	mb	4.6	39.43	29.4
293	1970	3	30	mb	4.2	39.4	30
294	1970	3	31	mb	4	39.41	29.32
295	1970	4	4	MS	4.3	39.7	30
296	1970	4	9	mb	4.7	39.4	27.9
297	1970	4	13	mb	4.2	39.4	28
298	1970	4	19	MS	5	40	30.9
299	1970	4	19	MS	5.3	39.6	30.7
300	1970	4	24	mb	4.4	39.6	29.6

301	1970	5	8	mb	4.1	39.93	30.07
302	1970	5	11	mb	4.1	39.61	29.37
303	1970	5	30	mb	4.3	39.4	28.8
304	1970	7	4	mb	4	39.9	28.8
305	1970	9	6	MS	4	40.2	28.5
306	1970	9	15	MS	4	39.7	28.54
307	1970	9	26	mb	4.4	41.8	26.6
308	1970	10	31	mb	4	39.92	26.16
309	1971	2	23	MS	5.4	39.623	27.343
310	1971	5	1	mb	4.6	40.868	28.017
311	1971	5	23	MS	4.1	39.96	28.72
312	1971	11	27	mb	4.6	39.7464	25.6557
313	1971	12	16	MS	4.1	39.52	27.78
314	1972	2	28	mb	4.1	40.4014	28.9993
315	1972	4	26	MS	5	39.451	26.383
316	1972	4	26	MS	4.1	39.4364	26.3374
317	1972	4	26	mb	4.8	39.454	26.336
318	1972	5	9	Ml	4.2	39.4617	26.3664
319	1972	6	4	mb	4	39.49	26.37
320	1972	6	21	mb	4.1	40.2583	30.0415
321	1972	12	30	mb	4.3	40.2724	25.7412
322	1973	6	27	Ml	4.2	40.72	27.49
323	1973	7	3	Ml	4.1	40.62	27.54
324	1973	11	22	mb	4.2	40.364	29.8804
325	1974	1	3	mb	4.2	39.7437	26.8157
326	1974	1	18	mb	4	40.5	28.94
327	1974	2	5	MS	4.3	39.7894	26.792
328	1974	2	7	mb	4.2	39.7022	26.8778
329	1974	2	7	Ml	4	39.53	27.01
330	1974	9	13	Ml	4.6	40.7932	28.2905
331	1974	12	1	mb	4.2	39.5269	26.3578
332	1974	12	1	mb	4.5	39.478	26.378
333	1975	3	16	mb	4.3	40.362	26.1443
334	1975	3	17	mb	4.5	40.4796	26.0294
335	1975	3	17	MS	5.3	40.48	25.95
336	1975	3	17	mb	4.8	40.429	26.156
337	1975	3	17	MS	5.9	40.475	26.118
338	1975	3	27	mb	5.5	40.422	26.147
339	1975	3	27	mb	4.7	40.376	26.239
340	1975	3	27	mb	4.5	40.4847	26.0827
341	1975	3	30	mb	4.5	40.5674	26.3606
342	1975	4	22	mb	4	40.2796	26.2436
343	1975	4	23	mb	4.4	40.3994	26.0428
344	1976	2	2	mb	4.1	40.387	26.2604

345	1976	5	29	mb	4	40.36	28.89
346	1976	5	31	mb	4.9	39.4771	29.1362
347	1977	1	10	mb	4.1	39.4807	27.383
348	1977	1	25	mb	4.2	39.408	28.3024
349	1977	3	23	mb	4.2	39.631	28.6496
350	1977	6	21	Ml	4.1	39.4772	27.6313
351	1978	2	13	Ml	4.2	40.1397	28.7435
352	1978	5	11	mb	4.3	40.1978	29.5804
353	1978	5	23	mb	4.1	39.5212	25.9402
354	1978	6	15	mb	4.6	40.7856	27.6835
355	1979	1	5	mb	4.4	39.8467	25.6239
356	1979	1	11	mb	4.3	40.3	29.26
357	1979	7	18	Mw	5.3	39.649	28.697
358	1979	8	23	mb	5	39.6877	28.5734
359	1980	1	3	mb	4.2	40.2654	30.8346
360	1980	2	15	mb	4.5	40.3775	25.949
361	1980	2	19	mb	4.2	40.4378	25.8083
362	1980	2	20	mb	4.2	40.4238	26.0354
363	1980	7	29	mb	4.1	39.8751	29.1371
364	1981	3	12	mb	4.7	40.813	28.12
365	1981	5	3	mb	4	40.7945	28.0902
366	1981	6	2	mb	4.1	39.4107	27.9635
367	1981	7	21	mb	4.1	40.2259	28.8565
368	1981	7	22	mb	4	40.2651	28.8984
369	1981	7	23	mb	4.5	40.2973	28.9364
370	1981	8	8	Ml	4	40.7091	28.2574
371	1981	8	12	Ml	4.3	39.514	26.994
372	1981	8	21	mb	4	39.7323	27.8112
373	1981	8	28	mb	4.1	40.466	29.2109
374	1981	12	26	mb	4.9	40.1476	28.74
375	1982	4	16	mb	4.1	39.5371	26.0757
376	1982	4	16	mb	4	40.7925	29.844
377	1982	4	17	Ml	4.6	40.6021	27.3387
378	1982	5	20	mb	4	40.4038	28.9825
379	1982	5	23	Ml	4.2	40.4507	29.0393
380	1982	5	23	mb	4.1	40.7501	30.547
381	1982	6	9	mb	4.4	40.1403	28.8944
382	1982	7	12	mb	4.6	40.9958	27.8284
383	1982	7	27	mb	4.3	40.3752	28.9501
384	1982	9	9	mb	4.4	40.9766	27.8697
385	1982	12	5	mb	4.6	39.8837	26.5031
386	1983	2	1	mb	4.8	40.2038	28.9369
387	1983	5	28	mb	4.4	40.0165	26.8905
388	1983	6	15	Ml	4.2	39.4617	28.2395

389	1983	7	5	Mw	6.1	40.311	27.256
390	1983	7	5	mb	4.1	40.264	27.1643
391	1983	7	8	Ml	4.2	40.2288	27.1842
392	1983	9	24	mb	4.1	39.4932	25.9874
393	1983	10	21	Mw	5.4	40.108	29.402
394	1983	10	27	mb	4.3	40.1558	29.3011
395	1983	10	30	Ml	4.7	40.1387	29.3779
396	1983	11	2	mb	4.6	40.1004	29.3592
397	1983	11	3	mb	4	40.1552	29.2794
398	1983	11	15	mb	4.4	40.1242	29.2767
399	1983	11	23	mb	4.1	40.1116	29.2916
400	1983	12	7	mb	4	40.0701	29.3713
401	1983	12	28	Ml	4.5	40.7286	30.3814
402	1983	12	30	mb	4.1	40.1006	29.4119
403	1984	1	21	mb	4	39.3973	26.3495
404	1984	1	24	mb	4.1	39.4597	25.693
405	1984	3	29	mb	4.6	39.6375	27.867
406	1984	3	31	mb	4	39.6156	28.758
407	1984	4	1	mb	4.1	39.5586	28.7598
408	1984	5	26	mb	4.1	40.6741	30.2693
409	1984	7	29	mb	5	40.418	26.001
410	1984	7	29	mb	4.8	40.382	26
411	1984	7	29	mb	4.5	40.426	25.928
412	1984	7	29	mb	4.1	40.4365	26.0204
413	1984	7	29	mb	4.2	40.3857	25.9934
414	1984	8	8	mb	4.1	39.4448	26.296
415	1984	8	27	mb	4	40.7375	30.0009
416	1984	10	28	mb	4.8	40.0692	29.2577
417	1984	11	14	mb	4.1	40.3275	27.2282
418	1985	4	11	mb	4.2	40.7036	29.009
419	1985	4	27	mb	4.4	40.7354	27.3803
420	1985	5	14	Ml	4	39.7109	26.0902
421	1985	6	4	mb	4.1	40.8584	27.8355
422	1985	6	20	mb	4.1	39.4245	25.6734
423	1985	9	14	mb	4.7	40.7249	29.112
424	1985	12	19	Ml	4.1	40.1958	27.2636
425	1986	5	14	mb	4.5	39.4921	28.417
426	1986	5	15	mb	4.6	40.7203	27.5684
427	1986	5	27	mb	4.4	39.4564	28.4385
428	1986	6	3	mb	4.3	39.4599	28.3601
429	1986	6	25	Ml	4.2	39.4628	28.3629
430	1986	6	27	mb	4.1	40.8907	28.3459
431	1986	9	12	Ml	4.1	40.2494	27.3151
432	1986	10	12	mb	4.4	39.6591	28.9652

433	1986	10	26	Ml	4.6	40.8005	28.993
434	1986	10	30	mb	4	39.7359	28.7815
435	1987	4	24	Ml	4	40.4475	25.9719
436	1987	9	3	mb	4	40.4566	29.2403
437	1987	10	27	mb	4.4	40.4182	28.4575
438	1987	12	31	Ml	4.1	39.4261	27.9823
439	1988	1	1	mb	4.5	40.1365	29.232
440	1988	1	14	mb	4.2	39.9554	29.157
441	1988	4	24	Mw	5.3	40.892	28.317
442	1988	5	30	mb	4.1	40.2772	25.8542
443	1989	1	4	mb	4.3	39.7833	30.6953
444	1989	1	27	mb	4.1	40.4259	29.1492
445	1989	5	10	mb	4.2	39.6684	27.8826
446	1989	5	10	Ml	4.2	39.7105	27.9189
447	1989	5	31	Ml	4.2	39.6268	27.8105
448	1990	1	31	mb	4.3	39.4761	26.0912
449	1990	2	10	mb	4	39.5693	27.9383
450	1990	9	13	mb	4.3	39.5387	28.5276
451	1990	10	24	mb	4.3	39.8444	30.2326
452	1990	12	17	mb	4.5	40.3658	31.3256
453	1991	1	4	Md	4	39.9222	30.167
454	1991	1	7	Md	4	40.6902	28.5579
455	1991	1	19	Ml	4	39.43	28.0345
456	1991	2	12	mb	4.8	40.788	28.844
457	1991	3	3	mb	4.6	40.637	29.078
458	1991	3	8	mb	4.5	40.8504	27.9093
459	1991	5	28	mb	4.1	40.5299	26.419
460	1991	6	26	Md	4.2	39.6029	27.8109
461	1991	10	12	mb	4.5	40.2021	25.6466
462	1992	3	22	mb	4.9	40.172	28.414
463	1992	4	1	mb	4	39.4	28.68
464	1992	4	5	mb	4	40.7961	27.9314
465	1993	1	23	Ml	4.1	40.7843	28.7635
466	1993	3	18	mb	4.1	40.3995	28.0061
467	1993	3	18	mb	4.4	40.4552	27.9811
468	1993	3	18	mb	4.4	40.4271	28.004
469	1993	5	21	mb	4	39.8	28.93
470	1993	5	25	Ml	4.1	40.4701	28.0711
471	1993	6	6	mb	4	39.4198	28.3514
472	1993	9	2	Ml	4.4	40.1918	27.2555
473	1993	12	12	mb	4.9	41.5494	28.786
474	1994	1	22	Ml	4	40.7778	27.4859
475	1994	1	26	Ml	4	40.7309	27.327
476	1994	2	21	mb	4	40.2039	29.3188

477	1994	3	28	mb	4	40.3946	29.9607
478	1994	4	6	Ml	4	40.0729	28.1002
479	1994	5	7	mb	4.1	39.46	27.84
480	1994	5	28	mb	4	40.6889	29.878
481	1994	6	20	mb	4.1	40.5711	27.3396
482	1994	6	22	Ml	4	40.1659	27.4254
483	1994	8	19	mb	4.1	40.4	25.78
484	1994	9	6	Ml	4	40.43	25.76
485	1995	1	5	mb	4	39.7565	25.7073
486	1995	2	8	mb	4.4	40.8032	27.7735
487	1995	4	13	mb	4.8	40.85	27.74
488	1995	4	18	mb	4.7	40.8648	27.7453
489	1995	7	7	mb	4.1	40.4849	29.3264
490	1995	8	19	mb	4.2	40.2287	29.6105
491	1995	10	28	mb	4	40.8354	27.9717
492	1996	2	22	mb	4.1	40.27	25.96
493	1996	3	21	mb	4	40.252	29.574
494	1996	3	22	mb	4.6	40.3	25.877
495	1996	4	14	mb	4	40.7867	27.4739
496	1996	8	25	mb	4	39.5585	26.112
497	1997	5	2	mb	4	39.6729	28.5904
498	1997	10	18	Ml	4.4	39.8034	28.6668
499	1997	10	18	Ml	4	39.814	28.6228
500	1997	10	21	mb	4.2	40.7143	30.4301
501	1997	10	25	mb	4.2	40.45	26.39
502	1997	12	28	mb	4.1	39.7731	26.8792
503	1998	1	19	Ml	4	40.4171	26.0935
504	1998	3	5	mb	4.5	39.555	27.388
505	1998	3	5	mb	4.4	39.561	27.477
506	1998	7	19	Ml	4.1	40.7165	27.3965
507	1998	9	25	mb	4	40.1997	28.8815
508	1999	2	28	Ml	4	40.41	25.95
509	1999	4	8	Ml	4	40.187	27.329
510	1999	7	13	Ml	4.1	40.412	25.907
511	1999	8	17	Mw	7.6	40.77	30.004
512	1999	8	17	mb	4.5	40.707	30.666
513	1999	8	17	mb	5	40.711	29.911
514	1999	8	17	mb	4.5	40.664	30.346
515	1999	8	17	mb	4	39.779	30.484
516	1999	8	17	mb	4	40.955	30.002
517	1999	8	17	mb	4.2	40.703	30.535
518	1999	8	17	mb	4.1	40.624	30.389
519	1999	8	17	mb	4.1	40.721	29.717
520	1999	8	17	mb	4.6	40.798	30.021

521	1999	8	17	mb	4.3	40.714	29.027
522	1999	8	17	mb	4.7	40.785	29.201
523	1999	8	17	mb	4	40.363	30.272
524	1999	8	17	mb	4	40.776	30.914
525	1999	8	17	mb	4.3	40.526	29.42
526	1999	8	17	mb	4.2	40.764	30.749
527	1999	8	17	mb	4.4	40.622	30.619
528	1999	8	17	mb	4.9	40.649	30.614
529	1999	8	17	mb	4.9	40.837	30.108
530	1999	8	17	mb	4.2	40.687	30.815
531	1999	8	17	mb	4.9	40.711	30.684
532	1999	8	17	mb	4.2	40.744	30.255
533	1999	8	17	mb	4.2	40.722	30.31
534	1999	8	17	mb	4	40.751	30.701
535	1999	8	17	mb	4.3	40.755	29.154
536	1999	8	17	mb	4.6	40.673	30.451
537	1999	8	17	mb	4.1	39.761	27.819
538	1999	8	17	mb	4.3	40.752	30.261
539	1999	8	17	mb	4.2	40.906	30.797
540	1999	8	17	mb	4.7	40.778	30.23
541	1999	8	17	mb	4.3	40.744	30.023
542	1999	8	17	mb	4.2	40.995	31.116
543	1999	8	17	mb	4.1	40.774	29.91
544	1999	8	17	mb	4.8	40.707	31.133
545	1999	8	17	mb	4.1	40.693	30.486
546	1999	8	17	mb	4.1	40.732	30.596
547	1999	8	17	mb	4.2	40.724	30.726
548	1999	8	17	mb	4	40.869	30.59
549	1999	8	17	mb	4	40.905	31.111
550	1999	8	17	mb	4.6	40.787	31.175
551	1999	8	17	mb	4.2	40.722	30.067
552	1999	8	17	mb	4.2	40.899	31.088
553	1999	8	17	mb	4	40.717	30.3
554	1999	8	17	mb	4.4	40.633	30.51
555	1999	8	17	mb	4	40.42	28.7
556	1999	8	17	mb	4.1	40.768	29.79
557	1999	8	17	mb	4.2	40.788	30.247
558	1999	8	17	mb	4.1	40.43	28.72
559	1999	8	17	mb	4.1	40.74	29.27
560	1999	8	17	mb	4.1	40.71	30.68
561	1999	8	17	mb	4.1	40.821	30.007
562	1999	8	17	mb	4	40.77	30.607
563	1999	8	18	mb	4.2	40.705	30.72
564	1999	8	18	mb	4	40.797	30.069

565	1999	8	18	mb	4.2	40.768	30.63
566	1999	8	19	mb	4.4	40.767	31.033
567	1999	8	19	mb	4.7	40.668	30.715
568	1999	8	19	mb	4.5	40.6	29.194
569	1999	8	19	mb	4.1	40.611	29.021
570	1999	8	19	Mw	5.1	40.571	29.205
571	1999	8	19	mb	4.1	40.619	29.098
572	1999	8	19	mb	4.1	40.73	30.55
573	1999	8	20	mb	4.3	40.766	29.846
574	1999	8	20	mb	4.5	40.605	29.193
575	1999	8	20	mb	4	40.738	29.802
576	1999	8	20	mb	4.3	40.653	30.599
577	1999	8	20	mb	4.3	40.832	30.783
578	1999	8	21	mb	4	40.715	30.447
579	1999	8	22	mb	4.1	40.609	29.075
580	1999	8	22	mb	4.6	40.607	30.716
581	1999	8	23	mb	4.1	40.781	30.562
582	1999	8	24	mb	4.2	40.749	30.023
583	1999	8	26	mb	4.8	40.769	30.003
584	1999	8	29	mb	4.5	40.77	31.093
585	1999	8	31	Mw	5.1	40.7064	29.8943
586	1999	8	31	mb	4.6	40.697	29.908
587	1999	8	31	mb	4.4	40.613	29.077
588	1999	9	2	mb	4.1	40.603	30.604
589	1999	9	4	mb	4	40.7	29.935
590	1999	9	4	mb	4.1	40.72	30.29
591	1999	9	5	mb	4	40.641	30.567
592	1999	9	6	mb	4	40.788	29.746
593	1999	9	6	mb	4.1	40.77	31.11
594	1999	9	9	mb	4	40.71	29.14
595	1999	9	9	mb	4.1	40.255	25.813
596	1999	9	9	mb	4.9	40.268	25.811
597	1999	9	13	Mw	5.8	40.7327	30.0169
598	1999	9	17	mb	4.4	40.774	30.134
599	1999	9	18	mb	4.6	40.599	29.225
600	1999	9	19	mb	4.2	40.691	30.481
601	1999	9	20	mb	4.7	40.618	27.616
602	1999	9	29	Mw	5.2	40.734	29.354
603	1999	10	20	mb	4.7	40.816	28.992
604	1999	11	7	Mw	4.9	40.701	30.728
605	1999	11	7	mb	4.2	40.754	30.682
606	1999	11	8	mb	4	40.724	30.645
607	1999	11	11	Mw	5.6	40.7425	30.2422
608	1999	11	11	mb	4	40.804	30.208

609	1999	11	12	Mw	7.1	40.806	31.226
610	1999	11	12	mb	4.4	40.794	31.261
611	1999	11	12	mb	4.3	40.864	31.018
612	1999	11	12	mb	4.7	40.785	31.03
613	1999	11	12	mb	5.2	40.78	31.139
614	1999	11	12	mb	4.6	40.782	31.127
615	1999	11	12	mb	4.4	40.716	31.544
616	1999	11	12	mb	5	40.723	31.516
617	1999	11	12	mb	4.5	40.805	31.009
618	1999	11	12	mb	4	40.878	31.148
619	1999	11	12	mb	4	40.615	31.371
620	1999	11	12	mb	4	40.64	30.694
621	1999	11	12	mb	4.2	40.769	31.232
622	1999	11	12	mb	4	40.89	31.519
623	1999	11	12	mb	4.6	40.779	31.355
624	1999	11	12	mb	4	40.797	31.07
625	1999	11	12	mb	4.2	40.892	31.02
626	1999	11	12	mb	4.1	40.683	31.338
627	1999	11	12	mb	4.3	40.768	31.175
628	1999	11	12	mb	4.3	40.785	31.468
629	1999	11	12	mb	4.5	40.753	31.177
630	1999	11	12	mb	4	40.903	31.461
631	1999	11	12	mb	4.1	40.815	31.471
632	1999	11	12	mb	4	40.972	31.387
633	1999	11	12	mb	4.1	40.65	31.06
634	1999	11	12	mb	4.4	40.828	31.103
635	1999	11	12	mb	4	40.838	31.201
636	1999	11	12	mb	4	40.818	31.343
637	1999	11	12	mb	4.3	40.849	31.414
638	1999	11	12	mb	4.1	40.776	30.941
639	1999	11	13	mb	4.2	40.831	31.406
640	1999	11	13	mb	4.9	40.773	31.031
641	1999	11	13	mb	4	40.885	31.404
642	1999	11	13	mb	4.2	40.85	31.097
643	1999	11	13	mb	4	40.718	31.445
644	1999	11	13	mb	4.3	40.829	31.447
645	1999	11	13	mb	4	40.805	31.048
646	1999	11	13	mb	4.2	40.811	30.947
647	1999	11	13	mb	4.2	40.822	31.386
648	1999	11	13	mb	4.1	40.802	31
649	1999	11	13	mb	4.3	40.831	31.509
650	1999	11	13	mb	4	40.835	31.504
651	1999	11	14	mb	4	40.894	31.478
652	1999	11	15	mb	4	40.813	31.069

653	1999	11	17	mb	4.1	40.765	31.353
654	1999	11	17	mb	4.7	40.832	31.509
655	1999	11	18	mb	4	40.823	31.403
656	1999	11	19	mb	4.3	40.854	30.99
657	1999	11	19	mb	4.2	40.852	30.85
658	1999	11	19	mb	4.8	40.794	31.044
659	1999	11	20	mb	4	40.858	31.462
660	1999	11	21	mb	4.2	40.817	31.292
661	1999	11	21	mb	4.1	40.82	30.911
662	1999	11	21	mb	4	40.746	31.174
663	1999	11	21	mb	4.3	40.761	31.544
664	1999	12	13	mb	4.3	40.766	30.718
665	1999	12	20	mb	4.2	40.817	30.957
666	2000	1	4	mb	4	40.755	30.69
667	2000	1	5	mb	4.1	40.846	31.238
668	2000	1	20	mb	4.6	40.759	31.402
669	2000	1	31	mb	4.1	40.712	29.252
670	2000	2	9	mb	4.1	40.77	29.94
671	2000	4	2	mb	4.5	40.853	30.328
672	2000	7	5	mb	4	40.364	25.988
673	2000	7	7	mb	4.5	40.863	29.339
674	2000	8	23	Mw	5.3	40.787	30.781
675	2000	9	8	mb	4.3	39.395	27.667
676	2000	11	7	mb	4	39.414	26.276
677	2000	11	13	mb	4	40.808	30.777
678	2001	1	16	mb	4.1	40.9	29.07
679	2001	1	24	Ml	4	39.59	26.083
680	2001	2	1	Ml	4	40.081	27.77
681	2001	3	14	Md	4.1	40.845	27.611
682	2001	4	1	mb	4	40.944	31.155
683	2001	5	31	mb	4	39.46	26.34
684	2001	8	26	mb	4.9	40.936	31.522
685	2002	2	28	mb	4.1	40.802	28.14
686	2002	3	5	mb	4.3	40.652	25.622
687	2002	3	23	mb	4	40.863	27.83
688	2002	5	5	mb	4	40.545	28.304
689	2002	9	17	mb	4.1	40.72	30.61
690	2003	3	9	mb	4	40.7742	30.6035
691	2003	3	20	mb	4.2	40.005	28.7787
692	2003	4	1	mb	4.1	40.7781	30.6629
693	2003	5	21	mb	4.2	40.8731	30.9584
694	2003	6	9	mb	4.5	40.201	28.083
695	2003	6	16	mb	4.1	39.4715	25.8105
696	2003	7	5	Md	4	40.4185	26.0478

697	2003	7	6	Mw	5.7	40.445	26.074
698	2003	7	6	Mw	5.2	40.443	26.039
699	2003	7	6	Md	4.1	40.3811	25.9852
700	2003	7	6	mb	4.4	40.4128	25.9607
701	2003	7	6	mb	4.3	40.405	25.949
702	2003	7	9	Ml	4	40.3882	25.8769
703	2003	7	9	mb	4	40.3954	25.9244
704	2003	7	9	Mw	4.8	40.419	25.836
705	2003	7	10	Md	4.1	40.3939	25.8695
706	2003	7	13	mb	4.1	40.8018	27.434
707	2003	7	13	mb	4.1	40.3728	25.8881
708	2003	7	25	mb	4.3	40.9866	31.5222
709	2003	8	31	Md	4	40.4141	25.9407
710	2003	12	23	mb	4.6	39.88	29.265
711	2003	12	23	mb	4.1	39.8762	29.2787
712	2004	4	19	Ml	4.3	40.6599	27.6444
713	2004	5	16	mb	4.4	40.727	29.338
714	2004	6	15	Mw	5.2	40.372	25.901
715	2004	6	27	mb	4.3	40.931	25.9875
716	2004	7	11	Ml	4.1	40.5382	27.1943
717	2004	8	13	mb	4.1	40.83	26.43
718	2004	9	29	Ml	4.3	40.7907	28.999
719	2005	4	9	mb	4	40.48	25.81
720	2005	6	20	mb	4.2	39.716	29.22
721	2005	11	4	mb	4.1	40.68	27.3
722	2006	2	8	mb	4.3	40.731	30.402
723	2006	2	21	Md	4	40.4206	25.8161
724	2006	10	17	mb	4.2	40.8293	31.0709
725	2006	10	20	mb	4.8	40.238	28.032
726	2006	10	24	Mw	5	40.443	29.079
727	2006	10	25	mb	4	40.4686	29.0075
728	2006	12	19	Md	4	40.3855	28.3113
729	2007	1	8	mb	4.1	39.4936	25.7799
730	2007	1	28	Ml	4	40.5924	28.3862
731	2007	8	28	mb	4	40.36	25.86
732	2007	9	29	Md	4	39.7439	27.7464
733	2007	10	21	Ml	4	40.3605	25.8381
734	2007	12	16	Ml	4.1	39.4273	26.2937
735	2007	12	28	mb	4.5	39.521	25.965
736	2008	1	22	Ml	4	39.55	25.98
737	2008	3	12	mb	4.2	40.638	28.9981
738	2008	5	12	Ml	4.5	40.6369	27.3714
739	2008	5	19	Ml	4	40.5	27.8
740	2008	6	1	mb	4	40.1522	26.9157

741	2008	6	3	Ml	4	40.16	26.92
742	2008	7	10	mb	4.3	39.994	27.7128
743	2008	7	15	Ml	4.1	40.37	27.44
744	2008	10	5	Ml	4.2	40.6103	29.0142
745	2008	12	28	Mw	5.2	40.3749	25.7855
746	2009	1	24	mb	4	40.8008	27.78
747	2009	4	1	Ml	4	40.84	31.06
748	2009	4	27	Md	4.2	40.7405	27.5233
749	2009	8	1	Ml	4.3	40.37	28.28
750	2009	8	8	mb	4.2	40.3505	27.4303
751	2010	5	11	mb	4.3	39.4486	25.9369
752	2010	5	15	Ml	4.3	41.2	30.13
753	2010	5	29	mb	4	40.95	26.65
754	2010	6	11	mb	4.2	40.4264	28.9573
755	2010	8	12	mb	4.3	39.6865	27.5781
756	2010	8	23	Ml	4.1	40.3769	25.9446
757	2010	10	3	mb	4.4	40.8323	28.176
758	2010	10	29	Ml	4.1	40.31	25.81
759	2010	11	3	Mw	5.3	40.425	26.2214
760	2010	12	26	mb	4.1	40.3222	25.8821
761	2010	12	31	Ml	4	40.58	27.34
762	2011	1	20	Ml	4.1	40.71	29.76
763	2011	3	9	Ml	4	40.43	28.06
764	2011	3	30	Ml	4.3	40.05	27.83
765	2011	7	11	Ml	4.7	40.1382	29.9733
766	2011	7	25	Mw	5.1	40.8195	27.7498
767	2011	8	16	Ml	4	40.44	28.89
768	2012	2	24	Ml	4	39.5937	26.0725
769	2012	3	23	Ml	4	39.6112	26.065
770	2012	5	4	Ml	4.2	40.3278	27.018
771	2012	5	18	Ml	4	39.4612	27.9018
772	2012	6	7	Mw	5	40.854	27.9235
773	2012	7	4	Ml	4.2	39.9467	27.891
774	2012	7	7	Ml	4	40.7608	30.4077
775	2012	7	25	Ml	4.6	40.427	26.2208
776	2013	1	8	Mw	5.6	39.68	25.67
777	2013	1	9	Ml	4.9	39.7075	25.658
778	2013	1	11	Ml	4.2	40.3985	25.9448
779	2013	1	12	Ml	4	39.6447	25.6733
780	2013	1	13	Ml	4.3	39.652	25.6377
781	2013	1	19	Ml	4.2	39.6382	25.6795
782	2013	2	11	Ml	4	39.7292	25.6595
783	2013	4	27	Ml	4	40.0497	25.9223
784	2013	7	12	Ml	4.3	40.3738	25.946

785	2013	7	30	Ml	5.3	40.3028	25.7902
786	2013	7	30	Ml	4.1	40.297	25.7933
787	2013	7	30	Ml	4.1	40.2687	25.8168
788	2013	7	31	Ml	4	40.3037	25.7712
789	2013	8	17	Ml	4.5	40.4132	29.1193
790	2013	8	29	Ml	4.3	40.3493	27.459
791	2013	11	27	Mw	4.5	40.8338	27.9051
792	2013	11	27	Mw	4	40.8155	27.908
793	2014	1	7	Mw	4	39.7968	26.141
794	2014	1	10	Mw	4	39.4531	27.9588
795	2014	1	13	ML	4.1	39.8125	26.1363
796	2014	5	24	Mw	5.3	40.3951	26.3058
797	2014	5	24	ML	4.4	40.4213	26.2166
798	2014	5	24	Mw	4.6	40.3888	26.1786
799	2014	5	24	Mw	4.3	40.397	26.1291
800	2014	5	24	ML	4	40.3861	26.2146
801	2014	5	24	Mw	4.5	40.2765	25.77
802	2014	5	24	Mw	4.5	40.3816	26.0231
803	2014	5	24	Mw	4	40.377	26.1345
804	2014	5	24	Mw	4.2	40.3895	25.9876
805	2014	5	25	Mw	4.8	40.4128	26.1851
806	2014	5	25	Mw	4.5	40.4411	26.041
807	2014	5	28	Mw	4.1	40.3923	26.177
808	2014	5	30	Mw	4.1	40.1746	25.6383
809	2014	6	26	Mw	4.1	39.6745	25.648
810	2014	7	3	Mw	4.5	40.1931	27.9231
811	2014	7	9	ML	4.2	40.4121	26.2645
812	2014	7	16	Mw	4	40.2411	26.2518
813	2014	8	3	Mw	4	40.5916	29.1678
814	2014	8	11	Mw	4.1	40.321	26.0166
815	2014	10	22	Mw	4.5	40.4113	30.1001
816	2014	12	16	Mw	4.3	40.1298	27.0845
817	2015	1	17	Mw	4	39.8775	30.3785
818	2015	1	23	Mw	4.3	40.0455	28.5788
819	2015	2	2	Mw	4.1	40.3083	26.0295
820	2015	7	24	Mw	4.3	40.2488	26.2651
821	2015	7	24	Mw	4.8	40.2473	26.2661
822	2015	7	24	Mw	4.4	40.2425	26.2778
823	2015	9	18	Mw	4	39.8125	30.4296
824	2015	10	26	Mw	4.3	39.7781	26.2648
825	2015	10	28	Mw	4.4	40.8003	27.7446
826	2015	11	16	Mw	4	40.8181	28.7631
827	2016	1	1	Mw	4	40.0415	30.5338
828	2016	6	7	Mw	4.3	40.259	29.1605

829	2016	6	25	Mw	4.2	40.6985	29.2016
830	2016	6	28	Mw	4	39.4206	25.937
831	2017	1	14	Mw	4.6	39.5373	26.1518
832	2017	1	15	Mw	4.3	39.5418	26.151
833	2017	2	6	Mw	5.3	39.5495	26.137
834	2017	2	6	Mw	4	39.5333	26.1288
835	2017	2	6	Mw	5.3	39.5303	26.1351
836	2017	2	6	Mw	4.4	39.5366	26.1183
837	2017	2	7	Mw	5.2	39.5205	26.151
838	2017	2	7	Mw	4.3	39.52	26.1555
839	2017	2	7	Mw	4.2	39.5313	26.1865
840	2017	2	7	Mw	4.4	39.5326	26.1705
841	2017	2	7	Mw	4.1	39.5163	26.177
842	2017	2	7	Mw	4.1	39.5243	26.1065
843	2017	2	8	Mw	4.5	39.5256	26.1916
844	2017	2	8	Mw	4.1	39.5333	26.1775
845	2017	2	9	Mw	4	39.5415	26.1036
846	2017	2	10	ML	5	39.5236	26.1946
847	2017	2	12	Mw	4	39.5496	26.1183
848	2017	2	12	Mw	5.3	39.5336	26.17
849	2017	2	16	Mw	4.6	39.5178	26.0885
850	2017	2	23	Mw	4.3	39.5486	26.1225
851	2017	2	27	Mw	4	39.4975	26.0835
852	2017	2	28	Mw	4.7	39.492	26.0968
853	2017	3	8	Mw	4.1	39.965	27.6536
854	2017	3	20	Mw	4.3	39.5446	26.1765
855	2017	3	24	Mw	4.2	39.5541	26.1126
856	2017	4	20	Mw	4.2	39.3975	28.463
857	2017	7	22	Mw	4	40.0158	27.1296
858	2017	9	16	Mw	4.1	39.4273	26.3946
859	2017	12	31	Mw	4	40.5491	27.8495
860	2018	1	14	Mw	4.1	39.5368	26.0538

Appendix B

This appendix presents borehole logs data used for PLHA in the Chapter 3.

ID	Lat.	Lon.	V_{s0-5}	V_{s5-10}	V_{s0-10}	SPT_{0-5}	SPT_{5-10}	SPT_{0-10}	GWL
0	40.7792	30.3946	121	142	131	4	20	12	0.90
1	40.7792	30.3949	164	426	237	10	28	19	0.87
2	40.7851	30.4002	225	278	224	6	8	7	3.10
3	40.7845	30.4004	137	253	178	8	31	16	1.68
4	40.7838	30.3923	90	205	125	5	14	9	0.96
5	40.7835	30.3923	101	117	108	5	22	13	1.42
6	40.7693	30.4083	145	180	161	7	28	18	1.68
7	40.7778	30.4052	111	217	146	5	22	13	0.50
8	40.7715	30.4080	116	170	138	5	12	9	1.64
9	40.7745	30.4090	130	142	136	5	8	7	0.41
10	40.7792	30.3949	114	146	128	5	9	7	1.72
11	40.7765	30.3925	122	252	164	6	30	17	0.71
12	40.7752	30.4108	112	135	123	4	15	10	0.89
13	40.7775	30.4034	99	206	133	4	19	11	0.80
14	40.7786	30.4027	114	217	149	5	22	12	0.68
15	40.7735	30.3637	128	136	132	7	8	7	1.11
16	40.7738	30.3721	115	140	126	5	6	6	2.40
17	40.7745	30.3776	127	188	152	6	16	11	0.37
18	40.7764	30.3830	143	256	184	5	30	17	2.50
19	40.7765	30.3925	122	253	164	6	31	18	0.71
20	40.7791	30.4052	155	180	167	3	20	12	0.74
21	40.7795	30.4070	130	135	132	4	8	6	0.62
22	40.7797	30.3947	101	166	126	4	12	8	0.92
23	40.7788	30.3917	114	248	156	5	29	17	0.10
24	40.7750	30.4067	111	152	129	5	10	7	0.50
25	40.7749	30.4047	94	156	118	3	10	7	1.16
26	40.7858	30.4017	106	202	139	4	18	11	1.65
27	40.7761	30.4046	118	176	141	5	13	9	0.64
28	40.7646	30.4090	99	138	115	4	8	6	1.01
29	40.7792	30.3949	124	193	151	6	17	11	0.75
30	40.7425	30.3841	188	247	214	16	29	22	11.00
31	40.7590	30.3937	155	200	175	10	18	14	0.30
32	40.7566	30.3867	212	288	244	21	41	31	2.20
33	40.7662	30.3819	200	270	230	18	35	27	1.20
34	40.7686	30.3939	143	142	142	8	8	8	2.10
35	40.7693	30.3957	155	145	150	10	9	9	1.40
36	40.7723	30.3921	171	229	196	13	24	18	1.00
37	40.7686	30.3995	145	174	158	9	13	11	1.00

38	40.7724	30.4047	245	322	278	28	53	41	10.00
39	40.7709	30.4038	145	232	178	9	25	17	1.25
40	40.7725	30.4004	174	190	182	13	16	15	0.70
41	40.7738	30.4082	128	174	147	7	13	10	0.60
42	40.7764	30.4030	126	220	161	6	22	14	0.22
43	40.7815	30.4043	140	161	150	8	11	10	1.00
44	40.7853	30.4052	161	214	184	11	21	16	1.00
45	40.7841	30.4116	114	227	152	5	24	15	0.60
46	40.7733	30.4071	168	187	177	12	15	14	0.75
47	40.7850	30.4184	132	148	140	7	9	8	0.70
48	40.7969	30.4083	223	168	191	23	12	18	0.80
49	40.7934	30.3964	161	181	171	11	14	13	0.60
50	40.7955	30.4217	132	183	154	7	15	11	0.95
51	40.8001	30.4146	132	179	152	7	14	11	1.10
52	40.7895	30.3764	190	181	186	16	14	15	0.55
53	40.7894	30.3879	155	161	158	10	11	11	0.70
54	40.7854	30.3879	124	202	153	6	18	12	0.80
55	40.7850	30.3956	155	185	168	10	15	13	0.60
56	40.7784	30.3909	221	255	237	23	31	27	0.70
57	40.7816	30.3963	132	177	152	7	14	10	0.58
58	40.7791	30.3937	132	129	131	7	7	7	0.65
59	40.7878	30.3804	132	181	153	7	14	11	0.75
60	40.7745	30.3966	148	168	157	9	12	11	0.68
61	40.7682	30.3819	155	197	173	10	17	14	0.50
62	40.7809	30.4005	155	217	181	10	22	16	1.10
63	40.7791	30.4082	132	257	175	7	32	19	0.80
64	40.7657	30.4129	174	214	192	13	21	17	0.70
65	40.7888	30.3990	219	219	219	22	22	22	0.80
66	40.8088	30.4046	195	185	190	17	15	16	0.90
67	40.7718	30.4027	155	202	175	10	18	14	1.50
68	40.7929	30.4129	150	197	170	9	17	13	2.00
69	40.7734	30.4198	140	237	176	8	26	17	2.00
70	40.8007	30.3963	161	193	176	11	17	14	2.00
71	40.7864	30.4104	132	191	156	7	16	12	2.00
72	40.7781	30.4006	212	237	224	20	26	28	1.40
73	40.7778	30.3989	185	285	224	15	40	28	1.10
74	40.7759	30.3879	210	291	244	20	42	31	1.50

Appendix C

This appendix presents building stock data used for seismic risk assessment in the Chapter 4.

Cell ID	Number of buildings	Roof area (m^2)	Average storey number	Floor area (m^2)	Population
1.1	270	51835	2.7	139955	2729
1.2	149	28605	2.55	72943	1422
1.3	180	45624	2.45	111779	2180
1.4	775	164778	2.9	477856	9318
1.5	598	114804	2.85	327191	6380
1.6	481	92342	2.87	265022	5168
1.7	208	39932	3.4	135769	2647
2.1	389	74680	2.7	201636	3932
2.2	918	176238	2.58	454694	8867
2.3	720	150578	2.45	368916	7194
2.4	639	210267	2.98	626596	12219
2.5	840	204232	3.1	633119	12346
2.6	1133	233615	2.93	684492	13348
2.7	598	114804	3.15	361633	7052
3.2	236	45307	2.6	117798	2297
3.3	573	137263	2.47	339040	6611
3.4	1357	320001	2.68	857603	16723
3.5	482	146667	2.83	415068	8094
3.6	1289	250717	2.78	696993	13591
3.7	869	166831	2.87	478805	9337
3.8	124	23806	3	71418	1393
4.3	683	167276	2.47	413172	8057
4.4	875	213093	2.45	522078	10181
4.5	753	150504	2.98	448502	8746
4.6	980	170304	3.08	524536	10228
4.7	1234	233026	2.88	671115	13087
4.8	668	128243	3.05	391141	7627

5.2	224	50505	2.5	126263	2462
5.3	2098	315984	2.73	862636	16821
5.4	1296	282110	3	846330	16503
5.5	1307	229660	3.6	826776	16122
5.6	1167	247479	3.45	853803	16649
5.7	1556	277311	2.83	784790	15303
5.8	109	34047	2.9	98736	1925
6.1	720	138226	2.35	324831	6334
6.2	956	232874	2.37	551911	10762
6.3	1733	311189	3	933567	18205
6.4	1323	399618	3.35	1338720	26105
6.5	1910	312475	3.43	1071789	20900
6.6	1103	261641	3.4	889579	17347
6.7	782	186811	2.75	513730	10018
6.8	75	31635	2.45	77506	1511
7.1	181	34748	2.35	81658	1592
7.2	427	86355	2.3	198617	3873
7.3	1090	233119	2.75	641077	12501
7.4	1957	357557	3	1072671	20917
7.5	2249	370468	3.05	1129927	22034
7.6	1036	238983	2.93	700220	13654
7.7	162	52484	2.43	127536	2487
8.2	888	170478	2.25	383576	7480
8.3	1068	212032	2.25	477072	9303
8.4	801	176565	2.4	423756	8263
8.5	889	152951	2.85	435910	8500
8.6	941	177978	2.5	444945	8676
8.7	219	42044	2.25	94599	1845
9.1	204	39164	2.5	97910	1909
9.2	598	114804	2.5	287010	5597
9.3	193	37052	2.5	92630	1806
Total	**47283**	**9663719**	**-**	**27598951**	**538178**